MULTI-ANTENNA MULTI-CARRIER SPACE-TIME-FREQUENCY PRECODED CODE DIVISION MULTIPLE ACCESS EMPLOYING COMPLETE COMPLEMENTARY CODES

by

Nikolai de Figueiredo

Submitted in partial fulfilment of the requirements for the degree

Master of Engineering (Electronic Engineering)

in the

Department of Electrical, Electronic and Computer Engineering
Faculty of Engineering, Built Environment and Information Technology
UNIVERSITY OF PRETORIA

February 2014

SUMMARY

MULTI-ANTENNA MULTI-CARRIER SPACE-TIME-FREQUENCY PRECODED CODE DIVISION MULTIPLE ACCESS EMPLOYING COMPLETE COMPLEMENTARY CODES

by

Nikolai de Figueiredo

Supervisor(s):	Prof. L. P. Linde
Department:	Electrical, Electronic and Computer Engineering
University:	University of Pretoria
Degree:	Master of Engineering (Electronic Engineering)
Keywords:	Code division multiple access, cyclically rotated complete complementary codes, diversity, joint detection, linear detection, multiple-input multiple-output, orthogonal frequency division multiplexing, orthogonal space-time block codes, spatial multiplexing.

The industry of wireless digital communications has matured since the 1970s with the introduction of cellular technology, to the present rollout of fourth generation infrastructure. The discovery and refining of technology such as orthogonal frequency division multiplexing (OFDM), code division multiple access (CDMA) and later multiple-input multiple-output (MIMO) techniques has set the stage for the current and future high capacity broadband wireless cellular networks. A number of organisations have developed standards for wireless communication technologies, most notably the Third Generation Partnership Project with the Long Term Evolution series of standards and the Institute of Electrical and Electronics Engineers (IEEE) with its IEEE 802 series of standards.

This work aims to contribute to the afore mentioned field of research by amalgamating three key technologies into a wireless communication system. The methodology adopted has centred on orthogonality with the utilisation of OFDM, CDMA employing completely orthogonal complementary codes and MIMO techniques. OFDM provides a reduced complexity means for managing multipath environments by taking advantage of the fast Fourier transform (FFT) algorithm for modulation and demodulation. Furthermore the cyclic rotation scheme applied to the orthogonal complete complementary codes allows the use of spread spectrum technology without the inherent rate loss while

providing multiple access.

The recent advances in multiple antenna communication technology have led to the development of two branches in the field. The first of these was the introduction of the spatial multiplexing concept which increases the system capacity and the second was the development of many diversity achieving spatial coding techniques. Of the diversity achieving techniques orthogonal space-time block codes (OSTBC) are most notable due to their linear detectability.

The performance of two communication systems has been evaluated through simulation. Both employ the multi carrier CDMA based on the cyclically rotated complete complementary codes however the fundamental difference between them is the spatial coding. Spatial multiplexing and OSTBCs have been utilised with a matrix algebraic framework description unifying both. The spatial multiplexed signals are detected with a non-linear sphere decoder and the OSTBC data is detected linearly.

The results have shown that the systems achieve the expected diversity orders in flat fading conditions. The OSTBC system achieves added gains in multipath conditions due to the spread spectrum coding. The codes provide multiple access as well as extract added multipath diversity that would otherwise be unavailable. Interestingly, both systems were unaffected by Doppler since perfect channel state information was assumed and the spreading was performed in frequency domain.

OPSOMMING

VERSKEIE-ANTENNA VERSKEIE-DRAER RUIMTE-TYD-FREKWENSIE VOORAFGEKODEERED KODE AFDELING VEELVULDIGE TOEGANG MET BEHULP VAN VOLLEDIGE KOMPLEMENTÊRE KODES

deur

Nikolai de Figueiredo

Studieleier(s):	Prof. L. P. Linde
Departement:	Elektriese, Elektroniese en Rekenaar-Ingenieurswese
Universiteit:	Universiteit van Pretoria
Graad:	Magister in Ingenieurswese (Elektroniese Ingenieurswese)
Sleutelwoorde:	Kodedivisie Veelvuldige Toegang, Siklies-geroteerde Volledig-komplementêre kodes, Diversiteit, Gesamentlike opsporing, Liniêere opsporing, Multi-inset multi-uitset, Ortogonale Frekwensieskeiding multipleksering, Ortogonale Ruimte-Tyd Blokkodes, Ruimtelike multipleksering.

Die bedryf van draadlose digitale kommunikasie het gegroei sedert die bekendstelling van sellulêre tegnologie in die 1970's tot die huidige ontplooiing van vierde generasie infrastruktuur. Die ontwikkeling en suiwering van tegnologie soos ortogonale frekwensiedeling multipleksering (OFDM)-kodedivisie veelvuldige toegang (CDMA) en later multi-inset multi-uitset (MIMO) tegnieke het gelei tot die huidige en toekomstige hoë kapasiteit breeband draadlose sellulêre netwerke. 'n Aantal organisasies het draadlose kommunikasie tegnologiee gestandardiseer, veral die Derde Generasie Vennootskapprojek (3GPP) se Lang Termyn Evolusie (LTE) reeks van standaarde, asook die IEEE se 802-reeks van standaarde.

Hierdie studie het ten doel om 'n bydrae te maak deur die samevoeging van drie kern tegnologiee om 'n draadlose kommunikasie stelsel te vorm. Die metode wat gevolg is fokus op ortogonaliteit, deur die benutting van OFDM, CDMA wat ortogonale volledig-komplementêre kodes gebruik en MIMO tegnieke. OFDM bied 'n verlaagde kompleksiteit i.t.v. bestuur van die multi-pad omgewing, deur gebruik te maak van die Vinnige Fourier Transform (FFT) algoritme vir modulasie en de-

modulasie. Verder verseker die sikliese rotasie van die ortogonale volledig-komplementêre kodes dat sprei-spektrum tegnologie gebruik kan word om veelvuldige toegang te verskaf, sonder die inherente verlies in datatempo wat met CDMA geassosieer word.

Die onlangse vooruitgang in verskeie antenna kommunikasie tegnologieë het gelei tot die ontwikkeling van twee sytakke in die veld. Die eerste hiervan was die bekendstelling van die ruimtelike multiplekseringkonsep, wat die stelselkapasiteit verhoog. Die tweede hiervan is die ontwikkeling van veelvoudige diversiteitsbereiking ruimtelike koderingstegnieke. Van die diversiteitsbereikingstegnieke is ortogonale ruimte-tyd blokkodes (OSTBC) tegnieke die mees bruikbare a.g.v hulle lineere eieskappe.

Die prestasie van twee kommunikasiestelsels is deur simulasie geëvalueer. Beide maak gebruik van die multi-draer siklies-geroteerde volledig-komplementêre CDMA. Die fundamentele verskil tussen dié twee stelsels is egter hulle ruimtelike kodering. Ruimtelike multipleksering en OSTBCs is benut deur ’n matriks algebraiese raamwerk voorstelling te gebruik, wat albei verenig. Die ruimtelike gemultiplekseerde seine is waargeneem met ’n nie-liniÃłere sferiese dekodeerder, terwyl die OSTBC data liniêer waargeneem word. Resultate het getoon dat die stelsels die verwagte diversiteitsorde in plat deining toestande bereik. Die OSTBC stelsel het die bygevoegde winste a.g.v. sprei-spektrum kodering, in multi-pad toestande bereik. Die volledig-komplementêre kodes verskaf veelvuldige toegang asook die benutting van bygevoegde frekwensiediversiteit wat andersins nie beskikbaar sou wees nie. ’n Interessante waarneming was dat beide stelsels nie deur Doppler geaffekteer is nie, weens die feit dat ideale kanaaltoestandinligting aanvaar was en die spreiding in die frekwensievlak uitgevoer is.

ACKNOWLEDGEMENTS

Without,

- The guidance of Professor L. P. Linde,
- The patience of Mr. J. H. van Wyk,
- The funding received from the Centre for Telecommunication Engineering for the Information Society (CeTEIS) Telkom Centre of Excellence at the University of Pretoria,
- The High Performance Computing Centre in the Department of Electrical, Electronic and Computer Engineering at the University of Pretoria, maintained by Mr. H. Grobler,
- The tolerance and friendship of my fellow students at the university: P. A. Jansen van Vuuren; A. Swiatko; F. de Lange and,
- The love of my Father and Grandmother,

this would not have been possible.

LIST OF ABBREVIATIONS

1G	First generation
2.5G	Beyond second generation
2G	Second generation
3.5G	Beyond third generation
3.9G	See LTE
3G	Third generation
3GPP	Third generation partnership project
3GPP2	Third generation partnership project 2
4G	Fourth generation
AMPS	Advanced Mobile Phone Service
AWGN	Additive white Gaussian noise
BER	Bit error rate
BLAST	Bell Laboratories layered space-time
BS	Base station
CDMA	Code division multiple access
COST	European Cooperation in Science and Technology
CP	Cyclic prefix
CRCCC	Cyclically rotated complete complementary codes
DAMPS	Digital advanced mobile phone service
DD	Delay diversity
DFT	Discrete Fourier transform
DS	Direct sequence
DS-CDMA	Direct sequence-code division multiple access
EDGE	Enhanced data rate for GSM Evolution
FDM	Frequency division multiplexing
FEC	Forward error correction
FFT	Fast Fourier transform
FIR	Finite impulse response
FM	Frequency modulation
GPRS	General packet radio access

GSM	Groupe special mobile
HSDPA	High speed downlink packet access
HSPA+	High speed packet access
IDFT	Inverse discrete Fourier transform
IEEE	Institute of Electrical and Electronics Engineers
IFFT	Inverse fast Fourier transform
IO	Interacting object
ISI	Inter-symbol interference
ITU	International Telecommunication Union
LOS	Line-of-sight
LTE	Long term evolution
MAP	Maximum a posteriori
MBWA	Mobile broadband wireless access
MC-CDMA	multi-carrier code division multiple access
MF	Matched filter
MI	Multipath interference
MIMO	Multiple-input multiple-output
ML	Maximum likelihood
MMSE	Minimum mean-square error
M-QAM	M-ary quadrature amplitude modulation
MS	Mobile station
MUI	Multi-user interference
NLOS	non-line-of-sight
NMT	Nordic Mobile Telephone
NTT	Nippon Telegraph and Telephony
OCC	Orthogonal complete complementary
OFDM	Orthogonal frequency division multiplexing
OFDMA	Orthogonal frequency division multiple access
OSTBC	Orthogonal space-time block code
PDC	Pacific Digital Cellular
PDP	Power delay profile
PG	Processing gain
PSD	Power spectral density

QPSK	Quadrature phase shift keying
REAL	Real environment adaption linearisation
RF	Radio frequency
SIC	Successive interference cancellation
SISO	Single-input single-output
SNR	Signal-to-noise ratio
STBC	Space-time block code
STC	Space-time code
STTC	Space-time trellis code
TACS	Total Access Communication System
TDM	Time division multiplexing
UWB	Ultra-wideband
WCDMA	Wideband code division multiple access
WiMAX	Worldwide interoperability for microwave access
WLAN	Wireless local area network
WMAN	Wireless metropolitan area network
ZF	Zero forcing
CSI	Channel state information

NOTATION

$\mathscr{F}\{\cdot\}$	Fourier transform
$\mathscr{F}^{-1}\{\cdot\}$	Inverse Fourier transform
$(\cdot)^T$	Transpose operator
$(\cdot)^H$	Hermitian/conjugate transpose operator
$(\cdot)^{\frac{1}{2}}$	Hermitian square root operator
$(\cdot)^*$	Conjugate operator
$\Re\{\cdot\}$	Real part
$\Im\{\cdot\}$	Imaginary part
$\|\|\cdot\|\|$	Frobenius norm
$\|\cdot\|$	Norm
$*$	Convolution operator
$vec(\cdot)$	Vectorisation operator

LIST OF MATHEMATICAL SYMBOLS

W	Channel bandwidth/signal Bandwidth
Δf	Bandwidth of subbands
T	Symbol period
N_{FFT}	FFT length
f_i	The ith subcarrier centre frequency
ϕ_i	The ith subcarrier phase
$s(t)$	General OFDM signal/transmitted signal
$S(f)$	Frequency domain representation of the OFDM signal/ transmitted signal
d_i	The ith data symbol
N_{CP}	Cyclic prefix length
T_{CP}	Cyclic prefix period
T_{sa}	Sampling period
F_{sa}	Sampling frequency
L	Channel length
$s[n]$	Sampled transmitted signal
$s^{(CP)}[n]$	Cyclically extended sampled transmitted signal
$r(t)$	Received signal
$r[n]$	Sampled received signal
$h[n]$	Discrete time channel impulse response
$h[k]$	Discrete transfer function
$\mathbf{W}$	DFT matrix
$P(t\ ;\ T)$	The square pulse of duration Ts
$d_i(t)$	User data signal
$c(t)$	Continuous time spreading sequence
T_s	Symbol period
T_p	Pulse period
R_s	Symbol rate
R_c	Chip rate
T_c	Chip period

B_e	Bandwidth expansion factor
$s_i(t)$	DS spread data symbol
$d_{i,k}(t)$	The ith data symbol of the kth user's signal
N_c	Code length
M_c	Family size
K_u	Number of users
$R_{a,a}^{(P)}[n]$	Periodic autocorrelation of a
$R_{a,a}^{(A)}[n]$	Aperiodic autocorrelation of a
$R_{a,b}^{(P)}[n]$	Periodic cross-correlation of a and b
$R_{a,b}^{(A)}[n]$	Aperiodic cross-correlation of a and b
c_i	The ith chip of a code
$d_{i,k}$	The ith data symbol of the kth user's sequence
N	Element code length
M	Flock size
K	Complementary code family size
$c_{i,j}$	The ith chip of the jth element code
$c_{i,j,k}$	The ith chip of the jth element code of the kth flock
$R_{a,a}$	Autocorrelation
$R_{a,b}$	Cross-correlation
$\mathbf{C}$	Spreading code matrix
$\mathbf{c}_i^j$	The jth cyclic rotation of the ith element code
$\mathbf{c}_{i,j}$	The ith element code of the jth flock
$\mathbf{c}_i$	The ith spreading code
$\mathbf{C}^{(E)}$	Cyclically extended complementary code family
$\mathbf{C}_i^{(E)}$	Cyclically extended flock
R	Code rate
n_s	Number of unencoded symbols
N_s	Number of symbol periods
$\mathbf{A}_i$	The ith coding matrix for the real part
$\mathbf{B}_i$	The ith coding matrix for the imaginary part
$\mathbf{X}$	Encoded transmission matrix
N_{Tx}	Number of transmit antennas
N_{Rx}	Number of receive antennas

s_i	The ith unencoded complex data symbol
R_{max}	Maximum achievable rate
$\bar{s}_i$	Real part of the ith unencoded symbol
$\tilde{s}$	Imaginary part of the ith unencoded symbol
$\mathbf{I}$	The identity matrix
$\mathbf{I}_a$	The identity matrix of dimension $a \times a$
$\mathbf{Y}$	Received matrix
$\mathbf{H}$	Channel coefficient matrix
$\mathbf{N}$	Noise matrix
$\mathbf{r}$	Received vector/vectorised received matrix
$\mathbf{h}$	Vector of channel gains
$\mathbf{n}$	Noise vector/vectorised noise matrix
$\breve{s}_j^{(CP)}[n]$	Cyclically extended sequence transmitted from the jth transmit antenna
$\mathbf{n}_\sigma$	Vector of zero mean noise samples with variance σ
$\mathbf{G}$	Matched filter matrix
$\mathbf{R}_n$	Noise covariance matrix
N_0	Noise PSD
n_r	Length of received vector
$\hat{\mathbf{s}}_{ZF}$	ZF solution
$\mathbf{R}_{sr}$	Covariance matrix of the received and data vectors
$\mathbf{R}_r$	Covariance matrix of the received vector
$\mathbf{0}$	The all zero matrix
$\hat{\mathbf{s}}_{MMSE}$	MMSE solution
σ_n^2	Noise variance
σ_s^2	Signal variance
C_r	Sphere radius
$\breve{C}_r$	Modified sphere radius
$\hat{\mathbf{s}}_{ML}$	ML solution
$\mathscr{S}$	Finite symbol alphabet
W_D	Maximum Doppler spread
T	Symbol period
σ_τ	RMS delay spread

T_h	Coherence time
v_{ms}	Velocity of the mobile station
v_{io}	Velocity of the interacting object
n_σ	Noise sample
μ	Noise mean
σ^2	Noise variance
E_b	Bit energy
N_0	Noise PSD
$s(t)$	Continuous time transmitted signal
$h(t\ ;\ f)$	Time variant transfer function
$n(t)$	Noise process realisation
$r(t)$	Continuous time received signal
k_{n_σ}	Noise scaling constant
F_{bit}	Bit frequency
$h(t)$	Fading process envelope
$p(t)$	Flat fading process realisation
$f_h(t)$	Underlying envelope process
$\phi(t)$	Fading process phase
$f_\phi(t)$	Underlying phase process
σ^2_{NLOS}	Diffuse component power
$k_{(dB)}$	Rician K-factor expressed in decibels
$h(t\ ;\ \tau)$	Time variant impulse response
τ_{max}	Maximum excess channel delay
$n_\sigma(t)$	Zero mean AWGN process with variance of σ
$\Delta\tau$	Channel impulse sampling period
$h_i(t\ ;\ \tau)$	Fading process associated with the ith tap
$\phi_i(t\ ;\ \tau)$	Combined phase associated with the ith tap
$\theta_i(t\ ;\ \tau)$	Phase associated with the ith tap
f_c	Carrier frequency
$h(\tau)$	Time-invariant channel impulse response
$\bar{h}_i$	Time averaged amplitude associated with the ith tap
$\bar{\phi}_i$	Time averaged phase associated with the ith tap
F_D	Maximum Doppler shift

$\alpha_i(t)$	Normalised discrete gain for the ith tap
ζ	Correlation constant
$h_{i,n}$	The ith tap coefficient during the nth time interval
$h_i[n]$	The ith tap coefficient during the nth time interval
$n_\sigma[n]$	The nth sample of a zero mean AWGN process with variance σ
$\mathbf{h}_n$	A vector of the channel tap coefficients during the nth time interval
N_B	Block length
$\mathbf{r}$	The vector of the received samples
$\mathbf{H}$	The banded diagonal time variant channel coefficient matrix
$\mathbf{s}$	The vector of the transmitted samples
$\mathbf{n}_\sigma$	The vector of noise samples
$P_p(t\ ;\ \tau)$	Time varying power delay profile
$P_p(\tau)$	Time invariant power delay profile
$P_u(\tau)$	Uniform power delay profile
$P_e(\tau)$	Exponential decay power delay profile
τ_e	Exponential decay PDP time constant
$\bar{\tau}$	Mean excess delay
W_c	Coherence bandwidth
$r_i(t)$	Continuous time received signal at the ith receive antenna
$h_{i,j}(t\ ;\ \tau)$	Time variant channel impulse response between the jth transmit antenna and the ith receive antenna
$s_i(t)$	Continuous time signal transmitted from the ith transmit antenna
$h_{i,j}(t\ ;\ f)$	Time variant transfer function between the jth transmit antenna and the ith receive antenna
$n_{\sigma,i}(t)$	Zero mean AWGN process with variance σ at the ith receive antenna
$\mathbf{r}(t)$	The vector of received signals
$\mathbf{H}(t\ ;\ \tau)$	The matrix of time variant channel impulse responses
$\mathbf{s}(t)$	The vector of transmitted signals
$\mathbf{H}(t\ ;\ f)$	The matrix of time variant transfer functions
$\mathbf{H}(\tau)$	The matrix of time invariant transfer functions
$\mathbf{H}$	The time invariant frequency flat channel coefficients
$\mathbf{r}_n$	The vector of received samples during the nth time interval

$\mathbf{s}_n$	The vector of transmitted samples during the nth time interval
$\mathbf{H}(n\ ;\ \tau)$	Causal continuous time sampled channel impulse response
$\mathbf{H}_i[n]$	ith channel coefficient matrix during the nth time interval
$\mathbf{H}_{i,n}$	ith channel coefficient matrix during the nth time interval
$\mathbf{S}$	The matrix of transmitted samples
$\mathbf{s}_i$	The vector of transmitted samples during the ith time interval
$\mathbf{R}$	The matrix of the received samples
$\mathbf{r}_i$	The vector of received samples during the ith time interval
$\mathbf{H}_\omega$	The matrix of independent fading coefficients
$\mathbf{R}_{Tx}$	Transmit antenna correlation matrix
$\mathbf{R}_{Rx}$	Receive antenna correlation matrix
$\mathbf{d}_i$	The ith data block
$\check{\mathbf{s}}_i$	Vector of DS-CDMA signal samples
$\mathbf{s}_i$	Vector of MC-CDMA signal samples
Ψ	Cyclic prefix addition matrix
$\mathbf{s}_i^{(CP)}$	Cyclically extended OFDM symbol
$\mathbf{L}$	Modulation matrix
$\Phi[n]$	Encoded matrices of symbols
$\phi_i[n]$	Vectors making up the encoded matrices
$\mathbf{S}[k]$	OFDM transmission matrices
$\mathbf{S}^{(CP)}[k]$	Cyclically extended OFDM transmission matrices
$\mathbf{s}_i^{(CP)}$	ith cyclically extended OFDM symbol
$\bar{\mathbf{s}}_i^{(CP)}$	Real part of the ith cyclically extended OFDM symbol
$\tilde{\mathbf{s}}_i^{(CP)}$	Imaginary part of the ith cyclically extended OFDM symbol
$\mathbf{s}_i^{(CP)}[k]$	ith vector of the nth OFDM transmission after cyclic extension
$\hat{\mathbf{S}}^{(CP)}[k]$	Reordered cyclically extended OFDM transmission matrices
$\mathbf{Y}[k]$	Received matrices
$\mathbf{N}_\sigma$	Noise matrices
$\hat{\mathbf{s}}_{ML}[n]$	ML estimate
$\bar{\hat{\mathbf{s}}}_{ML}[n]$	Real part of the ML estimate
$\tilde{\hat{\mathbf{s}}}_{ML}[n]$	Imaginary part of the ML estimate
$\mathbf{z}[n]$	Vectorised demodulated received OFDM matrices
$\mathbf{Z}[n]$	Demodulated received OFDM matrices

$\mathbf{F}[n]$	OSTBC effective channel matrix
$\mathbf{F}_a[n]$	OSTBC effective channel matrix for the real part
$\mathbf{F}_b[n]$	OSTBC effective channel matrix for the imaginary part
$\check{\mathbf{H}}[\omega]$	Channel frequency response
$\hat{\mathbf{s}}[n]$	Sufficient statistic for ML detection
$\tilde{\mathbf{H}}$	Effective channel matrix
$\Phi^{(P)}$	Vectorisation matrix

LIST OF FIGURES

LIST OF TABLES

TABLE OF CONTENTS

CHAPTER 1

INTRODUCTION

The advent of cellular networks has led to the widespread accessibility of wireless communication. Consequently this has created an ever increasing demand for connectedness, as cultures the world over have adopted wireless technology as the primary means of communication.

Chapter 1 begins with an historical recount of the development of wireless networks followed by the "Crowded Room" analogy that describes wireless technology in extended metaphor. Readers familiar with wireless communications are directed to section 1.3.

1.1 HISTORICAL BACKGROUND OF WIRELESS AND CELLULAR NETWORKS

The evolution of modern cellular networks began with first generation (1G) analogue technology. The demonstration of the cellular concept at Bell Laboratories in 1968 and the invention of the microprocessor in 1971 paved the way for commercial cellular networks. The first of these was deployed in Japan by Nippon Telegraph and Telephony (NTT) in 1979 followed by Nordic Mobile Telephone (NMT) in Scandinavia, the Total Access Communication System (TACS) in the United Kingdom, the Advanced Mobile Phone Service (AMPS) in the United States of America and C-450 in Germany in 1981, 1982, 1983 and 1985 respectively [2]. These systems all used frequency modulation (FM) along with frequency division multiplexing (FDM) as radio and multiuser access techniques.

The second generation (2G) of wireless communication networks moved in to the realm of digital transmission in the late 1980s and early 1990s [2]. This allowed the transmission of both improved quality voice as well as data in higher capacity networks. Systems such as Groupe Spécial Mobile (GSM), Digital AMPS (DAMPS) and Pacific Digital Cellular (PDC) using time division multiplexing (TDM) and FDM were introduced. Code division multiple access (CDMA) was also first used in

the CDMAOne (IS-95A) standard as a multiple access method. Beyond 2G (commonly referred to as 2.5G) offered improved data services in the form of the General Packet Radio Service (GPRS), Enhanced Data Rate for GSM Evolution (EDGE) and IS-95B which improved on CDMAOne.

Paralleling the evolution of cellular networks was the Institute of Electrical and Electronics Engineers' (IEEE) working groups that developed numerous standards including: the IEEE802.11 for wireless local area networks (WLAN) employing spread spectrum modulation; and the IEEE802.16 (commercially known as WiMAX) for wireless metropolitan area networks (WMAN) [3, 4].

Third generation (3G) technologies then emerged near the end of the 1990s, being driven by the demand for multimedia via the internet [2]. Two competing CDMA implementations were created: Wideband-CDMA (WCDMA) and CDMA2000. These in turn initiated the creation of the Third Generation Partnership Project (3GPP) and the 3GPP2 which respectively manage the development of the standards that govern the two CDMA implementations, they then present recommendations for development to the International Telecommunication Union (ITU). Beyond 3G (or 3.5G) was then introduced in 2005 using the High Speed Downlink Packet Access (HSDPA) concept. Further development toward fourth generation (4G) technology led to the introduction of Evolved High Speed Packet Access (HSPA+) and the first long term evolution (LTE) standards commonly grouped as 3.9G. Subsequent LTE releases first included multiple antenna techniques as well as orthogonal frequency division multiple access (OFDMA).

Again in parallel the IEEE's working groups developed standards for WLAN and WMAN [3, 4]. These include the IEEE802.11a/n WLAN standard and IEEE802.16d/e WMAN standard as extensions of their respective predecessors. They include orthogonal frequency division multiplexing (OFDM), OFDMA and multiple antenna concepts. The IEEE802.20 or Mobile Broadband Wireless Access (MBWA) was developed for mobile wireless internet access but was discontinued in 2008.

Currently 4G is being standardised by the ITU. It includes advanced wireless technology such as smart antenna concepts, advanced coding and multiple access schemes, adaptive modulation and ultra wideband (UWB) signalling [2].

Future evolution of wireless communication technology beyond 4G will rely on the most efficient use of the resources that are available as well as new technology in the form of processing power, advanced wireless techniques and coordination among internetworked devices.

1.2 THE "CROWDED ROOM" ANALOGY

In much the same way as a crowded room of people, wireless technology uses a shared medium for the transmission of information. The medium for transmission of digitised information is free space and the mechanism is electromagnetic field variation. Analogously sound propagates through air as people speak to one another conveying information. For successful communication between two people within a room they might take turns to speak so as not to interfere with each another. This is essentially TDM. More people entering the room presents a problem for this approach as either some do not get a turn to speak or too little time to convey all they wish. Also the broadcast nature of this scheme is inefficient as some people may only wish to communicate with a subset of the people in the room.

Wireless networks present similar problems with solutions being found in the nature of the variations of the electromagnetic fields. The next step after time division is to divide the available spectrum into multiple parallel channels, either orthogonal or separated by guard bands, the result being FDM. This is slightly more difficult to describe metaphorically but if one imagines how separate voice types in a choir may be differentiated based on tone, for example the soprano voices may be easily distinguished from the bass voices. Another example would be the distinction between the voices of children and adults within the room and once again the conversations of the respective groups may be distinguished easily.

Suppose that the people within the room then organised themselves into smaller groups that were separated by enough space allowing softer speech so that the conversation of each group did not interfere with the other groups. This is much the same as the structure of cellular networks. Furthermore if a group, in unison, was to sing a message whilst facing in the direction of another group this may be viewed as beamforming or diversity transmission since the volume and lyrical quality, upon hearing the song, would be improved compared to a single person singing. If then the listening (or receiving) group was to confer about lyrical composition and meaning of the song, this may be thought of as diversity reception.

With the division of physical resources such as time, spectrum and space, communication using the shared medium becomes feasible. Language may be used as a further division allowing parallel communication while occupying the same physical resources. Code division is a mechanism that is analogous to language in wireless communication.

The preceding descriptions are of methods that allow multiple-access in an environment where physical layer resources are shared. Another factor to be considered is the nature of the environment or channel through which information is to be transmitted. There are many physical phenomena that interfere with, corrupt or distort the transmitted signal. The most fundamental of these is additive noise introduced by thermal variation in frontend electronics of devices. This may be thought of as the static buzz of environmental noise experienced in a crowded room. To make matters worse the strength, or loudness, of the transmitted signal attenuates inversely with the square of the distance between transmitter and receiver, and is further randomly attenuated by time varying channel conditions: movement of the transmitter or receiver results in Doppler shifting of the frequencies used as parallel channels, distorting orthogonality and resulting in cross channel interference; and multiple, reflected and scattered copies of the transmitted signal arriving at the receiver with different delays, phases and amplitudes interfere constructively and destructively causing frequency selectivity in the channel. The equivalent effect would be echoes within the room, while they may be loud or soft and clear or distorted they interfere with one another making messages indistinguishable and communication impossible.

1.3 MOTIVATION AND OBJECTIVES

"The fundamental problem of communication is that of reproducing at one point either exactly or approximately a message selected at another point." [5]

Information may be represented by messages and those messages in turn are represented by signals. The construction, transmission and reception of those signals are the challenges that must be faced for the future evolution of communication networks.

On the physical layer there is little concern for the meaning of the messages but rather their representation. A message in its simplest form is a bit or group of bits, which is transformed into a symbol. Symbols represent signals in complex baseband form with distinct quantities such as amplitude and phase. There are a number of issues that must be addressed before the symbols may be transmitted successfully. These include the mapping of data to symbols and the sharing of physical resources among multiple users. Resource usage will inevitably impact on the performance of the system. Improving that performance may not justify the complexity of the applied algorithm, it may not even be possible to implement in a functional communication system. Other than multi-access, the channel conditions and appropriate modulation must also be considered.

All of these issues imply that a selection of technologies must be made, but before this can be addressed the objectives of this research must be stated. The primary objective is to investigate modulation and demodulation algorithms that will allow high capacity digital wireless communication at reduced computational complexity while achieving diversity. Such algorithms would operate in a mobile multiuser environment where overall system performance is evaluated as bit error probabilities.

The aim is to contribute to the body of knowledge in the field of multiuser digital wireless communications by evaluating the error performance, through computer simulation, of a system employing various algorithms that achieve capacity, diversity or a combination thereof. Also the computational complexity of each algorithm will provide a measure of whether or not the algorithms will be implementable in future networks. There are three key technologies used in this work namely: code division multiple access (CDMA); multiple-input multiple-output (MIMO) techniques; and orthogonal frequency division multiplexing (OFDM).

These key technologies each address one or more of the abovementioned issues. CDMA provides a multiple-access method where physical resources are shared. With the correct choice of codes multiuser interference (MUI) can be mitigated. In order to increase capacity as well as improve performance MIMO techniques are employed because of their potential that has been demonstrated in recent years [6, 7]. Both diversity (manifested through improved performance) and high capacity (via layering techniques) may be achieved. Lastly OFDM provides a reduced complexity means to address the challenge posed by the environment. Along with the correct design, OFDM allows the reduction of a multipath frequency selective channel to multiple flat faded channels [8].

1.4 OVERVIEW OF RELEVANT LITERATURE

Shannon's classical theorem describing the maximum capacity of wireless links set both a goal and a limit for research [5]. With remarkable swiftness this limit was reached due in large to the introduction of advanced forward error correction (FEC) coding techniques. These developments were spurred on by the overwhelming demand for accessibility to a limited pool of resources and therefore efficiency became paramount. Achieving high data rates along with low error rates, while minimising power consumption for rapidly increasing numbers of users, is an arduous challenge. Meeting these needs requires the use of the most advanced modulation techniques [9, 10, 11, 12, 13]. Among these are OFDM, CDMA and MIMO techniques.

OFDM was originally deemed infeasible as a modulation technique since it required banks of subcarrier oscillators and coherent detection. This was until the discovery that the discreet Fourier transform (DFT) is an efficient algorithm that can be used for OFDM modulation [14]. OFDM is appealing since, with the addition of a cyclic prefix (CP), the convolution with the channel impulse response may be reduced to a frequency domain vector dot product [8].

Spread spectrum techniques were originally developed as a military application for the purpose of secure covert communication as well as for robustness against narrowband interference and jamming [15]. In later years it became apparent that spread spectrum techniques could be used as a multiple access method by employing sets of sequences that displayed favourable correlation properties, simultaneously retaining the resistance to frequency selectivity. As early as 1960 there was knowledge of sequence pairs that exhibited perfect correlation properties [16] and then later in 1972 sets of such sequences were discovered [17]. Initial implementations of CDMA technology used codes with imperfect properties such as Gold codes and Walsh-Hadamard codes that suffered from MUI and consequently led to reduced performance [18, Ch. 4]. This led to a loss of confidence in CDMA among researchers. More recently though a new class of sequences known as orthogonal complete complementary (OCC) sequences has been shown to possess both perfect periodic and aperiodic cross- and auto-correlation properties [18, 19, 20]. Furthermore a number of algebraic construction methods for OCC codes have been developed [21, 22, 23, 24]. With the perfect correlation properties of these codes it is also possible to achieve a rate of one symbol-per-chip using a cyclic rotation scheme thus mitigating the usual loss of spectral efficiency in older CDMA systems [25]. The method generates an extended family of codes known as cyclically rotated complete complementary codes (CRCCC). Another notable point concerning CDMA is that the resulting signals are characterised by multilevel waveforms. This signal property would ordinarily be used to increase system capacity, for example through M-ary quadrature amplitude modulation (M-QAM), however in the sequel CDMA is used for multiple access.

Without doubt MIMO is one of the most important improvements made in the field in recent years. This is because of the linearly increasing capacity in the minimum number of transmit and receive antennas [26, 27]. The potential available in the capacity gains of MIMO systems has even been demonstrated in field experiments achieving an astounding 50 bits/second/Hz spectral efficiency [28]. Furthermore the use of multiple antennas introduces multiple transmission channels and therefore simultaneously offers a diversity advantage improving link quality and error rate performance [29]. Initially rather rudimentary techniques such as antenna selection and beam switching were employed

[29, 30], after which more sophisticated techniques were developed. There are two schools when it comes to MIMO technology. The first of these, which is a capacity achieving technique, was introduced at Bell Laboratories in the form of spatial multiplexing [6]. Consequently this led to a receive diversity gain since the system required as many, if not more, receiving antennas as transmit. Soon after there was a drive for the realisation of transmit diversity as well. The result of this was the second school of space-time coding (STC), wherein researchers strove to adapt existing single antenna coding methods to the multi-antenna environment. This gave rise to space-time trellis coding (STTC), delay diversity (DD) and space-time block codes such as the well-known Alamouti code [31, 32]. It turns out that the Alamouti code was a special case of a set of space-time block codes (STBC) that were derived from amicable orthogonal designs with the appealing property of linear detection while still achieving transmit diversity [33]. The appeal of orthogonal space-time block codes (OSTBC) is that they require far lower complexity receivers than the multiple signal detection algorithm based receivers previously used for MIMO detection [31]. Examples of such algorithms are nulling and cancelling or successive interference cancellation (SIC) [6] and the sphere decoder based on the search for the closest lattice point [34, 35]. Unfortunately OSTBC suffer from two drawbacks in that complex orthogonal designs for more than eight antennas do not exist and the transmission rate is limited [36].

Development of these three technologies has not been independent from one another. They each address specific problems and it has become evident that integration of these and other technologies is necessary for future networks [37]. Four classes of systems have become prominent in the literature. There are three pairs of the abovementioned techniques and the last is the combination of all three.

Multicarrier CDMA (MC-CDMA) is the combination of OFDM and CDMA. The implementation may be achieved by spreading in the time domain, frequency domain or both [38]. Each of these implementations has its own benefits. Time domain spreading counteracts frequency selectivity while frequency domain spreading is resistant to multipath induced inter-symbol interference (ISI). A combination of the two can retain the benefits of both time and frequency spreading and simultaneously achieve a high processing gain with short codes. The use of OCC codes in a multicarrier architecture has been shown to mitigate both multiuser and multipath interference [39] because of the unique correlation properties of the codes [18].

CDMA has also been combined with MIMO in so called space-time spreading. Naturally there are

two approaches where the goals are to achieve multiple access with improved link quality or higher capacity. Applying orthogonal designs to transmitter structures can achieve transmit diversity [40] while multiplexing different streams of user data can increase user throughput [41]. Another approach is to use the spreading codes not for multiuser access but rather for the orthogonalisation of antennas or groups of antennas [42, 43]. A major computational burden is created by the combination of CDMA and MIMO in the joint detection problem. Some works have addressed linear detection attempting to alleviate this burden [44]. However in order to achieve the best performance available complex joint detection algorithms must still be applied [45].

The integration of MIMO and OFDM has become very popular. It is possible to achieve diversity at high capacity in a multiuser environment through the use of sophisticated space-time/frequency coding [10, 11, 12, 46]. The implementation required to attain this operation is the main limiting factor for these state-of-the-art and generally processing intensive algorithms [47]. Indoor experiments have verified that an increase in capacity is achievable however it is somewhat less than the theoretical predictions [48]. The reasons for this loss in theoretical potential are sensitivity to changing channel conditions in the case of multiplexing and the presence of correlation in the channel for the case of diversity systems [49].

Lastly, the most relevant amalgamation of technologies to this research is MIMO MC-CDMA. As in the cases of MIMO CDMA and MIMO-OFDM the duality between multiplexing and coding exists. MIMO MC-CDMA has the potential for future cellular networks [13]. The reason for this is the efficiency with which the various elements of the system can be processed. Both the orthogonal frequency modulation and the despreading operation can be efficiently implemented using the fast Fourier transform (FFT) algorithm [25]. The duality of time and frequency domain spreading can be exploited to counteract certain channel effects as well as provide a multiple access method in cellular networks [50]. In conjunction with MIMO techniques these robust MC-CDMA techniques can be tailored to achieve high capacity or high link quality [51, 52].

1.5 CONTRIBUTION AND OUTPUT

1.5.1 Contribution of this research

The contributions of this dissertation are as follows:

1. OFDM, CDMA and MIMO concepts have been combined into a unified baseband transceiver framework. Specifically, cyclically rotated complete complementary codes have been employed for CDMA.

2. A transmit diversity achieving modem has been presented. This simulation platform employs OSTBCs as the underlying linear space-time codes at the transmitter. A general linear ML receiver has been designed that decouples transmitted signals allowing subsequent independent despreading.

3. A spatially multiplexed modem has been presented. High capacity transmission is achieved at the transmitter while joint ML detection is performed at the receiver. The detection algorithm employed is based on the sphere decoder.

4. The SISO channel has been extended to the multi antenna environment. Both general and standardised channel models described in terms of PDPs and Doppler characteristics have been amalgamated into a MIMO channel structure.

5. Bit error probability has been estimated by means of Monte Carlo simulation for both modems under a variety of channel conditions.

1.5.2 Related publications

Derived from this work the following articles have been published and submitted for publication as a part of peer reviewed publications.

1.5.2.1 Journal publications

The following journal article has been submitted for publication:

1.5.2.2 Conference proceedings

The following conference article has been accepted for publication:

1. N. de Figueiredo, L. P. Linde and J. H. van Wyk, “Performance of a transmit diversity MIMO MC-CDMA communication system employing Cyclically Rotated Complete Complementary

Codes," *Proceedings of IEEE AFRICON Conference*, Mauritius, September 2013, accepted for publication.

1.6 OUTLINE

This document is structured as follows. In chapter 2 the mathematical concepts that form the foundation of this work are presented. These include OFDM, CDMA and MIMO concepts. Each distinct mathematical concept is first described in continuous time followed by discrete time and matrix algebraic formulations. Chapter 3 describes the model utilised for evaluation of the communication systems. Firstly the SISO channel is treated where a number of general and standardised channels are described. The statistical properties of these channels are presented following which is an extension to the MIMO environment. Finally the channel is presented in matrix algebraic formulation. The system model is then presented in chapter 4, which includes both the transmit diversity and spatially multiplexed modems. Along with system model is a unified matrix algebraic framework.

Chapters 2 - 4 cover the design elements of this work. Following this are chapters 5 and 6 which respectively detail the evaluation of the two systems presented. Each proposes an hypothesis and experimental setup, followed by results and conclusions drawn. This dissertation is then concluded in chapter 7.

CHAPTER 2

MATHEMATICAL FOUNDATION

2.1 INTRODUCTION

In chapter 2 the mathematical basis of this work is presented. OFDM is first treated with the definition and properties given. Following this is an exposition of classical CDMA which leads to a detailed description of the complementary codes employed in this work. The complementary sequence properties and the mechanism for their detection are described. Next, MIMO concepts are presented, including: achieving transmit diversity through OSTBCs; linear ML detection of OSTBCs as an example; exploiting the capacity gains offered via spatial multiplexing; and joint detection techniques. All three technologies that form the basis for this investigation are also described in a matrix algebraic formulation.

2.2 ORTHOGONAL FREQUENCY DIVISION MULTIPLEXING

OFDM is a method for performing orthogonal multicarrier modulation. The premise of multicarrier modulation is to divide the available channel bandwidth into many narrow subbands. Supposing the available channel bandwidth is W, then that bandwidth may be divided into N_{FFT} subbands each of bandwidth $\Delta f = \frac{W}{N_{FFT}}$. Each of the subbands may be used for the transmission of independently coded and modulated signals. These signals would require synchronous transmission with a symbol period of $T = \frac{1}{\Delta f} = \frac{N_{FFT}}{W}$. Provided that Δf is small enough, making the symbol time significantly larger than the channel delay spread, the ISI becomes negligible. Effectively the channel transfer function may be thought of as constant over each of the subbands.

Simply dividing the available bandwidth into an arbitrary number of subbands does not guarantee

orthogonality. In order to orthogonalise the subbands a centre frequency is associated with each. That is, a sinusoidal subcarrier,

$$s_k(t) = \cos 2\pi f_k t \quad k = 0, 1, \ldots, N_{FFT} - 1, \tag{2.1}$$

with f_k, the centre frequency of the kth subband. If the symbol rate $1/T$ is equal to the subcarrier spacing Δf the subcarriers become mutually orthogonal:

$$\int_0^T \cos(2\pi f_k t + \phi_k) \cos(2\pi f_j t + \phi_j) dt = 0, \tag{2.2}$$

which is independent of subcarrier phase ϕ_k and ϕ_j for $f_k - f_j = n/T, \quad n = 1, 2, \ldots, N_{FFT} - 1$.

In general an OFDM signal may be represented by,

$$s(t) = \sum_{k=0}^{N_{FFT}-1} d_k e^{j2\pi f_k t} \quad 0 \leq t < T, \tag{2.3}$$

for a single block of digital symbols $\mathbf{d} = [d_1 \; d_2 \; \ldots d_{N_{FFT}}]$. Consequently this is equivalent to the inverse discrete Fourier transform (IDFT) of the sequence $\{d_i\}$, $i = 1, 2, \ldots, N_{FTT}$, and the frequency domain representation of the resulting signal is,

$$S(f) = Te^{-j\pi fT} \sum_{k=0}^{N_{FFT}-1} d_k sinc\left[T\left(f - \frac{k}{T}\right)\right], \tag{2.4}$$

where,

$$sinc(x) = \begin{cases} 1 & x = 0 \\ \frac{\sin(\pi x)}{\pi x} & \text{elsewhere} \end{cases}. \tag{2.5}$$

Fig. 2.1 (a) illustrates the densely packed subcarrier spectra that make up the OFDM signal defined by each element in the sum 2.4 and Fig. 2.1 (b) illustrates the resulting baseband PSD of the combined spectra. From the figure it can be seen that the spectrum usage in an OFDM system is efficient due to the overlapping. It is not immediately obvious however (as can be seen from 2.4) the peaks and zero

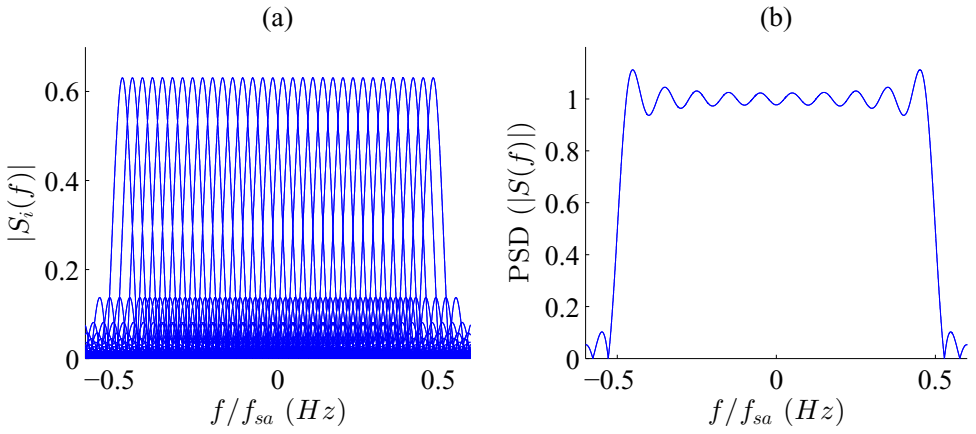

Figure 2.1: (a) Overlapping subcarrier spectra and (b) the resulting PSD of the OFDM signal.

crossings of the individual subcarrier spectra coincide and to this phenomenon the term orthogonal is attributed. Sampling 2.3 at a rate of $\frac{1}{T}$ the resulting digital signal is,

$$s[n] \equiv s(t)|_{t=\frac{nT}{N_{FFT}}} = \sum_{k=0}^{N_{FFT}-1} d_k e^{j2\pi f_k \frac{n}{N_{FFT}}} \quad n = 0,1,\ldots,N_{FFT}-1. \tag{2.6}$$

It is well known that OFDM signals are resistant to ISI due to the long symbol time, relative to the channel delay spread [8, 53]. ISI may further be eliminated from the received signal by appending a cyclic prefix and extending $s[n]$ as follows,

$$s^{(CP)}[n] = \begin{cases} s[N_{FFT}+n] & n = -N_{cp}, -N_{cp}+1,\ldots,-1 \\ s[n] & n = 0,1,\ldots,N_{FFT}-1 \end{cases}, \tag{2.7}$$

where N_{cp} is the number of samples in a cyclic prefix of period T_{cp}. According to the circular convolution theorem [54], provided the channel remains quasi-static over the duration of an OFDM symbol period, $T_{CP}+T$, the sampled received signal (in the absence of noise) may be expressed as,

$$r[n] \equiv r(t)|_{t=\frac{nT}{N_{FFT}}} = \int_{-\infty}^{\infty} h(\tau)s^{(CP)}(t-\tau)d\tau\Big|_{t=\frac{nT}{N_{FFT}}} \quad n = 0,1,\ldots,N_{FFT}-1, \tag{2.8}$$

where $h(\tau)$ is an infinite length time-invariant frequency selective channel and $s^{(CP)}(t)$ is the continuous time representation of $s^{(CP)}[n]$. Transformation of the expression 2.8 via the DFT results

in,

$$r[k] = H[k] \cdot d_k \quad k = 0, 1, \ldots, N_{FFT} - 1, \tag{2.9}$$

where $H[k]$ is the DFT of the sampled channel impulse response $h[n] \equiv h(\tau)|_{t=\frac{nT_{sa}}{L}}$, $n = 0, 1, \ldots, L$. The infinite continuous time channel now becomes a finite length sampled channel (sampled at a rate $F_{sa} = \frac{1}{T_{sa}}$) that may be modelled using a tapped delay line with $L+1$ taps,

$$H[k] = \sum_{n=0}^{L} h[n] e^{-j2\pi \frac{kn}{L+1}}, \quad k = 0, 1, \ldots, N_{FFT} - 1. \tag{2.10}$$

The OFDM modulation and demodulation (IDFT and DFT) operations may be represented in matrix form. For the DFT, a multiplication between the DFT matrix and the vector of time domain samples results in the frequency domain output samples,

$$\mathbf{X} = \mathbf{W}\mathbf{x} \quad \Longleftrightarrow \quad \mathbf{X} = \mathscr{F}\{\mathbf{x}\}, \tag{2.11}$$

where $\mathbf{X} = [X[0]\ X[1]\ \ldots\ X[N-1]]^T$, $\mathbf{x} = [x[0]\ x[1]\ \ldots\ x[N-1]]^T$, $\mathscr{F}\{\cdot\}$ is the discrete Fourier transform operator and,

$$\mathbf{W} = \begin{bmatrix} 1 & 1 & \ldots & 1 \\ 1 & \omega & & \omega^{N-1} \\ \vdots & & & \vdots \\ 1 & \omega^{N-1} & \ldots & \omega^{N-1^2} \end{bmatrix}, \tag{2.12}$$

where,

$$\omega = \frac{e^{\frac{-j2\pi}{N_{FFT}}}}{\sqrt{N_{FFT}}}. \tag{2.13}$$

The transpose operator is represented as $(\cdot)^T$. When this matrix is normalised it is unitary and consequently the IDFT operation may be expressed as,

$$\mathbf{x} = \mathbf{W}^H \mathbf{X} = \mathbf{W}^H \mathbf{W} \mathbf{x} \quad \Longleftrightarrow \quad \mathbf{x} = \mathscr{F}^{-1}\{\mathbf{X}\}, \tag{2.14}$$

here $(.)^H$ is the hermitian or conjugate transpose of a matrix and $\mathscr{F}^{-1}\{\cdot\}$ is the inverse discrete Fourier transform operator. The matrix formulation of the DFT is convenient for analysis purposes however the implementation may be achieved is a less complex manner. The FFT algorithm is an efficient method for performing the DFT operation along with the inverse fast Fourier transform (IFFT) for implementation of the IDFT operation [54].

2.3 CODE DIVISION MULTIPLE ACCESS

CDMA is a spread spectrum technique used for multiple access. The premise of CDMA is to share the physical resources of space, time and frequency between users in the form of a shared channel. Each user is assigned an orthogonal code (or set of codes) that allows simultaneous orthogonal transmission of data. The term spread spectrum arises from the resulting bandwidth expansion of a digital signal when it is multiplied by a code. The cause of the bandwidth expansion is the shifting of the phase of a digital signal according to the code sequence.

2.3.1 Classical code division multiple access

Assuming a user wishes to transmit a digital data signal,

$$d_i(t) = d_i P(t - iT_s \; ; \; T_s) \quad \begin{matrix} iT_s \leq t < (i+1)T_s \\ -\infty \leq i \leq \infty \end{matrix}, \tag{2.15}$$

which consists of symbols $\{d_i\}$ multiplied by a pulse train $P(t - iT_s \; ; \; T_s)$. $P(t \; ; \; T_p)$ is a pulse of unit magnitude and duration T_p,

$$P(t \; ; \; T_p) = \begin{cases} 1 & 0 \leq t < T_p \\ 0 & \text{otherwise} \end{cases}. \tag{2.16}$$

The symbol period of this signal is T_s and the symbol rate is $R_s = 1/T_s$. In order to shift the phase of each symbol within a single symbol period the spreading code consists of a sequence of bipolar

binary values known as *chips*, each of duration T_c and thus rate $R_c = 1/T_c$. A code sequence may be represented as,

$$c(t) = c_j P(t - jT_c \; ; \; T_c) \quad \begin{matrix} 0 \leq t < T_s \\ j = 0, 1, \ldots, B_e - 1 \end{matrix}, \tag{2.17}$$

where $\{c_j\}$ is a bipolar binary sequence again multiplied by a pulse train. The bandwidth expansion factor is,

$$B_e = \frac{W}{R_s} = \frac{T_s}{T_c}, \tag{2.18}$$

which for practical reasons should be an integer [8]. This value is equal to the number of phase shifts within one symbol period or the number of chips, N_c, that a spreading code consists of.

This quantity is also known as the processing gain (PG), attributed to CDMA systems. It is a measure of the advantage gained over interference from expansion of the transmitted signal bandwidth. The upper limit for the probability of bit error as a function of the PG is given by [8],

$$P_e \leq \sum_{m=2}^{M_c} Q\left(\sqrt{\frac{4B_e}{\gamma_i}\gamma_{CG}}\right), \tag{2.19}$$

where $Q(\cdot)$ is the Gaussian Q-function, γ_i is the interference margin or inverse signal-to-interference power ratio and γ_{CG} is the coding gain of the system. The interference margin of a DS spread spectrum system depends on both the processing gain and the coding gain; from 2.19 it can be seen that as the PG increases the probability of bit errors decreases.

The signal generated by spreading in the form,

$$s_i(t) = d_i(t)c(t) \quad \begin{matrix} iT_s \leq t < (i+1)T_s \\ -\infty \leq i \leq \infty \end{matrix}, \tag{2.20}$$

is known as a direct sequence (DS) spread spectrum signal [8, 55]. For K_u users each assigned a spreading sequence $c_i(t),\ i = 1, 2, \ldots, K_u$, the resulting multiuser signal is,

$$s_i(t) = \sum_{k=1}^{K_u} d_{i,k}(t-\tau_k)c_k(t-\tau_k) \quad -\infty \leq i \leq \infty, \tag{2.21}$$

where τ_k is the offset associated with the kth user's transmission time and $d_{i,k}$ is the ith symbol of the kth user's data stream. In a synchronous environment $\tau_k = 0$ for $k = 1,2,\ldots,K_u$.

2.3.2 Detection and ideal correlation properties

The detection of data transmitted in a CDMA environment is based on the discrete time correlation with the codes assigned to each user. Correlation of the received signal with the spreading codes results in an estimate of the transmitted data symbol associated with the respective code, this *de-spreading* operation is performed by the correlator-based receiver [55]. This procedure is naturally sensitive to the correlation properties of the code family. It is desirable for the codes assigned to each user to have zero auto-correlation for any chip shift except the zero shift. It is also desirable for the cross-correlation between all pairs of codes in the family to be zero for all chip shifts. Furthermore it is desirable for both the periodic and aperiodic correlations to exhibit these properties. These properties are known as *ideal* correlation properties. Sets of sequences that exhibit these properties are immune to MUI [18] and under certain conditions MI as well [18].

Sampling signals of the form 2.17 for each user at the beginning of each chip results in sequences $c_i = \{c_{k,i}\},\ k = 1,2,\ldots,N_c,\ i = 1,2,\ldots,K_u$. $c_{k,i}$ is the kth chip of the ith user's spreading sequence. The aperiodic correlation function indicated by the superscript $(\cdot)^{(A)}$ of a family of sequences that exhibit ideal properties is represented as follows for cross-correlation between length N_c sequences c_i and c_j:

$$R^{(A)}_{c_i,c_j}[n] = \sum_{k=-\infty}^{\infty} c_{k,i}c_{k+n,j} = 0 \quad \forall\, n, \tag{2.22}$$

and auto-correlation for any code c_i with the ideal property,

$$R^{(A)}_{c_i,c_i}[n] = \sum_{k=-\infty}^{\infty} c_{k,i}c_{k+n,j} = \begin{cases} N_c & n = 0 \\ 0 & \text{otherwise} \end{cases}. \tag{2.23}$$

The ideal periodic cross-correlation function indicated by the superscript $(\cdot)^{(P)}$ is given by,

$$R^{(P)}_{c_i,c_j}[n] = \sum_{k=1}^{n} c_{k,i}c_{N_c-n+k,j} \pm \sum_{k=n+1}^{N_c} c_{k,i}c_{k-n,j} = 0 \quad \forall\, n, \tag{2.24}$$

and ideal periodic auto-correlation

$$R^{(P)}_{c_i,c_i}[n] = \sum_{k=1}^{n} c_{k,i}c_{N_c-n+k,j} \pm \sum_{k=n+1}^{N_c} c_{k,i}c_{k-n,j} = \begin{cases} N_c & n = 0 \\ 0 & \text{otherwise} \end{cases}. \tag{2.25}$$

The importance of ideal correlation properties in a CDMA system can be seen by cross-correlating 2.21 (in the synchronous case) sampled at the beginning of each chip, with the mth user's sequence c_m resulting in,

$$\begin{aligned} R^{(A)}_{s_k,c_m}[n] &= \sum_{j=-\infty}^{\infty} s_k(t)|_{t=kT_s+jT_c} c_{n+j,m} && (2.26)\\ &= \sum_{j=-\infty}^{\infty} s_{j,k} c_{n+j,m} && (2.27)\\ &= \sum_{j=-\infty}^{\infty} \left[\sum_{i=1}^{K_u} d_{i,k} c_{j,i}\right] c_{n+j,m} && (2.28)\\ &= \sum_{i=1}^{K_u} d_{i,k} \sum_{j=-\infty}^{\infty} c_{j,i} c_{n+j,m} && (2.29)\\ &= \sum_{i=1}^{K_u} d_{i,k} R^{(A)}_{c_i,c_m}[n] && (2.30)\\ &= d_{m,k} R^{(A)}_{c_m,c_m}[n] + \sum_{i=1}^{m-1} d_{i,k} R^{(A)}_{c_i,c_m}[n] + \sum_{i=m+1}^{K_u} d_{i,k} R^{(A)}_{c_i,c_m}[n], && (2.31) \end{aligned}$$

where $s_{j,k} = s_k(t)|_{t=kT_s+jT_c}$. From 2.31 it can be seen that, with non-ideal cross-correlation properties, the last two terms introduce MUI to the detection process.

As in the case of OFDM the spreading operation may also be represented as a matrix multiplication. With the K_u spreading sequences as the columns of the code matrix,

$$\mathbf{C} = [\mathbf{c}_1\ \mathbf{c}_2\ \ldots\ \mathbf{c}_{K_u}], \tag{2.32}$$

and

$$\mathbf{c}_i = [c_{1,i}\ c_{2,i}\ \ldots\ c_{N_c,i}]^T, \tag{2.33}$$

the multi-user spreading operation then becomes,

$$\mathbf{s}_k = \mathbf{C}\mathbf{d}_k, \tag{2.34}$$

where $\mathbf{s}_k = [s_{1,k}\ s_{2,k}\ \ldots\ s_{N_c,k}]^T$ and $\mathbf{d}_k = [d_{1,k}\ d_{2,k}\ \ldots\ d_{K_u,k}]^T$.

2.4 ORTHOGONAL COMPLETE COMPLEMENTARY AND CYCLICALLY ROTATED COMPLETE COMPLEMENTARY CODES

2.4.1 Complementary code structure

Classical CDMA code sets are made up of a set of M_c sequences. Each of the sequences is composed of N_c chips. A single sequence is used to spread a stream of data which may be associated with a particular user in a communication system. An improved approach to the construction of sequences for multiple access, is to have multi-element sequences that function in a complementary fashion. Such a complementary family of codes is composed of K multi-element sequences. Each of the K sequences, termed *flocks*, is split into M *element* codes which are in turn composed of N chips. Therefore the total complementary sequence or flock length is MN as opposed to the classical code length N_c.

Fig. 2.2 illustrates the difference in structure between a classical code and a complementary code. A direct consequence of the structure of a complementary code is the need for orthogonal element code transmission. The element codes must be transmitted either orthogonally in time via TDM or on different carriers via FDM [19, 39]. This is because of the method of calculation of the cross-correlation between two codes and is also the reason for the term *complementary codes*.

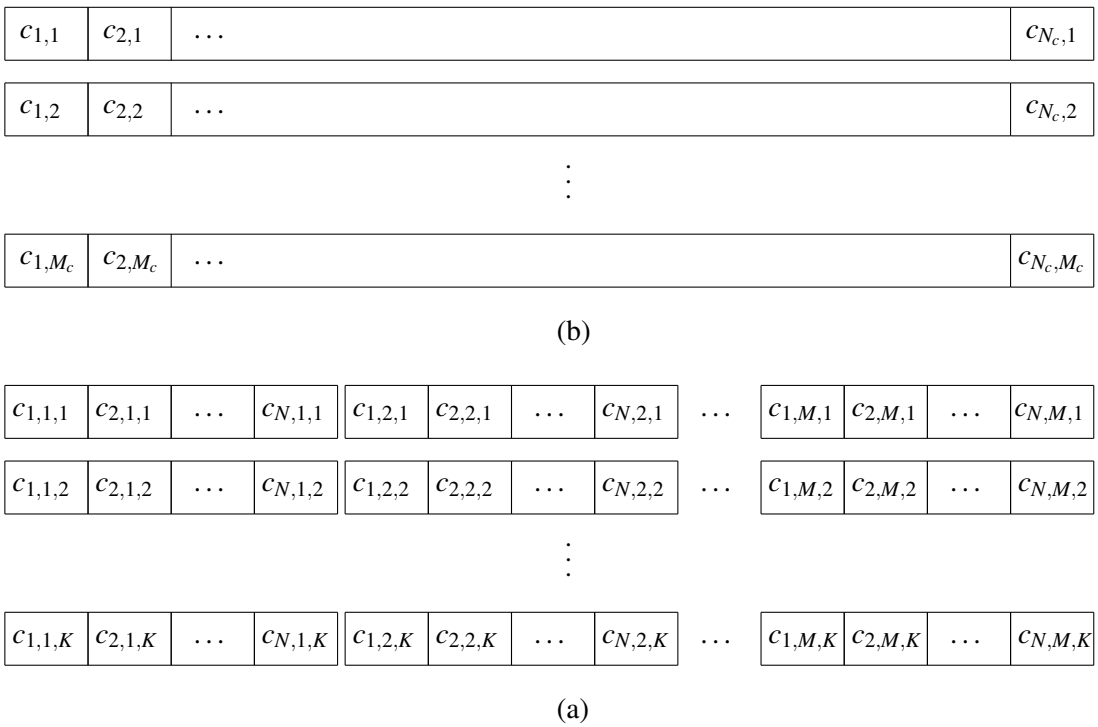

Figure 2.2: The structure of (a) classical and (b) complementary codes.

2.4.2 Correlation properties and orthogonal complete complementary codes

The computation of the auto-correlation of a complementary code and the cross-correlation between pairs of codes is performed on an element code basis. The correlations of pairs of corresponding element codes are computed and then summed to form the resulting correlation of the codes. Supposing a complementary code $\mathbf{C}$ is made up of K length MN flocks as described previously. This code may be represented as,

$$\mathbf{C} = \begin{bmatrix} \mathbf{c}_{1,1} & \mathbf{c}_{1,2} & \dots & \mathbf{c}_{1,K} \\ \mathbf{c}_{2,1} & \mathbf{c}_{2,2} & \dots & \mathbf{c}_{2,K} \\ \vdots & & & \vdots \\ \mathbf{c}_{M,1} & \mathbf{c}_{M,2} & \dots & \mathbf{c}_{M,K} \end{bmatrix}, \tag{2.35}$$

where the columns form the flocks and each element code,

$$\mathbf{c}_{m,k} = [c_{1,m,k}\ c_{2,m,k}\ \ldots c_{N,m,k}]^T \quad \begin{matrix} m & = 1,2,\ldots,M \\ k & = 1,2,\ldots,K \end{matrix} \tag{2.36}$$

is a vector with elements that take on the values of the constituent chips.

The calculation of the discrete aperiodic cross-correlation between any two columns of $\mathbf{C}$ now becomes a double sum,

$$R^{(A)}_{c_a,c_b}[n] = \sum_{i=1}^{N-n}\sum_{j=1}^{M} c_{i,j,a}c_{j,j+n,b}. \tag{2.37}$$

A similar modification gives rise to the discrete periodic correlations as well.

$$R^{(P)}_{c_a,c_b}[n] = \sum_{j=1}^{M}\left[\sum_{i=1}^{n} c_{i,j,a}c_{i,j+n,b} \pm \sum_{i=n+1}^{N} c_{i,j,a}c_{i,j+n,b}\right]. \tag{2.38}$$

OCC sequences are a class of complementary sequences that possess the following properties:

$$R_{c_a,c_b}[n] = 0 \quad \forall\, n, \tag{2.39}$$

and

$$R_{c_a,c_a}[n] = \begin{cases} MN & n = 0 \\ 0 & \text{otherwise} \end{cases}. \tag{2.40}$$

This includes both the aperiodic and periodic correlations. In fact it has been shown that a family of sequences with ideal periodic correlation properties will have ideal aperiodic properties as well [18]. Furthermore a family with ideal aperiodic correlation properties will have ideal periodic correlation properties [18].

The consequence of these properties is that a CDMA system using OCC codes will have zero MUI, and with the correct delay introduced between successive transmissions of the same code multipath interference (MI) may also be eliminated [18, 19].

2.4.3 Generation of orthogonal complete complementary codes

There are a number of methods for the generation of OCC sequence sets. Among these are systematic approaches that result in sets which support moderate numbers of users. One particular algorithm is based on the expansion of N-shift cross orthogonal sequence sets, details of which are given in appendix A. This algorithm is grounded in a number of theorems [20]. Other construction methods are detailed in [20, 22].

It is desirable to have large numbers of users supported in a multiple access scheme. In order to create OCC sequence sets that support more users under the same processing gain, an algebraic method was developed [23]. This algorithm is called the real environment adaption linearization (REAL) approach. By creating a set of non-linear equations based on the auto- and cross-correlation functions of a set of unknown complementary sequences that exhibit ideal correlation properties and then selecting a complementary sequence with ideal auto-correlation properties as a starting point, the non-linear equations may be linearised systematically. In doing so each of the unknown complementary sequences in the set may be solved for chip-by-chip, leading to an OCC set. This method may be used to generate larger sets know as super complementary code sets. The REAL approach algorithm is however computationally intensive. Super complementary sets and OCC sets exhibit identical correlation properties and belong to the same class of complementary sequence sets [23].

2.4.4 Cyclically rotated complete complementary codes

In any CDMA scheme, be it classical or complementary, one sequence is used per symbol. In the case of classical CDMA an entire code family may be used to simultaneously transmit M symbols and in the case of complementary codes, K symbols. There is an inherent loss of spectral efficiency in either of these schemes since $M_c < N_c$ and $K < MN$, respectively. A cyclic rotation scheme may be applied to the OCC codes in order to extend the family, leading to increased throughput of the system and thus improving spectral efficiency [25]. Taking the kth vectors $\mathbf{c}_{i,k}$ and cyclically rotating them one chip at a time produces a new flock for each rotation. With element codes of length N, a family of K flocks may be extended to KN flocks. Fig. 2.3 illustrates the cyclic rotation approach.

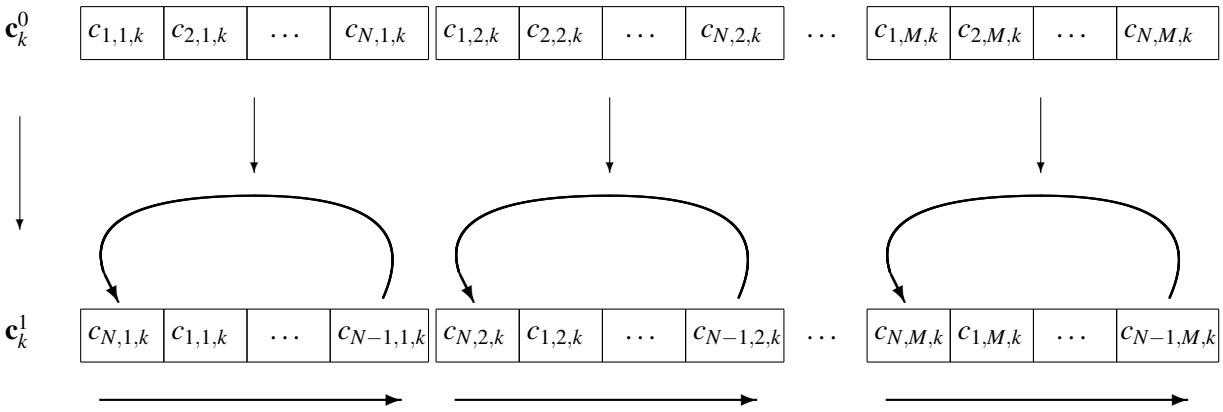

Figure 2.3: Cyclic rotation of element codes.

For the kth flock $\mathbf{c}_k = [\mathbf{c}_{1,k}^T \ \mathbf{c}_{2,k}^T \ \ldots \ \mathbf{c}_{N,k}^T]^T$ the extended flock may be expressed as,

$$\mathbf{C}_k^E = \begin{bmatrix} \mathbf{c}_{1,k}^0 & \mathbf{c}_{1,k}^1 & \ldots & \mathbf{c}_{1,k}^{N-1} \\ \mathbf{c}_{2,k}^0 & \mathbf{c}_{2,k}^1 & \ldots & \mathbf{c}_{2,k}^{N-1} \\ \vdots & & & \vdots \\ \mathbf{c}_{M,k}^0 & \mathbf{c}_{M,k}^1 & \ldots & \mathbf{c}_{M,k}^{N-1} \end{bmatrix}, \tag{2.41}$$

where $\mathbf{c}_{i,k}^l$ is the lth cyclic rotation of the ith element code $\mathbf{c}_{i,k}$ of the kth user's flock. The entire extended set is then,

$$\mathbf{C}^E = [\mathbf{C}_1^E \ \mathbf{C}_2^E \ \ldots \mathbf{C}_K^E]. \tag{2.42}$$

Provided each extended flock (that is all the flocks produced from cyclic rotations of an original flock) of the CRCCC is transmitted synchronously the extended set will have no MUI [25, 39]. The main advantage of this technique is increased throughput and in the case of an OCC code with $K = M$, the extended set will contain MN flocks. Therefore a transmission rate of $\frac{KN}{MN} = 1 \quad symbol/chip$ may be achieved.

As in the case of the classical CDMA the processing gain associated with complementary codes is equal to the length of the code or flock. For classical CDMA this is simply M_c and for complementary codes it is MN. It has been shown that in the case of OCC codes the MUI is zero and so the

interference which plays a role in the bit error probability (as in expression 2.19) is attributed solely to noise [18]. It stands to reason that a system employing OCC codes can achieve error performance of a narrowband BPSK system without the rate loss associated with CDMA. It has been shown that a cyclically extended set achieves this [25].

2.4.5 Efficient detection via correlation

Detection of data conveyed via a CDMA signal is achieved by making decisions based on the correlation between the received signal and the code sequences. Typically a bank of correlators is used for this operation, each correlator in the bank correlates the input with each of the user codes. Therefore a bank of KMN correlators is required for detection of a family when KN flocks are employed. Fortunately it is possible to detect CRCCC signals with the FFT algorithm.

With aid of the circular convolution theorem [54], the correlation operation between sequences **a** and **b** may be calculated as [25],

$$R_{\mathbf{a},\mathbf{b}}^{(P)} = \mathscr{F}^{-1}\left\{\mathscr{F}\{\mathbf{a}\}\cdot[\mathscr{F}\{\mathbf{b}\}]^*\right\}. \tag{2.43}$$

The correlation operation is of complexity $O(N^2)$ but making use of this fast correlation algorithm reduces the complexity to $O(NlogN)$ due to the use of the FFT. Thus the detection of a CRCCC extended flock becomes,

$$R_{\mathbf{r},\mathbf{c}_k^0}^{(P)} = \sum_{m=1}^{M} \mathscr{F}^{-1}\left\{\mathscr{F}\{\mathbf{r}^{(m)}\}\cdot\left[\mathscr{F}\left\{\mathbf{c}_{m,k}^0\right\}\right]^*\right\}. \tag{2.44}$$

The result of this expression is a sequence of estimates that may be used by a decision algorithm to detect the data spread by the extended flock. Furthermore the index of each symbol in the resulting sequence is equal to the number of rotations used to generate the corresponding flock.

2.5 MULTIPLE-INPUT MULTIPLE-OUTPUT SYSTEMS

There are two major developments when it comes to MIMO systems, each depending on the desired outcome. Intuitively a MIMO channel offers a number of parallel spatial channels. Thinking about the channel in this way leads first to the spatial multiplexing or layering concept. The core of these

technologies is simultaneous transmission of independent data with the goal of increasing the system capacity. These data are transmitted using the same time and frequency resources but with multiple antennas there is now a new degree of freedom: space. In a spatial multiplexing architecture it stands to reason that there must be the same number of (or more) receive antennas than transmit antennas. In this way, during a single symbol period, there will be a sufficiently defined system of linear equations and detection of the transmitted data is possible. Another consequence of having more than one receive antenna is receive diversity since each receive antenna will receive a copy of each transmitted signal.

However there are situations where multiple receive antennas are not available, for example in the downlink (forward channel) the mobile station most often will not possess the required number of receive antennas for layering. In this case it is desirable to achieve diversity from a transmit perspective. This approach gives rise to architectures that achieve transmit diversity such as delay diversity and STC based systems. STTC emerged along with STBC, with OSTBCs gaining widespread popularity due to their linear detectability.

2.5.1 Transmit diversity - Orthogonal space-time block coding

The simple Alamouti code was the first STBC that offered the linear detectability that OSTBCs share [31, 32]. After its introduction the subclass of OSTBCs was explored based on the theory of amicable orthogonal designs [31, 33]. The basic idea to STBCs, is to map symbols to antennas over a number of symbol periods. More specifically, in the case of OSTBCs a symbol, its complex conjugate, the negative of either or zero may be transmitted on each antenna during one symbol period. OSTBC are a subclass of linear STBC since this mapping is linear in the real and imaginary parts of the symbols. The number of symbol periods required for transmission is defined by the rate of the code and the number of antennas used. The rate of a STBC is defined as,

$$R = \frac{n_s}{N_s}, \tag{2.45}$$

where n_s is the number of symbols mapped to antennas and N_s is the number of symbol periods used for transmission. The general construction of a linear STBC is,

$$\mathbf{X} = \sum_{i=1}^{n_s} \left(\bar{s}_i \mathbf{A}_i + j\tilde{s}_i \mathbf{B}_i \right), \tag{2.46}$$

where $\bar{s}_n$ and $\tilde{s}_n$ are real and imaginary parts of the symbols s_n and $\{\mathbf{A}_n, \mathbf{B}_n\}$ are a set of fixed and generally complex valued matrices of dimension $N_{Tx} \times N_s$. The resulting matrix of coded symbols is also of dimension $N_{Tx} \times N_s$. Each of its columns is transmitted during one symbol period with each of the entries therein being transmitted from the antenna relative to its index.

It has been shown that for the subclass of OSTBCs the maximum number of antennas that a complex amicable orthogonal design exists for is four [33]. Furthermore orthogonal designs with maximal rates exist for rates equivalent to [36],

$$R_{max} = \frac{m+1}{2m}, \tag{2.47}$$

where $N_{Tx} = 2m-1$ or $N_{Tx} = 2m \quad \{m \in \mathbb{N} | m \leq 8\}$. This compromise is justified by the simplicity of detection of OSTBC.

The main advantage of using OSTBC is the simplicity of their detection. The coherent maximum likelihood (ML) detection of the symbols s_n is decoupled. This is a result of the property,

$$\mathbf{X}\mathbf{X}^H = \sum_{i=1}^{n_s} |s_i|^2 \cdot \mathbf{I}, \tag{2.48}$$

which holds for all complex $\{s_n\}$ if and only if $\{\mathbf{A}_n, \mathbf{B}_n\}$ is an amicable orthogonal design [31]. That is,

$$\begin{aligned} &\mathbf{A}_n\mathbf{A}_n^H = \mathbf{I}, && \mathbf{B}_n\mathbf{B}_n^H = \mathbf{I} \\ &\mathbf{A}_n\mathbf{A}_p^H = -\mathbf{A}_p\mathbf{A}_n^H, && \mathbf{B}_n\mathbf{B}_p^H = -\mathbf{B}_p\mathbf{B}_n^H \quad n \neq p \\ &\mathbf{A}_n\mathbf{B}_p^H = \mathbf{B}_p\mathbf{A}_n^H \end{aligned}, \tag{2.49}$$

for $n = 1, 2, ..., n_s,\ p = 1, 2, ..., n_s$.

2.5.2 Maximum likelihood detection of OSTBCs

When data are transmitted using space-time codes, the ML detection of the transmitted data may be achieved by minimising the ML metric of the form [31],

$$||\mathbf{Y} - \mathbf{HX}||^2, \tag{2.50}$$

where $\mathbf{Y}$ represents the received corrupted signal, $\mathbf{H}$ the channel and $\mathbf{X}$ the estimate. This requires a "brute force" approach, as the minimisation is performed over the symbol constellation alphabet. In the case that OSTBCs are used as the underlying space-time code, there is another means for ML detection that decouples the transmitted data. This is well illustrated using the Alamouti code as an example.

2.5.2.1 Alamouti detection example

The Alamouti code, using two antennas, transmits two symbols over two symbol periods. The space-time transmission matrix is structured as follows:

$$\mathbf{X} = \begin{bmatrix} s_1 & s_2^* \\ s_2 & -s_1^* \end{bmatrix}, \tag{2.51}$$

where s_1 and s_2 are the two transmitted symbols. When transmission is through a flat faded time-invariant channel the received signals (at a single antenna) may be represented as,

$$r_1 = s_1 h_1 + s_2 h_2 + n_1, \tag{2.52}$$

and

$$r_2 = s_2^* h_1 - s_1^* h_2 + n_2, \tag{2.53}$$

where r_1 and r_2 are the samples received in the first and second symbol periods respectively and h_1

and h_2 are the fading channel coefficients from transmit antennas 1 and 2, respectively. This may conveniently be represented in vector notation as,

$$\mathbf{r} = \mathbf{h}^T\mathbf{X} + \mathbf{n} \tag{2.54}$$

$$= \begin{bmatrix} h_1 & h_2 \end{bmatrix} \begin{bmatrix} s_1 & s_2^* \\ s_2 & -s_1^* \end{bmatrix} + \begin{bmatrix} n_1 \\ n_2 \end{bmatrix} \tag{2.55}$$

$$= \begin{bmatrix} s_1h_1 + s_2h_2 \\ s_2^*h_1 - s_1^*h_2 \end{bmatrix} + \begin{bmatrix} n_1 \\ n_2 \end{bmatrix} \tag{2.56}$$

$$= \begin{bmatrix} s_1h_1 + s_2h_2 + n_1 \\ s_2^*h_1 - s_1^*h_2 + n_2 \end{bmatrix}, \tag{2.57}$$

where $\mathbf{n}$ is a vector of noise samples. In order to generate the decoupled statistics for detection of the transmitted symbols, the second entry in 2.57 must be conjugated, that is,

$$\tilde{\mathbf{r}} = \begin{bmatrix} s_1h_1 + s_2h_2 + n_1 \\ s_2h_1^* - s_1h_2^* + n_2^* \end{bmatrix}. \tag{2.58}$$

With this formulation, the received vector may be written as,

$$\tilde{\mathbf{r}} = \begin{bmatrix} h_1 & h_2 \\ -h_2^* & h_1^* \end{bmatrix} \begin{bmatrix} s_1 \\ s_2 \end{bmatrix} + \begin{bmatrix} n_1 \\ n_2^* \end{bmatrix} \tag{2.59}$$

$$= \tilde{\mathbf{H}}\mathbf{s} + \tilde{\mathbf{n}}, \tag{2.60}$$

where $\tilde{\mathbf{n}}$ is the equivalently transformed noise vector. Now the matrix $\tilde{\mathbf{H}}$ has the property,

$$\tilde{\mathbf{H}}^H\tilde{\mathbf{H}} \tag{2.61}$$

$$= \begin{bmatrix} h_1^* & -h_2 \\ h_2^* & h_1 \end{bmatrix} \begin{bmatrix} h_1 & h_2 \\ -h_2^* & h_1^* \end{bmatrix} \tag{2.62}$$

$$= \begin{bmatrix} |h_1|^2+|h_2|^2 & 0 \\ 0 & |h_1|^2+|h_2|^2 \end{bmatrix} \tag{2.63}$$

$$=(|h_1|^2+|h_2|^2)\mathbf{I}_2, \tag{2.64}$$

which is similar to unitary matrices. Therefore, with knowledge of the fading coefficients, the sufficient statistics for ML detection are calculated by,

$$\tilde{\mathbf{H}}^H\tilde{\mathbf{r}} = (|h_1|^2+|h_2|^2)\mathbf{s}+\tilde{\mathbf{H}}^H\tilde{\mathbf{n}}. \tag{2.65}$$

The entries in the resulting vector may then be passed to the detector or decoder in order to retrieve the transmitted data symbols.

2.5.3 Capacity - Spatial multiplexing

Spatial multiplexing (or layering) was first introduced at Bell Laboratories with the BLAST system [6]. The further study of the layering concept led to the discovery that the capacity of a MIMO system increases linearly in the minimum of the number of transmit and receive antennas [26, 27]. This capacity may be achieved by transmitting independent data from each of the transmit antennas. The data may then be recovered by applying multiple-signal detection algorithms at the receiver. This research aims to combine CDMA and OFDM in a multi antenna environment. In this way the symbols transmitted synchronously from the jth of N_{Tx} transmit antennas (before the addition of the CP) may be represented by,

$$s_j[n] = \sum_{a=0}^{MN-1}\sum_{k=1}^{K_u} d_{j,k}c_{a,k}e^{j2\pi f_a \frac{n}{MN}} \quad \begin{matrix} j=1,2,\ldots,N_{Tx} \\ n=1,2,\ldots,N_c \end{matrix}, \tag{2.66}$$

where $d_{j,k}$ is the kth data symbol that is transmitted on the jth antenna and $c_{a,k}$ is the ath chip of the sequence associated with the kth data symbol. The symbols $\{s_j\}$ may be referred to as space-frequency

spread symbols. Before digital-to-analogue conversion and transmission through the channel the cyclic prefix must be appended to the symbols to eliminate the ISI, this means lengthening the OFDM symbols in the following manner:

$$\check{s}_j = \begin{cases} \mathbf{s}_j[MN-n] & n = -N_{cp}, -N_{cp}+1, \ldots, -1 \\ \mathbf{s}_j[n] & n = 0, 1, \ldots, MN-1 \end{cases} . \tag{2.67}$$

The layering may also be thought of as a space-time block code (STBC) where independent OFDM symbols are transmitted during a single symbol interval, which is opposed to classical STBCs where symbols are repeated over a number of symbol periods with different antenna mappings. Without the repetition of the symbols over a number of symbol periods there can be no transmit diversity. The code matrices in 2.46 are then constructed by choosing $\{\mathbf{A}_n, \mathbf{B}_n\}$ as the nth columns of $\mathbf{I}_{N_{Tx}}$ and $n_s = N_{Tx}$ [31],

$$\mathbf{X} = \left[\mathbf{s}_1^T \ \mathbf{s}_2^T \ \ldots \ \mathbf{s}_{n_s}^T\right]^T . \tag{2.68}$$

2.5.4 Joint detection

As will be seen in chapter 3 a MIMO system may be represented by a system of linear equations. The received signals in a MIMO system may be expressed in the form,

$$\mathbf{r} = \mathbf{H}\mathbf{s} + \mathbf{n}_\sigma , \tag{2.69}$$

which is solvable for $\mathbf{s}$ given that the matrix $\mathbf{H}$ has full rank and the system is not underdetermined. If this is the case then a number of detection algorithms may be applied to the system to retrieve the transmitted data. The most simple of these algorithms is the zero forcing (ZF) algorithm, an extension of the matched filter (MF) detector. Other approaches include the minimum mean-square error (MMSE), maximum likelihood (ML) and maximum *a posteriori* (MAP) detectors.

2.5.4.1 Matched filter detector

The MF detector aims to maximise the SNR at the output of the filter for each symbol. The filter itself is matched to the waveform of the transmitted signal. Assuming the classical linear filter model of a multipath channel the received vector $\mathbf{r}$ is,

$$\mathbf{r} = \mathbf{h} * \mathbf{s} + \mathbf{n}_\sigma, \tag{2.70}$$

where $\mathbf{s}$ is the transmitted vector of symbols, $\mathbf{h}$ is the channel impulse response vector and $\mathbf{n}_\sigma$ is a vector of i.i.d. zero mean AWGN samples with variance σ^2. Following the approach in [55, pp. 99] and taking the z-transform of the elements in each of these vectors, 2.70 may be rewritten as,

$$R(z) = H(z)S(z) + N(z), \tag{2.71}$$

where $A(z)$ is the z-transform of some vector $\mathbf{a}$. The estimates of the transmitted data may be expressed as,

$$\hat{S}(z) = G(z)H(z)S(z) + G(z)N(z), \tag{2.72}$$

where $G(z)$ is the z-transform of the MF. The signal component power spectral density (PSD) in this expression is,

$$|S(z)|^2|G(z)H^*(z)|^2 = \sigma_S^2|G(z)H^*(z)|^2, \tag{2.73}$$

where it is assumed that the variance of the data is σ_S^2. The noise component PSD with double-sided PSD of AWGN equal to $\frac{N_0}{2}$ is,

$$|N(z)|^2|G(z)|^2 = \frac{N_0}{2}|G(z)|^2. \tag{2.74}$$

Therefore the SNR, when applying the Cauchy-Schwartz inequality [56] is,

$$\frac{\sigma_S^2|G(z)H^*(z)|^2}{\frac{N_0}{2}|G(z)|^2} \leq \frac{\sigma_S^2|G(z)|^2|H^*(z)|^2}{\frac{N_0}{2}|G(z)|^2}, \tag{2.75}$$

which is maximised when,

$$|G(z)H^*(z)|^2 = |G(z)|^2|H^*(z)|^2, \tag{2.76}$$

$$|G(z)|^2 = c|H^*(z)|^2, \tag{2.77}$$

where $c \neq 0$ is a scalar constant. In vector notation this may be expressed as,

$$\mathbf{G} = \mathbf{H}^H, \tag{2.78}$$

where $\mathbf{G}$ is the vector valued MF with respect to 2.69.

2.5.4.2 Zero forcing detector

Again considering 2.69 the detection of $\mathbf{s}$ may be concisely described from a statistical standpoint. Here $\mathbf{H}$ represents the effective channel impulse response in the discrete domain. The covariance matrix of the vector $\mathbf{n}_\sigma$ may be expressed as [55, pp. 102],

$$\mathbf{R}_n = \frac{N_0}{2}\mathbf{I} = \frac{\sigma_n^2}{2}\mathbf{I}, \tag{2.79}$$

where the noise variance σ_n^2 is equal to the noise PSD N_0. With this assumption the conditional joint probability density function of the received vector $\mathbf{r}$ is given by [55, eq. (3.99)],

$$p(\mathbf{r}|\mathbf{s}) = \frac{1}{\sqrt{(2\pi)^{n_r}|\mathbf{R}_n|}} e^{-\left[\frac{1}{2}(\mathbf{r}-\mathbf{Hs})^H\mathbf{R}_n^{-1}(\mathbf{r}-\mathbf{Hs})\right]}, \tag{2.80}$$

where n_r is the length of the received vector. Maximising 2.80 in the ZF sense amounts to minimising the expression in the exponent,

$$(\mathbf{r}-\mathbf{Hs})^H \mathbf{R}_n^{-1} (\mathbf{r}-\mathbf{Hs}) = \frac{1}{\sigma_n^2} ||\mathbf{r}-\mathbf{Hs}||^2, \tag{2.81}$$

by solving the following,

$$\begin{aligned} \mathbf{r} &= \mathbf{H}\hat{\mathbf{s}}_{ZF} \\ \therefore \quad \hat{\mathbf{s}}_{ZF} &= \mathbf{H}^{-1}\mathbf{r} \end{aligned}, \tag{2.82}$$

where $\hat{\mathbf{s}}_{ZF}$ is the estimated transmitted vector. The ZF detector is essentially the inversion of the channel operation. If the channel matrix $\mathbf{H}$ is not square the pseudo inverse may be taken. Left multiplying by the Moore-Penrose pseudo inverse [57] of $\mathbf{H}$ gives,

$$\hat{\mathbf{s}}_{ZF} = \left(\mathbf{H}^H\mathbf{H}\right)^{-1} \mathbf{H}^H\mathbf{r}. \tag{2.83}$$

The first important observation is that 2.83 contains the MF solution and can therefore be considered a derivative of the MF detector. The second observation is that this detection method does not take the noise into account and so is suboptimal. In fact the decorrelation of ISI from the received vector leads to noise enhancement [55, pp. 104]. This may be improved on by using the MMSE detector.

2.5.4.3 Minimum mean-square error detector

The MMSE detector aims to minimise the mean-square error between the transmitted vector and the estimated vector. This finds a balance between the noise and ISI rather than simply eliminating the effects of the channel. The mean-square error is expressed as [55, eq. (3.108)],

$$E\left[(\mathbf{s}-\hat{\mathbf{s}})^H (\mathbf{s}-\hat{\mathbf{s}})\right] = E\left[||\hat{\mathbf{s}}-\mathbf{s}||^2\right], \tag{2.84}$$

where $E[\cdot]$ is the expectation operator. This may be minimised by setting the error vector orthogonal to the received vector [55, pp. 105] and solving for $\mathbf{G}$ [55, eq. (3.109)],

$$E\left[(\mathbf{s}-\hat{\mathbf{s}})\,\mathbf{r}^H\right]=0 \tag{2.85}$$

$$\therefore E\left[(\mathbf{s}-\mathbf{G}\mathbf{r})\,\mathbf{r}^H\right]=0 \tag{2.86}$$

$$\therefore E\left[\mathbf{s}\mathbf{r}^H-\mathbf{G}\mathbf{r}\mathbf{r}^H\right]=0 \tag{2.87}$$

$$\therefore E\left[\mathbf{s}\mathbf{r}^H\right]-\mathbf{G}E\left[\mathbf{r}\mathbf{r}^H\right]=0 \tag{2.88}$$

$$\therefore \mathbf{R}_{\mathbf{sr}}-\mathbf{G}\mathbf{R}_{\mathbf{r}}=0 \tag{2.89}$$

$$\therefore \mathbf{G}=\mathbf{R}_{\mathbf{sr}}\mathbf{R}_{\mathbf{r}}^{-1}, \tag{2.90}$$

where $\mathbf{R}_{\mathbf{sr}}$ is the covariance matrix of the data and the received vector and $\mathbf{R}_{\mathbf{r}}$ is the auto-covariance matrix of the received vector. The same solution may be found explicitly from [8, pp. 970],

$$E\left[||\hat{\mathbf{s}}-\mathbf{s}||^2\right]=E\left[||\mathbf{G}\mathbf{r}-\mathbf{s}||^2\right] \tag{2.91}$$

$$=E\left[||\mathbf{G}\mathbf{H}\mathbf{s}+\mathbf{G}\mathbf{n}-\mathbf{s}||^2\right] \tag{2.92}$$

$$=\frac{\sigma_s^2}{2}||\mathbf{G}\mathbf{H}-\mathbf{I}||^2+\frac{\sigma_n^2}{2}||\mathbf{G}||^2 \tag{2.93}$$

$$=\frac{\sigma_s^2}{2}\left|\left|[\mathbf{I}\quad\mathbf{0}]-\mathbf{G}\left[\mathbf{H}\quad\sqrt{\frac{\sigma_n^2}{\sigma_s^2}}\mathbf{I}\right]\right|\right|^2, \tag{2.94}$$

assuming that the data symbols are uncorrelated as well as the and noise samples, with variance σ_s^2 and σ_n^2 respectively. The MMSE detector may be formulated as,

$$\hat{\mathbf{s}}_{MMSE}=\mathbf{G}\mathbf{r} \tag{2.95}$$

$$=\left(\mathbf{H}^H\mathbf{H}+\frac{\sigma_n^2}{\sigma_s^2}\mathbf{I}\right)^{-1}\mathbf{H}^H\mathbf{r}. \tag{2.96}$$

Again this solution contains the MF solution and therefore is also a derivative thereof. Also the structure is similar to the ZF solution however the noise is compensated for in the term $\frac{\sigma_n^2}{\sigma_s^2}\mathbf{I}$.

2.5.4.4 Maximum likelihood detector

Neither the ZF nor the MMSE detectors are optimal in the ML sense. A true ML estimator is one that maximises the expression 2.80 for $\mathbf{s} \in \mathscr{S}$ where $\mathscr{S}$ is a finite constellation alphabet. The ML metric for coherent detection may be expressed as [31, eq. (4.2.5)],

$$\hat{\mathbf{s}}_{ML} = \underset{s\in\mathscr{S}}{\text{argmax}} \quad p(\mathbf{r}|\mathbf{s}) \tag{2.97}$$

$$= \underset{s\in\mathscr{S}}{\text{argmax}} \quad \frac{1}{\sqrt{(2\pi)^{n_r}\,|\mathbf{R_n}|}} e^{-\left[\frac{1}{2}(\mathbf{r}-\mathbf{Hs})^H \mathbf{R_n}^{-1}(\mathbf{r}-\mathbf{Hs})\right]} \tag{2.98}$$

$$= \underset{s\in\mathscr{S}}{\text{argmax}} \quad e^{-\frac{1}{2\sigma_n^2}||\mathbf{r}-\mathbf{Hs}||^2} \tag{2.99}$$

$$= \underset{s\in\mathscr{S}}{\text{argmin}} \quad ||\mathbf{r}-\mathbf{Hs}||^2 . \tag{2.100}$$

The ML estimator is optimal in the sense that it minimises the probability of erroneous detection [8]. The computation of the ML solution is often infeasible due to large constellations as well as simultaneous joint decoding and detection. A number of algorithms, derived from the "search for the closest lattice point" problem, have been developed in order to achieve near ML performance [34]. These are collectively termed sphere decoders and may be used to jointly perform equalisation, decoding and detection.

The sphere decoder operates as follows. The received vector $\mathbf{r}$ may be thought of as a point in a multi-dimensional space. The ML solution is the closest lattice point, of a finite lattice formed by the transformation of the constellation alphabet via the channel $\mathbf{H}$ [34]. The means to achieve this is to enumerate all the lattice points that fall within a hyper-sphere of radius C_r centred at the received vector [34]. Thus the search space is reduced and computation of the ML solution becomes feasible. Naturally this approach poses its own problems in terms of selecting the radius C_r since choosing too large a radius does not reduce the number of possible transmitted signals and choosing too small a radius may result in zero possible transmitted signals. The decoder enumerates vectors $\{\mathbf{s}\}$ that fulfil the condition,

$$||\mathbf{r}-\mathbf{Hs}||^2 \leq C_r^2. \tag{2.101}$$

The sphere decoder has been further refined so that the detection of the transmitted symbols may be performed sequentially while simultaneously reducing the radius of the sphere [35]. This eliminates the problem of radius selection. This approach involves solving a system of the form 2.69 by decomposing the channel matrix (or some variation thereof) into a triangular form. This may be done by performing the Cholesky decomposition of,

$$\mathbf{H}^H\mathbf{H} = \mathbf{R}^H\mathbf{R}, \tag{2.102}$$

where $\mathbf{R}$ is an upper triangular matrix. The expression 2.101 may then be reformulated as,

$$||\mathbf{R}(\hat{\mathbf{s}}_{ZF} - \hat{\mathbf{s}})||^2 \leq \check{C}_r^2, \tag{2.103}$$

where $\{\hat{\mathbf{s}}\}$ is the set of candidate ML solutions and $\check{C}_r^2 = C_r^2 - ||\mathbf{r}||^2 + ||\mathbf{H}\hat{\mathbf{s}}_{ZF}||^2$ is the modified radius [35]. Cholesky decomposition is a favourable algorithm since it is of lower complexity than other triangular decomposition algorithms [58] however the QR decomposition may also be used to solve the ML problem. Performing the QR decomposition of the channel matrix yields,

$$\mathbf{H} = \mathbf{QR}, \tag{2.104}$$

where $\mathbf{Q}$ is a unitary matrix and $\mathbf{R}$ is an upper triangular matrix [58]. With this formulation the enumeration of points within the sphere is based on the condition,

$$||\mathbf{r} - \mathbf{Hs}||^2 \leq C_r^2 \tag{2.105}$$

$$\therefore ||\mathbf{r} - \mathbf{QRs}||^2 \leq C_r^2 \tag{2.106}$$

$$\therefore \left|\left|\mathbf{Q}^H\mathbf{r} - \mathbf{Rs}\right|\right|^2 \leq C_r^2 \tag{2.107}$$

$$\therefore ||\tilde{\mathbf{r}} - \mathbf{Rs}||^2 \leq C_r^2. \tag{2.108}$$

Due to the structure of the triangular matrix a set of symbols $\{\hat{\mathbf{s}}\}$ may be enumerated sequentially through the process of back substitution with decisions fed back. This leads to a tree structure listing

the possible transmitted sequences, which may be searched using a greedy depth first strategy [1]. Once the search reaches the bottom of the tree a candidate solution has been found and the residual distance between the solution and the surface of the sphere may be subtracted from the sphere radius, C_r. This reduces the number of possible solutions by 'pruning' the tree. The search continues until only one candidate solution remains as the ML solution. The QR decomposition may be further refined by performing a variation known as the sorted QR decomposition [59]. This is akin to performing successive interference cancellation (SIC) as in the BLAST architectures [6].

2.5.4.4.1 The sorted QR decomposition algoritm A further refinement of the QR decomposition is the sorted QR decomposition. The difference between these two triangular decomposition algorithms is that the sorted QR decomposition attempts to order the diagonal elements of the matrix R in descending order of magnitude [59]. This is much like the SIC decoder used in the BLAST systems. There is however an issue with the sorted QR decomposition algorithm. It in some instances results in an ordering that of the diagonal elements of R that is not ideal. This in turn may result in a propagation of errors while the remainder of the block is decoded since the algorithm attempts to sequentially decode the symbols that are received in parallel.

2.6 CONCLUDING REMARKS

Mathematical descriptions of the foundational technologies have been presented. OFDM has been shown to be an efficient (in terms of spectrum usage and implementation) modulation method that is succinctly represented as a matrix multiplication. Classical CDMA has been described in terms of its formulation and correlation properties with the ideal property being stated. The complementary CDMA approach, specific to this work, has also been described along with its matrix formulation. Furthermore the correlation properties, generation algorithms, extension method and detection have been treated. MIMO techniques that achieve the goals set out for this work have been described together with respective detection algorithms. Again a matrix formulation has been given.

CHAPTER 3

CHANNEL MODEL

3.1 INTRODUCTION

In chapter 3 the channel models used for the evaluation of the proposed communication system are described, beginning with an abstracted view of noise and the mechanisms of signal propagation. Then, a statistical exposition of the SISO channel is provided, including fading in frequency and time. After this the discrete time channel model is described in the form of the tapped delay line leading to generalised channel models. These concepts are then extended to the MIMO environment in the general sense after which the standardised LTE MIMO channel is presented. Additionally the MIMO channel is described in vector notation that is consistent with the descriptions of the fundamental technologies presented in chapter 2.

3.2 NOISE AND FADING

3.2.1 Noise

Inherent to any communication system is interference caused by noise. Additive noise observed in receivers is due, in the most part, to thermal noise generated in the frontend electronics of transceivers [8, pp. 10]. This form of interference is present in all systems and plays an integral role in performance evaluation. The performance measure being bit error rate (BER) or bit error probabilities versus signal-to-noise ratio (SNR). If the noise is a linear addition of wideband noise with constant spectral density across the system bandwidth, it may be modelled as AWGN.

3.2.2 Fading channels

Further impairments of the received signal that lead to random amplitude variations are known as fading effects. These effects are due largely to the environment through which the transmission propagates as well as the relative motion of transceivers and other interacting objects (IOs).

Electromagnetic waves radiated into the environment around the transmitter are reflected, diffracted and scattered about resulting in many propagation paths to the receiver. This leads to several copies of the transmitted signal, each attenuated and delayed arriving at the receiver. These waves interfere with one another, either constructively or destructively, leading to the randomly varying received amplitude. If the resulting amplitude gain is constant and the phase is linear over the signal bandwidth for a given time instant the channel is termed *flat fading*. If the channel is flat fading the relations, $W \ll W_D$ and $T \gg \sigma_\tau$ hold, where W is the signal bandwidth, W_D is the channel maximum Doppler spread, T is the symbol period and σ_τ is the RMS delay spread. In the flat fading case the spectral characteristics of the transmitted signal are preserved by the channel and may be modelled as a single propagation path [60, pp. 205-206].

Alternatively the range spanning the bandwidth of the transmission may be faded to different degrees for different frequencies, which is called *frequency selective fading*. This occurs when the channel does not exhibit a constant gain and linear phase response over the entire signal bandwidth. Therefore $W > W_D$ and $T < \sigma_\tau$ as opposed to the flat fading case and this results in ISI [60, pp. 207-208]. Fig. 3.1 illustrates multipath propagation.

Relative movement of the transmitter and receiver as well as movement of IOs (that give rise to multiple propagation paths) results in Doppler related fading or temporal selectivity. There are two types of Doppler spread fading related to the rate of change of the channel impulse response, namely: *fast fading* and *slow fading* [60, pp. 208-210]. Fast fading is caused when the impulse response changes to a large degree within one symbol period. This implies that the symbol period of the transmitted signal is larger than the channel coherence time T_h. If $T_h < T$ or $W < W_D$ the channel may be said to be fast fading. Slow fading on the other hand occurs when the channel impulse response does not change significantly within one symbol period. This is when $T_h \gg T$ and $W \gg W_D$.

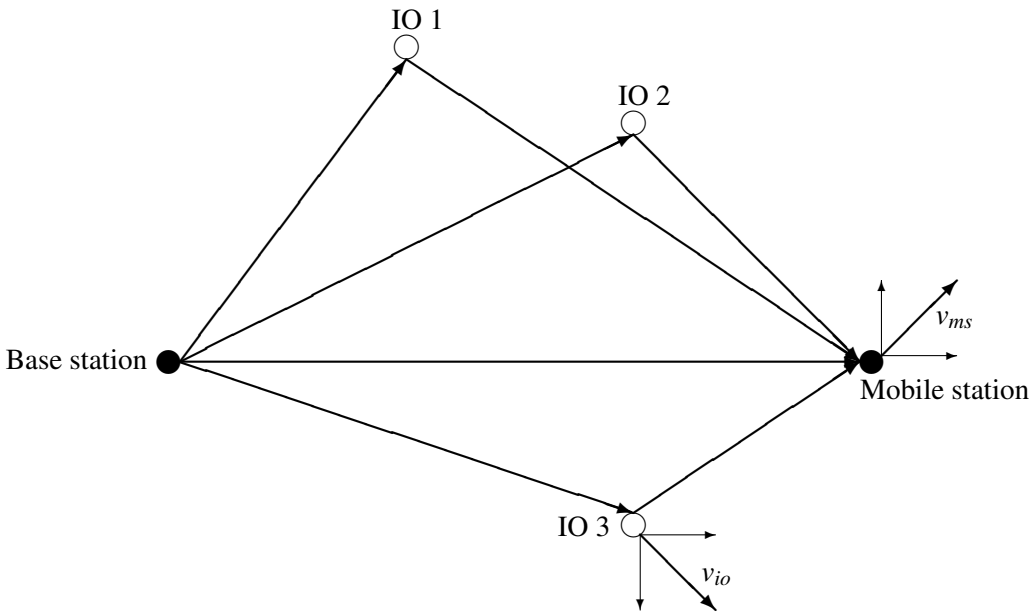

Figure 3.1: Multipath propagation between the base station (BS) and the mobile station (MS) with three IOs (v_{ms} is the velocity of the MS and v_{io} is the velocity of IO 3).

3.3 STATISTICAL MODEL OF SISO CHANNELS

The general structure of a SISO channel is shown in Fig. 3.2. The transfer function $h(t\ ;\ f)$ may either be constant or may vary according to frequency for flat or frequency selective fading respectively.

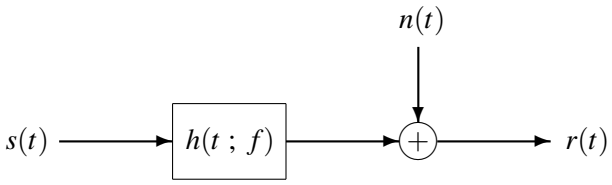

Figure 3.2: General structure of the SISO channel.

3.3.1 Additive white Gaussian noise

The noise observed in a communication system is characterised by the addition of many sources of statistically independent noise. According to the central limit theorem, the amplitude may be modelled by the Gaussian probability density function [61, pp. 214],

$$p(n_\sigma|\mu,\ \sigma^2) = \frac{1}{\sqrt{2\pi\sigma^2}} e^{-\frac{(n_\sigma-\mu)^2}{2\sigma^2}}, \tag{3.1}$$

where $\mu = 0$ is the mean and σ^2 is the variance or power of the random variable n_σ. In order to generate the abovementioned performance results as a function of SNR, the noise bandwidth must be specified and in doing so, systems with different noise bandwidths are not easily compared. To rectify this problem the SNR is normalised to E_b/N_0, which is the average bit energy-to-noise density ratio. This is done in simulation by scaling the variance of the noise samples by [43, eq. (2.35)],

$$k_{n_\sigma} = \frac{\sigma_s^2 F_{sa}}{10^{\frac{E_b}{10N_0}} 2F_{bit}}, \tag{3.2}$$

where σ_s^2 is the variance of the channel input (usually normalised to unity for practical reasons), F_{sa} is the sampling frequency of the system as well as the rate at which noise samples are generated and F_{bit} is the bit rate of the system. In the case where super complementary codes are employed the sampling rate and the bit rate are equal and 3.2 reduces to,

$$k_{n_\sigma} = \frac{1}{20^{\frac{E_b}{10N_0}}}. \tag{3.3}$$

Noise samples generated with zero mean and unit variance may then be scaled by the factor $\sqrt{k_{n_\sigma}}$ in order to acquire the correct bit energy-to-noise density ratio.

3.3.2 Flat fading

Generally flat fading is experienced in narrowband systems where the random variations of the received signal amplitude are almost constant and phase response is linear over the entire bandwidth of the signal. This is congruous to an OFDM subcarrier with long symbol period, where ISI becomes

negligible. The narrowband condition is not present in spread spectrum systems (such as DS-CDMA systems) however for comparative purposes results in flat fading conditions are simulated. Furthermore it will be seen that frequency selective channels may be simulated as a linear combination of multiple independent flat faded channels.

Flat fading may be modelled as a stochastic process,

$$p(h(t)) = \begin{cases} f_h(h(t)) & 0 \leq h(t) < \infty \\ 0 & \text{otherwise} \end{cases}, \tag{3.4}$$

and

$$p(\phi(t)) = f_\phi(\phi(t)) \quad -\pi \leq \phi(t) \leq \pi, \tag{3.5}$$

where $h(t)$ (here h is used as the symbol for amplitude to maintain consistency with the channel impulse response) is the envelope and $\phi(t)$ is the phase of the fading process and $f_h(\cdot)$ and $f_\phi(\cdot)$ are the functions determining the nature of the process. The most commonly employed statistical models for flat fading are Rayleigh and Rician distributed processes.

3.3.2.1 Rayleigh fading

In a wireless channel when there is no line-of-sight (LOS) component present in the received signal and only the other indirect multipath components, the amplitude distribution may be modelled as a Rayleigh process and the phase may be modelled as a uniform process on the interval $[-\pi, \pi]$ [60]. The implication of this in terms of the complex baseband representation of the transmitted signal, is that the received signal may be modelled by the product of the transmitted signal and a Rayleigh distributed stochastic process. This represents the random attenuation or fading imposed on the signal during transmission. The variance σ^2_{NLOS} [1], of this random variable represents the power of the received signal. The pdf of a Rayleigh distributed amplitude is given by [53, eq. 5.16],

[1] NLOS is an acronym for non-line-of-sight and σ^2_{NLOS} refers to the power of the diffuse component in a multipath channel.

$$p(h(t)) = \begin{cases} \frac{h(t)}{\sigma^2_{NLOS}} e^{-\frac{h^2(t)}{2\sigma^2_{NLOS}}} & 0 \leq h(t) < \infty \\ 0 & \text{otherwise} \end{cases}, \tag{3.6}$$

and uniformly distributed phase by,

$$p(\phi(t)) = \frac{1}{2\pi} \quad -\pi \leq \phi(t) \leq \pi, \tag{3.7}$$

3.3.2.2 Rician fading

In a wireless channel when there is LOS between the transmitter and receiver as well as the other NLOS paths, the amplitude distribution may be modelled by the Rician process [53]. Rician fading is caused when there is significantly more power present in the LOS component than the other paths. The ratio of the power of LOS component to the power of the other paths (diffuse component) is known as the Rician K-factor, $K = A^2/2\sigma^2_{NLOS}$ where A is the amplitude of the LOS component. The Rician distribution is given by the joint pdf [53, eq. 5.26],

$$p(h(t), \phi(t)) = \frac{x(t)}{2\pi\sigma^2_{NLOS}} e^{-\frac{x^2(t)+A^2-2x(t)Acos(\phi(t))}{2\sigma^2_{NLOS}}}, \tag{3.8}$$

from which the amplitude distribution,

$$p(x(t)) = \begin{cases} \frac{x(t)}{\sigma^2_{NLOS}} e^{-\frac{x^2(t)+A^2}{2\sigma^2_{NLOS}}} I_0\left(\frac{Ax(t)}{\sigma^2_{NLOS}}\right) & A \geq 0 \text{ and } x(t) \geq \infty \\ 0 & x(t) < 0 \end{cases}, \tag{3.9}$$

and the phase distribution,

$$p(\phi(t)) = \begin{array}{l} \frac{1}{2\pi} e^{-\frac{A^2}{2\sigma^2_{NLOS}}} \left[1 + \frac{A}{\sigma^2_{NLOS}} \sqrt{\frac{\pi}{2}} cos(\phi(t) + \theta_R) \cdot \right. \\ \left. exp\left(\frac{A^2 cos^2(\phi(t)-\theta_R)}{2\sigma^2_{NLOS}}\right)\left(1 + erf\left[\frac{Acos(\phi(t)-\theta_R)}{\sigma^2_{NLOS}\sqrt{2}}\right]\right)\right] \quad -\pi \leq \phi(t) \leq \pi \end{array}, \tag{3.10}$$

may be derived. Here $I_0(\cdot)$ is the modified Bessel function of the first kind and zero-th order. From these expressions it can be seen that Rician fading approaches Rayleigh fading as $K_{(dB)} \to 0$ dB and

for large K, it approximates a Gaussian random process with mean, $\mu = A$. It is common practice for the K-factor to be expressed in logarithmic form as,

$$K_{(dB)} = 10log_{10}\left(\frac{A^2}{2\sigma_{NLOS}^2}\right). \tag{3.11}$$

3.3.3 Frequency selective fading

Frequency non-selectivity is present when $\frac{1}{W} \gg \tau_{max}$ where W is the system (or signal) bandwidth and τ_{max} is the maximum excess channel delay or channel delay spread [53]. In all other situations the channel may be considered to be frequency selective [60]. In this case the received signal may be described by,

$$\begin{aligned} r(t) &= h(t\ ;\ \tau) * s(t) + n_\sigma(t) \\ &= \int_{-\infty}^{\infty} h(t\ ;\ \tau)s(t-\tau)d\tau + n_\sigma(t) \end{aligned}, \tag{3.12}$$

where $s(t)$ is the transmitted signal, $h(t\ ;\ \tau)$ is the time variant impulse response of the channel and $n_\sigma(t)$ is a zero mean AWGN process with variance σ^2. Under certain conditions the channel may be assumed to be time-invariant and 3.12 reduces to,

$$\begin{aligned} r(t) &= h(\tau) * s(t) + n_\sigma(t) \\ &= \int_{-\infty}^{\infty} h(\tau)s(t-\tau)d\tau + n_\sigma(t) \end{aligned}, \tag{3.13}$$

In order to develop a discrete time statistical channel model consider $\Delta\tau$ the sampling period of the channel impulse response in 3.12. If $\Delta\tau \ll 1/W$ the channel impulse response may be approximated by [53],

$$\begin{aligned} h(t\ ;\ \tau) &= \sum_{i=0}^{L} h_i(t\ ;\ \tau)\delta(\tau - i\Delta\tau)e^{j(2\pi f_c i\Delta\tau + \theta_i(t\ ;\ \tau))} \\ &= \sum_{i=0}^{L} h_i(t\ ;\ \tau)\delta(\tau - i\Delta\tau)e^{j\phi_i(t\ ;\ \tau)} \end{aligned}, \tag{3.14}$$

where the random variables $\{h_i\}$ are characterised by either Rayleigh or Rician processes, f_c is the carrier frequency and $\theta_i(t\ ;\ \tau)$ is the time variant phase. Only the first $L+1$ bins or samples are

considered [53], those being the $L+1$ most significant contributions to the received signal power. The transfer function of 3.14 is,

$$h(t\ ;\ f) = \int_{-\infty}^{\infty} \sum_{i=0}^{L} h_i(t\ ;\ \tau)\delta(\tau - i\Delta\tau)e^{j\phi_i(t\ ;\ \tau)}e^{-j2\pi f\tau}d\tau \tag{3.15}$$

$$= \sum_{i=0}^{L} h_i(t\ ;\ i\Delta\tau)e^{j\phi_i(t\ ;\ i\Delta\tau)}e^{-j2\pi fi\Delta\tau} \tag{3.16}$$

$$= \sum_{i=0}^{L} h_i(t\ ;\ i\Delta\tau)e^{-j(2\pi fi\Delta\tau - \phi_i(t\ ;\ i\Delta\tau))}, \tag{3.17}$$

which is only flat in the case of one path ($L = 0$).

The time-invariant version of the channel may be expressed as,

$$h(\tau) = \sum_{i=0}^{L} \bar{h}_i\delta(\tau - i\Delta\tau)e^{j\bar{\phi}_i}, \tag{3.18}$$

where $\bar{h}_i$ and $\bar{\phi}_i$ are the time averaged amplitude and phase for the ith tap over the interval $[i\Delta\tau,\ i\Delta\tau + \Delta\tau]$.

3.3.4 Temporal channel variation and Doppler spectra

When the conditions under which time-invariance are not present, a time varying model for the fading induced by the channel must be adopted. Generally this occurs when the relative velocity between the transmitter and receiver as well as the IOs is large [60]. The resulting spectral broadening of the transmitted signal is called *Doppler spread*.

Typically Doppler is associated with a single path, in other words it describes the spectral broadning that occurs due to transmission along that path. Considering this, Doppler spread may be associated with each of the different multipath components in a multipath channel. The Doppler effect is caused by relative motion between the transmitter and receiver and the IOs. It should be noted that Doppler spread is a function of relative motion between transmitter and receiver as well as the angle of arrival of different multipath components.

An important parameter concerning Doppler spread is the maximum Doppler shift F_D. This para-

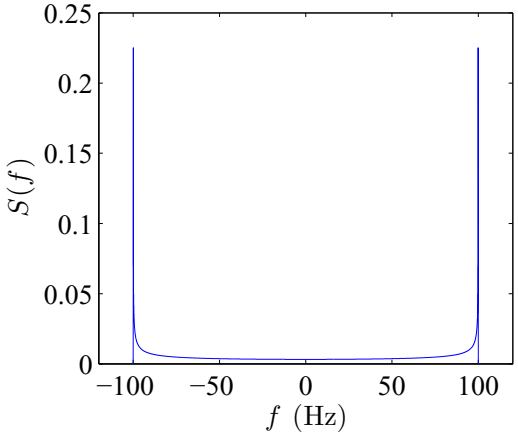

Figure 3.3: Normalised Doppler PSD of the classical Jakes model with a maximum Doppler shift of $F_D = 100\ Hz$.

meter is a measure of the frequency shift observed in a system when the relative velocity between the transmitter and receiver is in the direction of propagation (there is no orthogonal component of velocity with respect to the direction of propagation).

It has been shown that the received signal PSD of a sinusoidal input signal to the channel may be approximated by [53, 60],

$$S(f) = \frac{1}{\pi F_D \sqrt{1 - (\frac{f}{F_D})^2}}. \tag{3.19}$$

This function is known as the classical Doppler spectrum or Jakes PSD, which is illustrated by Fig. 3.3. The Jakes model for Doppler PSD is limited since it assumes omnidirectional antennas with uniform scattering and no LOS component. However, it is adopted in many standards as the Doppler spectrum including the LTE specification [62].

Another parameter of interest is the channel *coherence time*. The coherence time is a statistical measure of the maximum time interval over which the channel exhibits flat fading; in general it may be expressed as [43],

$$T_h = \frac{\zeta}{F_D}. \tag{3.20}$$

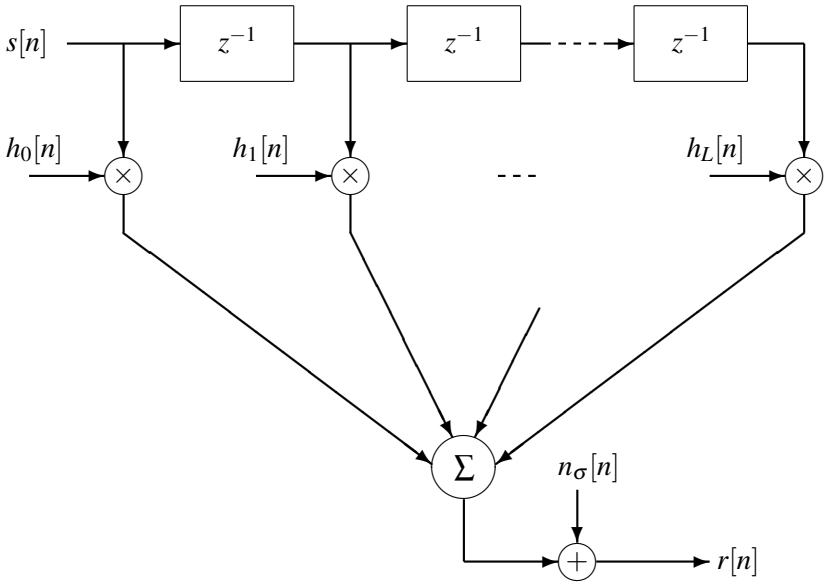

Figure 3.4: Tapped delay line model.

ζ is a constant value that is determined by the required pre-set amplitude correlation [43]. Typical values of ζ for specified correlations may be found in [60].

3.4 DISCRETE MULTIPATH CHANNEL MODELS

3.4.1 Tapped delay line and matrix representation

The operation of the channel in 3.14 may viewed as a finite impulse response (FIR) filter and be implemented using the tapped delay line model [63]. This consists of a complex valued shift register where the value stored by each delay element is tapped to a complex multiplier following which all the taps are summed. Fig. 3.4 illustrates the tapped delay line structure. Each of the tapped values is multiplied by its respective gain sampled from the channel impulse response,

$$h_{i,n} \equiv h_i[n] = \left[h_i(t\ ;\ \tau)e^{j\phi(t\ ;\ \tau)}\right]|_{t=nT_{sa},\tau=(n-i)T_{sa}} \quad i = 0,1,\ldots,L. \tag{3.21}$$

If the channel coefficients in 3.14 are represented as a sequence of vectors,

$$\mathbf{h}_n = [h_{0,n}\ h_{1,n}\ \ldots h_{L,n}]^T \quad n = 0,1,\ldots,N_B-1, \tag{3.22}$$

the operation of the tapped delay line for a length N_B block of data may conveniently be represented in vector notation as,

$$\mathbf{r} = \mathbf{H}\mathbf{s} + \mathbf{n}_\sigma, \tag{3.23}$$

where,

$$\mathbf{s} = [s[0]\ s[1]\ \ldots s[N_B-1]\ ]^T, \tag{3.24}$$

$$\mathbf{n}_\sigma = [n_\sigma[0]\ n_\sigma[1]\ \ldots n_\sigma[N_B-1+L]\ ]^T, \tag{3.25}$$

$$s[n] = s(t)|_{t=nT_{sa}}, \tag{3.26}$$

$$n_\sigma[n] = n_\sigma(t)|_{t=nT_{sa}}, \tag{3.27}$$

and

$$\mathbf{H} = \begin{bmatrix} h_{0,0} & 0 & \ldots & 0 \\ h_{1,0} & h_{0,1} & \ldots & 0 \\ \vdots & h_{1,1} & \ldots & 0 \\ h_{L,0} & \vdots & \ddots & h_{0,N_B-1} \\ 0 & h_{L,1} & \ddots & h_{1,N_B-1} \\ \vdots & \vdots & \ddots & \vdots \\ 0 & 0 & \ldots & h_{L,N_B-1} \end{bmatrix}. \tag{3.28}$$

3.4.2 Discrete multipath channel profiles

The complex channel gains in expression 3.22 may be modelled in a number of ways. One approach is to sample stochastic processes for each tap (each vector in the sequence 3.22 represents a set of samples from the processes at a particular time instant) with variance derived from the pre-defined

power of each tap. A function of τ describing the channel power delay spread serves this purpose and is known as the power delay profile (PDP) [60, pp. 185]. Beginning with a time varying expression for the channel power,

$$P(t\ ;\ \tau) = |h(t\ ;\ \tau)|^2, \tag{3.29}$$

and averaging over time, the power delay profile is derived as,

$$P(\tau) = \sum_{i=0}^{L} \bar{h}_i^2 \delta(\tau - i\Delta\tau). \tag{3.30}$$

Here the coefficients $\{\bar{h}_i^2\}$ represent time-invariant average power of the ith multipath component [60]. When designing these values for simulation they are normalised according to the condition,

$$\sum_{i=0}^{L} \bar{h}_i^2 = 1, \tag{3.31}$$

ensuring that the total power transferred by the simulated channel is equal to unity. There are a number of standardised channels for which a PDP is defined as well as the underlying stochastic process that characterises the fading of each tap. To further illustrate the channel as described herein a number of general channel PDPs are treated.

Firstly an example of the two ray PDP is shown in Fig. 3.5 [53]. This model describes a channel with two discrete paths to the receiver. Assuming the relative delay between the paths is an integer multiple, i, of the sampling frequency, T_{sa}, the channel may be represented by the tapped delay line shown in Fig. 3.6. If the path delays of a general $L+1$ tap channel are not integer multiples of the sampling frequency techniques such as tap interpolation, resampling or rounding may be used to estimate the tap powers that coincide with the sampling period.

Other general PDPs include the uniform profile,

$$P_u(\tau) = \sum_{i=0}^{L} h^2 \delta(\tau - i\Delta\tau), \tag{3.32}$$

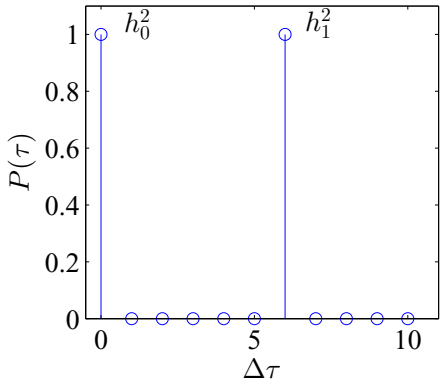

Figure 3.5: Two ray PDP with an excess delay of $6\Delta\tau$ (See page 44 for the definition of $\Delta\tau$, the sampling frequency. In this example the differential path delay is an integer multiple of the sampling frequency for illustrative purposes).

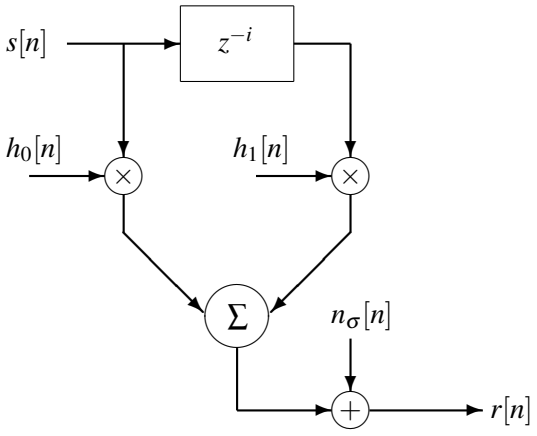

Figure 3.6: Tapped delay line model of the two ray channel.

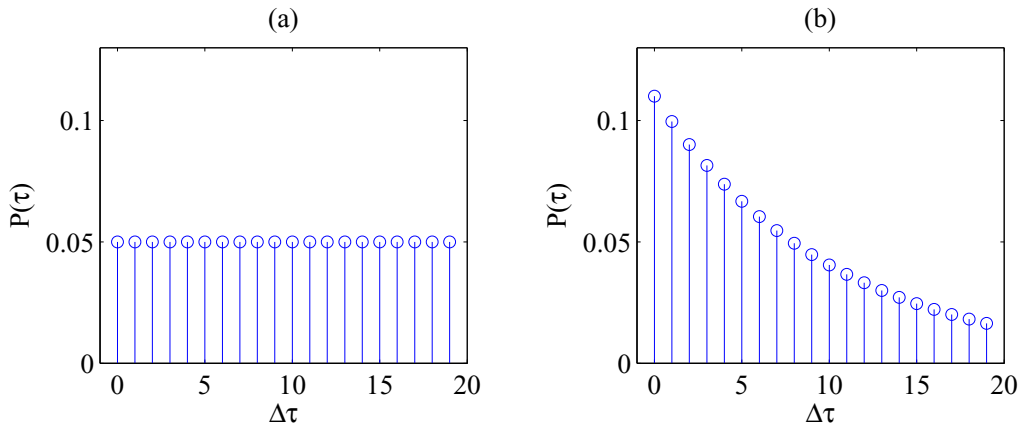

Figure 3.7: 20 tap (a) uniform and (b) exponential decay PDP examples.

where $h = \frac{1}{\sqrt{L+1}}$ is constant with respect to i; and the exponential decay profile,

$$P_e(\tau) = \sum_{i=0}^{L} A e^{-\frac{i\Delta\tau}{\tau_e}} \delta(\tau - i\Delta\tau), \tag{3.33}$$

$$A = \frac{1}{\sum_{i=0}^{L} e^{-\frac{i\Delta\tau}{\tau_e}}}, \tag{3.34}$$

with a time constant equal to τ_e. Examples of these channel model PDPs are shown in Fig. 3.7.

3.4.3 Multipath channel parameters

There are many different multipath channel models that exist and in order to compare them certain quantitative parameters exist. These include time dispersion parameters, coherence bandwidth, Doppler spread and coherence time (the last two parameters have been discussed in section 3.3.4).

3.4.3.1 Time dispersion paramters

The delay between the transmission and the reception of the first multipath component is the *first arrival delay*, τ_0 [60, pp. 199]. The difference between the first arrival delay and the lth multipath component is the excess delay for the lth path, τ_l. Time dispersion parameters are measures of power delay caused by the channel. The first of these is the mean excess delay which quantifies the average delay of a transmitted signal through the multipath channel. The mean excess delay is calculated by

[60, eq. (5.35)],

$$\bar{\tau} = \frac{\sum_{i=0}^{L} \bar{h}_i^2 (\tau_i - \tau_0)}{\sum_{i=0}^{L} \bar{h}_i^2}. \tag{3.35}$$

The next parameter of interest is the root-mean-square (RMS) delay spread given by [60, eq. (5.36)],

$$\sigma_\tau = \sqrt{\bar{\tau^2} - (\bar{\tau})^2}, \tag{3.36}$$

where,

$$\bar{\tau^2} = \frac{\sum_{i=0}^{L} \bar{h}_i^2 (\tau_i - \tau_0)^2}{\sum_{i=0}^{L} \bar{h}_i^2}. \tag{3.37}$$

Lastly the maximum excess delay is the excess delay of the last $(L+1)$th multipath component equal to,

$$\tau_{max} = \tau_L - \tau_0. \tag{3.38}$$

3.4.3.2 Coherence bandwidth

The final parameter of concern is the channel coherence bandwidth. This is a statistical measure of the width of a subband within the channel bandwidth that may be considered flat. Defining a minimum for the correlation between amplitudes of the subband edges the coherence bandwidth may be expressed as [43],

$$W_C = \frac{1}{\psi \sigma_\tau}, \tag{3.39}$$

where ψ is a constant determined from the predefined minimum correlation between bandedge amplitudes [43].

3.5 EXTENSION TO THE MULTIPLE ANTENNA ENVIRONMENT

Thus far only SISO channels have been considered. The SISO channel may however be extended to the MIMO environment as can be seen from the model depicted in Fig. 3.8. A MIMO system may be viewed conceptually as a superposition of a number of SISO systems. The received signals, in the absence of noise, in a system with N_{Tx} transmit antennas and N_{Rx} receive antennas will be linear combinations of the transmitted signals.

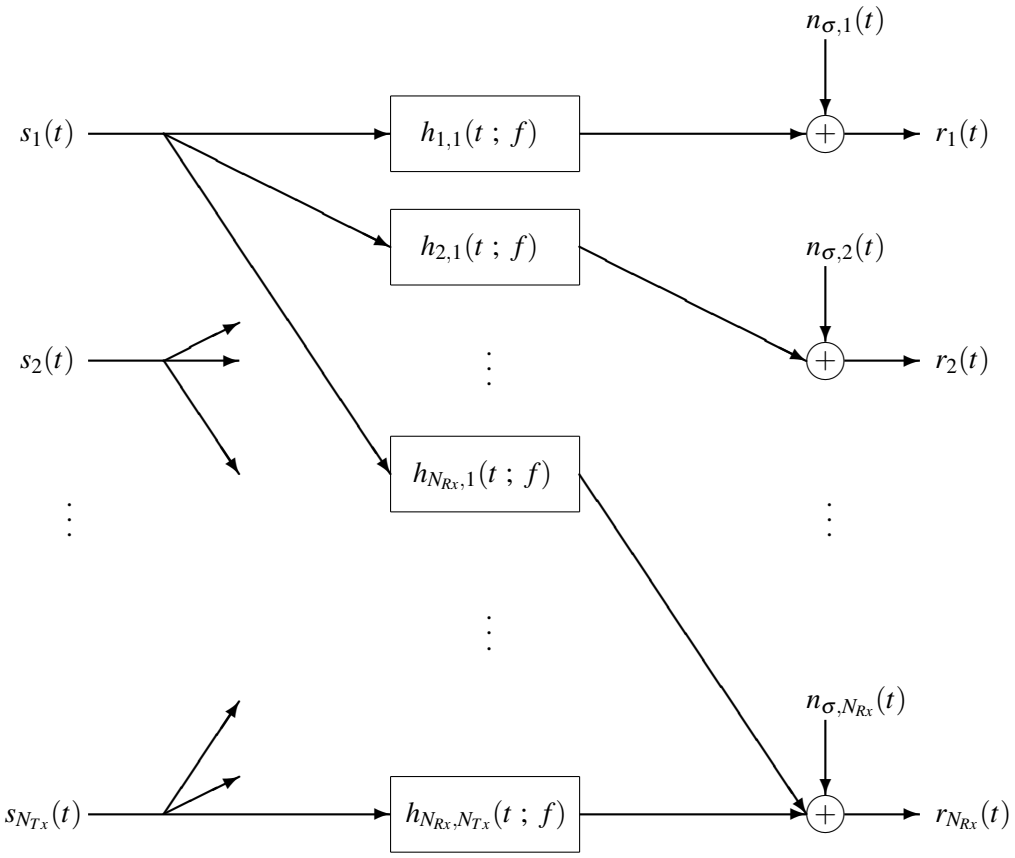

Figure 3.8: General structure of the MIMO channel [1]. Copyright © 2004, IEEE.

3.5.1 The multiple-input multiple-output channel

The signal received at the *i*th receive antenna in the absence of noise may be expressed as,

$$r_i(t) = \sum_{j=1}^{N_{Tx}} \int_{-\infty}^{\infty} h_{i,j}(t\ ;\ \tau) s_j(t-\tau) d\tau \tag{3.40}$$

$$= \sum_{j=1}^{N_{Tx}} h_{i,j}(t\ ;\ \tau) * s_j(t), \tag{3.41}$$

where $h_{i,j}(t\ ;\ \tau)$ is the lowpass equivalent channel impulse response between the jth transmit antenna and the ith receive antenna and $s_j(t)$ is the signal transmitted from the jth transmit antenna. The variable τ in the channel impulse response is known as the channel age or delay variable [8]. This system may be further represented in vector notation as [31],

$$\mathbf{r}(t) = \mathbf{H}(t\ ;\ \tau) * \mathbf{s}(t), \tag{3.42}$$

where $\mathbf{s}(t)$ and $\mathbf{r}(t)$ are $N_{Tx} \times 1$ and $N_{Rx} \times 1$ vectors respectively and,

$$\mathbf{H}(t\ ;\ \tau) = \begin{bmatrix} h_{1,1}(t\ ;\ \tau) & h_{1,2}(t\ ;\ \tau) & \dots & h_{1,N_{Tx}}(t\ ;\ \tau) \\ h_{2,1}(t\ ;\ \tau) & h_{2,2}(t\ ;\ \tau) & \dots & h_{2,N_{Tx}}(t\ ;\ \tau) \\ \vdots & & & \vdots \\ h_{N_{Rx},1}(t\ ;\ \tau) & h_{N_{Rx},2}(t\ ;\ \tau) & \dots & h_{N_{Rx},N_{Tx}}(t\ ;\ \tau) \end{bmatrix}. \tag{3.43}$$

The corresponding time-variant channel transfer function may be expressed as,

$$\mathbf{H}(t\ ;\ f) = \begin{bmatrix} h_{1,1}(t\ ;\ f) & h_{1,2}(t\ ;\ f) & \dots & h_{1,N_{Tx}}(t\ ;\ f) \\ h_{2,1}(t\ ;\ f) & h_{2,2}(t\ ;\ f) & \dots & h_{2,N_{Tx}}(t\ ;\ f) \\ \vdots & & & \vdots \\ h_{N_{Rx},1}(t\ ;\ f) & h_{N_{Rx},2}(t\ ;\ f) & \dots & h_{N_{Rx},N_{Tx}}(t\ ;\ f) \end{bmatrix}, \tag{3.44}$$

where $h_{i,j}(t\ ;\ f)$ is the time variant transfer function associated with the channel impulse response between the jth transmit antenna and the ith receive antenna.

If the channel is assumed to be time-invariant, the channel matrix 3.43 may be simplified to,

$$\mathbf{H}(\tau) = \begin{bmatrix} h_{1,1}(\tau) & h_{1,2}(\tau) & \dots & h_{1,N_{Tx}}(\tau) \\ h_{2,1}(\tau) & h_{2,2}(\tau) & \dots & h_{2,N_{Tx}}(\tau) \\ \vdots & & & \vdots \\ h_{N_{Rx},1}(\tau) & h_{N_{Rx},2}(\tau) & \dots & h_{N_{Rx},N_{Tx}}(\tau) \end{bmatrix}. \tag{3.45}$$

A further simplification may be made to the impulse response matrix, for illustrative purposes, in the case that the channel is frequency non-selective. The resulting channel impulse response and transfer function are simply $\mathbf{H}$, populated by complex scalar values.

When the received signals during the nth symbol interval are sampled on each receive antenna (in the absence of noise and assuming the time-invariant frequency non-selective channel) the samples may conveniently be represented by the following matrix formulation:

$$\mathbf{r}_n = \mathbf{H}\mathbf{s}_n. \tag{3.46}$$

where $\mathbf{r}_n$ and $\mathbf{s}_n$ are vectors of dimension $N_{Rx} \times 1$ and $N_{Tx} \times 1$ respectively. As in the SISO channel this may be extended to the frequency selective case by reformulating the channel matrix according to the tapped delay line model [31]. The causal continuous-time channel may be expressed as,

$$\mathbf{H}(n\ ;\ \tau) = \sum_{i=0}^{L} \mathbf{H}_i[n]\delta(\tau - \tau_i), \tag{3.47}$$

where $\mathbf{H}_i[n] \equiv \mathbf{H}_{i,n}$ is the coefficient matrix associated with the ith path, with delay $\tau_i = i\Delta\tau$, at time instant nT_{sa} (again only the $L+1$ strongest taps are considered). This can be interpreted as truncating the infinite length channel to an effective delay spread of L ($L = 0$ corresponds with the frequency non-selective case). With this formulation of the channel, when transmitting a block $\mathbf{S} = [\mathbf{s}_0, \mathbf{s}_1, \dots, \mathbf{s}_{N_B-1}]$ where each length N_{Tx} column of $\mathbf{S}$ is a vector of symbols transmitted in one symbol period from the corresponding N_{Tx} transmit antennas, the received signal is then expressed as,

$$\mathbf{r}_n = \sum_{i=0}^{L} \mathbf{H}_{i,n}\mathbf{s}_{n-i} + \mathbf{n}_{\sigma,n}, \tag{3.48}$$

where $\mathbf{R} = [\mathbf{r}_0, \mathbf{r}_1, \dots, \mathbf{r}_{N_B-1+L}]$ is a matrix of received samples (vectors of length N_{Rx}) structured in

a similar way to $\mathbf{S}$ and $\{\mathbf{n}_{\sigma,n}\}$ are length N_{Rx} vectors of i.i.d. zero mean complex Gaussian noise samples with variance σ.

Considering the formulation 3.47 and 3.48, the channel may be represented as a banded diagonal matrix,

$$\mathbf{H} = \begin{bmatrix} \mathbf{H}_{0,0} & 0 & \dots & 0 \\ \mathbf{H}_{1,0} & \mathbf{H}_{0,1} & \dots & 0 \\ \vdots & \mathbf{H}_{1,1} & \dots & 0 \\ \mathbf{H}_{L,0} & \vdots & \ddots & \mathbf{H}_{0,N_B-1} \\ 0 & \mathbf{H}_{L,1} & \ddots & \mathbf{H}_{1,N_B-1} \\ \vdots & \vdots & \ddots & \vdots \\ 0 & 0 & \dots & \mathbf{H}_{L,N_B-1} \end{bmatrix}. \tag{3.49}$$

The received samples may now be expressed in the form,

$$\mathbf{r} = \mathbf{H}\mathbf{s} + \mathbf{n}_\sigma, \tag{3.50}$$

where $\mathbf{r}$ and $\mathbf{s}$ are the vectorisation of $\mathbf{R}$ and $\mathbf{S}$ respectively and $\mathbf{n}_\sigma$ is a noise vector of length equal to $\mathbf{r}$ or $N_{Rx}(N_B + L)$.

Considering the MIMO channel matrix 3.43, each $h_{i,j}(t\ ;\ \tau)$ may be viewed as a SISO channel impulse response. Thus the MIMO frequency selective channel may be constructed from multiple SISO channels. Two considerations must be made concerning the constituent SISO channels. Firstly the PDP for each antenna pair must be defined and a fair assumption is that all the links exhibit the same PDP [1]. Secondly the correlation between antennas must be considered.

3.5.2 Spatial selectivity

The statistics that describe the antenna correlation are directly related the spatial selectivity of the system. A commonly made assumption is that the fading between pairs of antennas in a MIMO system is statistically independent [31] however in reality this not the case. Often the fading between pairs of antennas is correlated since the radiated waves interact with the same objects in the propagation

environment. One approach to modelling this spatial correlation is to model the channel matrix $\mathbf{H}$ (assuming time-invariant flat fading again for illustrative purposes) as [31],

$$\mathbf{H} = \mathbf{R}_{Rx}^{\frac{1}{2}} \mathbf{H}_{\omega} \mathbf{R}_{Tx}^{\frac{1}{2}}, \tag{3.51}$$

where $\mathbf{R}_{Rx}^{\frac{1}{2}}$ and $\mathbf{R}_{Tx}^{\frac{1}{2}}$ are the receive and transmit antenna correlation matrices respectively and $(\cdot)^{\frac{1}{2}}$ is the Hermitian square root of a matrix.

$\mathbf{H}_{\omega}$ is a matrix populated by independent realisations of random variables. The expression 3.51 may be rewritten as,

$$\mathbf{h} = \left(\left[\mathbf{R}_{Tx}^{\frac{1}{2}} \right]^{T} \otimes \mathbf{R}_{Rx}^{\frac{1}{2}} \right) \mathbf{h}_{\omega}, \tag{3.52}$$

where $\mathbf{h} = vec(\mathbf{H})$ and $\mathbf{h}_{\omega} = vec(\mathbf{H}_{\omega})$. Alternatively, if the matrix $\mathbf{H}_{\omega}$ is populated by realisations of i.i.d. complex zero mean Gaussian random variables with unit variance,

$$\mathbf{h} \sim N_{\mathbb{C}}(\mathbf{0},\ \mathbf{R}_{Tx}^{T} \otimes \mathbf{R}_{Rx}), \tag{3.53}$$

where $N_{\mathbb{C}}(\cdot)$ is the circular complex Gaussian distribution.

3.6 THE LONG TERM EVOLUTION MIMO CHANNEL

Thus far the MIMO channel has been shown to be composed of a number of SISO channels. By defining the PDP of each SISO link, a composite MIMO PDP can be created. Furthermore by defining the Doppler characteristics of each tap of each SISO link, a frequency selective Doppler time varying MIMO model is created. Lastly by defining the antenna correlation at each sampling instant a triply selective MIMO channel model can be described [1]. Reiterating, by combining multiple SISO channels in a correlated MIMO environment the result is a model that incorporates frequency, temporal and spatial selectivity.

By assuming that the PDP for each SISO link is the same and that the correlation between antennas is time invariant, a realistic and practical MIMO simulation model is fully defined. A set of such

standardised models for MIMO channels is included in the LTE specification for user equipment (this specification refers to the downlink channel) [62].

Firstly there are three PDP for three different scenarios: the Extended Pedestrian A (EPA), Extended Vehicular A (EVA) and Extended Typical Urban (ETU) models are provided. Secondly, the Doppler characteristics are then described in the form of maximum Doppler spread-power delay profile combinations. All the taps have a classical Jakes Doppler power spectral density. Thirdly, the antenna correlation matrices are provided for three levels of correlation: low, medium and high. The transmit antenna correlation matrices when using uniform linear arrays at both the transmitter and receiver are given by [62]:

$$\mathbf{R}_{Tx}^{\frac{1}{2}} = 1, \quad \mathbf{R}_{Tx}^{\frac{1}{2}} = \begin{bmatrix} 1 & \alpha_{Tx} \\ \alpha_{Tx}^{*} & 1 \end{bmatrix}, \quad \mathbf{R}_{Tx}^{\frac{1}{2}} = \begin{bmatrix} 1 & \alpha_{Tx}^{\frac{1}{9}} & \alpha_{Tx}^{\frac{4}{9}} & \alpha_{Tx} \\ \alpha_{Tx}^{\frac{1}{9}\,*} & 1 & \alpha_{Tx}^{\frac{1}{9}} & \alpha_{Tx}^{\frac{4}{9}} \\ \alpha_{Tx}^{\frac{4}{9}\,*} & \alpha_{Tx}^{\frac{1}{9}\,*} & 1 & \alpha_{Tx}^{\frac{1}{9}} \\ \alpha_{Tx}{}^{*} & \alpha_{Tx}^{\frac{4}{9}\,*} & \alpha_{Tx}^{\frac{1}{9}\,*} & 1 \end{bmatrix}, \tag{3.54}$$

for one, two and four antennas respectively.

The receive antenna correlation matrices are given by [62]:

$$\mathbf{R}_{Rx}^{\frac{1}{2}} = 1, \quad \mathbf{R}_{Rx}^{\frac{1}{2}} = \begin{bmatrix} 1 & \beta_{Rx} \\ \beta_{Rx}^{*} & 1 \end{bmatrix}, \quad \mathbf{R}_{Rx}^{\frac{1}{2}} = \begin{bmatrix} 1 & \beta_{Rx}^{\frac{1}{9}} & \beta_{Rx}^{\frac{4}{9}} & \beta_{Rx} \\ \beta_{Rx}^{\frac{1}{9}\,*} & 1 & \beta_{Rx}^{\frac{1}{9}} & \beta_{Rx}^{\frac{4}{9}} \\ \beta_{Rx}^{\frac{4}{9}\,*} & \beta_{Rx}^{\frac{1}{9}\,*} & 1 & \beta_{Rx}^{\frac{1}{9}} \\ \beta_{Rx}{}^{*} & \beta_{Rx}^{\frac{4}{9}\,*} & \beta_{Rx}^{\frac{1}{9}\,*} & 1 \end{bmatrix}, \tag{3.55}$$

for one, two and four antennas respectively.

The three levels of correlation are then defined in terms of α_{Tx} and β_{Rx} and are listed in table 3.1.

Table 3.1: LTE antenna correlation level parameters.

	Low	Medium	High
α_{Tx}	0	0.3	0.9
β_{Rx}	0	0.9	0.9

The spatial correlation $\mathbf{R}_{spat}$ is then fully defined for the $\{N_{Tx} \times N_{Rx}\} \in \{1 \times 2,\ 2 \times 2,\ 4 \times 2,\ 4 \times 4\}$ cases by,

$$\mathbf{R}_{spat} = \mathbf{R}_{Tx}^{\frac{1}{2}} \otimes \mathbf{R}_{Rx}^{\frac{1}{2}}. \tag{3.56}$$

In this way the 3GPP has provided a standardised channel model set that may be used for testing of wireless communication technology in order to determine performance in terms of the LTE standard.

3.7 CONCLUDING REMARKS

This chapter provides a framework for the development of MIMO channels, beginning with abstracted descriptions of interference and propagation mechanisms which lead to a mathematical description of the SISO channel. The statistical properties of time-variant frequency selective channels have been presented along with the discrete time model for simulation. General channel models have been treated before extension to the multiple antenna environment. The framework provided includes temporal, frequency and spatial selectivity and a mechanism for including standardised channel PDPs therein. The channel has also been described in a matrix formulation that is consistent with those of chapter 2. Lastly the LTE MIMO channel has been presented.

CHAPTER 4

MIMO MC-CDMA SYSTEM MODEL

4.1 INTRODUCTION

Chapter 4 describes the functional composition of a MIMO system employing spread spectrum techniques. Both transmit diversity and spatial multiplexing may be achieved using the same functional model of a communication system. Concepts described in the preceding chapters are combined herein by taking a modular approach. This chapter provides a platform from which further investigation into MIMO and CDMA may be conducted. Along with the functional description of the system is a concise mathematical description in the form of a matrix algebraic framework. Finally the methods for ML detection are described.

4.2 FUNCTIONAL SYSTEM DESCRIPTION

4.2.1 Block diagram

Since the real world is inherently causal it is of use to approach the system model in a sequential manner, beginning first with the transmitter and then the receiver. The functional system block diagram is shown in Fig. 4.1. Functional units 1 and 3 are the transmitter and receiver respectively and functional unit 2 is the channel already described in detail in chapter 3.

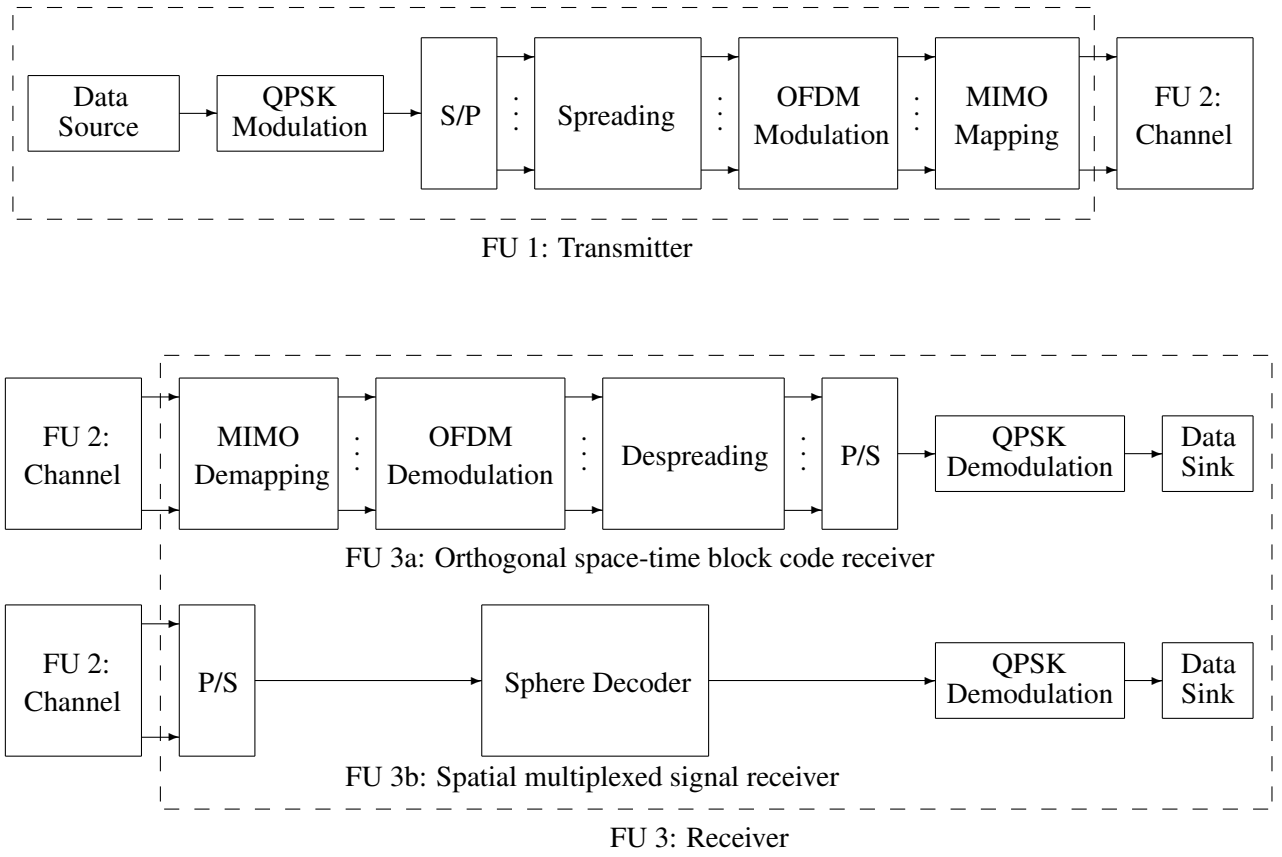

Figure 4.1: Functional system block diagram.

4.2.2 Transmitter

The transmitter consists of a data source which generates uniformly distributed random binary data. The data are then modulated digitally, the result of which is quadrature phase shift keyed (QPSK) symbols. Due to the modular nature of the system any complex digital modulation scheme may replace the QPSK modulator. This will however lead to an increase in the number of digital levels composing the MC-CDMA signal, therefore QPSK is adopted throughout. The resulting stream of complex digital symbols is then split into the appropriate number of parallel streams (the number of streams depends on the number of antennas employed at the transmitter). Each of these parallel streams of data is then spread using the CRCCCs generating the DS spread spectrum signal of the same rate as the symbol stream. Following spreading is the OFDM modulation which is implemented by means of the FFT algorithm.

The MC-CDMA streams are then either mapped to the antennas according to an OSTBC or transmitted simultaneously as in the case of spatial multiplexing. This subtle difference at the transmitter forms the basis for the fundamental difference between the transmit diversity achieving system and the increased capacity system. These two systems are presented in chapters 5 and 6 respectively. Once the mapping or multiplexing is complete the signals are passed to the MIMO channel as described in chapter 3. The different antenna mappings facilitate separate receiver structures. Other than the effects due to propagation the channel may also include transmit and receive filtering. At the transmitter the signals mapped to the antennas would then be upsampled, filtered and digital-to-analogue converted before being passed to the radio frequency (RF) chain associated with each antenna. Such filtering is multipurpose in that it eliminates ISI (in this case interference between subsequent samples) in band limited channels and limits the noise bandwidth at the receiver. In the case where perfect synchronisation is assumed the effects of such filtering and RF chains need not be considered as is the case in this study.

4.2.3 Receiver

The signals received on the RF chains associated with each receive antenna are sampled at the correct sampling instant. The results are digital signals synchronised with the transmitted signals. These digital signals may then be passed to the detection structures in order to reproduce the transmitted data.

Two approaches to detection have been investigated, one for each of the transmission techniques. The methodology that has been adopted is to maximise the likelihood of a transmitted message. The OSTBC receiver (functional unit 3a in Fig. 4.1) is appealing since linear detection of the transmitted signals is possible in the maximum likelihood sense. Thus a compromise is struck between the receiver complexity and the rate of transmission with the gains being in the form of increased SNR at the receiver and thus improved BER performance. On the other hand the spatial multiplexing transmitter improves system capacity by taking advantage of the added degree of freedom: the spatial dimension. The penalty paid for this increase in capacity is the need for a complex non-linear detector at the receiver. The ML detection of these messages may be achieved through the utilisation of the sphere decoder (functional unit 3b in Fig. 4.1). Much research has been conducted in order to reduce the complexity of such a "brute force" algorithm. The result of which, is an algorithm akin to tree search algorithms such as the A* [35]. These have been developed from the matrix formulation of the

MIMO channel, its triangular decomposition and the resulting mathematical properties thereof that allow for sequential detection of parallel symbols.

4.3 MATRIX ALGEBRAIC FRAMEWORK

This treatise describes an amalgamation of the various technologies that have thus far been described in chapter 2. Each of these technologies has been described in terms of a matrix formulation with the goal of a unified matrix algebraic description of the system as a whole. The following framework serves this purpose. Reiterating the previous developments, the data that forms part of an OFDM symbol may be represented as,

$$\mathbf{d}_b = [d_{1,b} \quad d_{2,b} \quad \dots \quad d_{KN,b}]^T, \tag{4.1}$$

with $d_{a,b}$ the ath symbol of the bth data block. These symbols may take on values from a finite complex constellation alphabet $\mathscr{S}$. This data vector is then spread using the CRCCC extended family 2.42. Multiplying 2.42 and 4.1 results in a vector comprised of samples of a DS-CDMA signal,

$$\check{\mathbf{s}}_b = \mathbf{C}^E \mathbf{d}_b. \tag{4.2}$$

The matrix 2.42 is of dimension $MN \times KN$, therefore the vectors 4.1 and 4.2 are of dimension $MN \times 1$. The next step in the process of OFDM symbol generation is to transform 4.2 via the MN-point IDFT. In practice this would be done using the IFFT operation however it is conveniently represented in matrix form as,

$$\mathbf{s}_b = \mathbf{W}^H \mathbf{C}^E \mathbf{d}_b = \mathbf{W}^H \check{\mathbf{s}}_b, \tag{4.3}$$

which results in the vector of samples from a MC-CDMA signal. A typical example of the continuous time baseband signal generated from the vector $\mathbf{s}_b$ is shown in Fig. 4.2. This vector may be thought of as a single OFDM symbol, however before transmission the cyclic prefix must be appended to ensure elimination of ISI. This is achieved by the multiplication of 4.3 with a cyclic extension matrix,

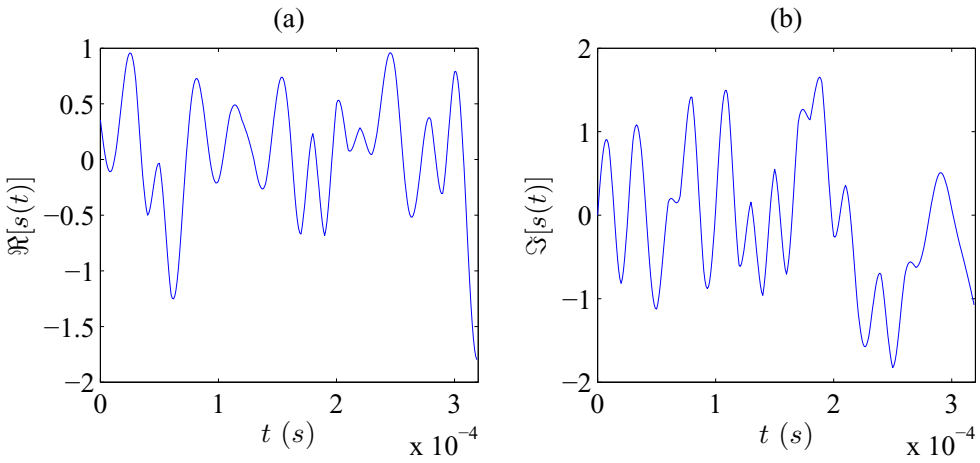

Figure 4.2: (a) The in-phase and (b) quadrature components versus time that make up the baseband MC-CDMA signal (The power of the complex baseband signal has been normalised to unity).

$$\Psi = \begin{bmatrix} \mathbf{0}_{N_{CP},KN-N_{CP}} & \mathbf{I}_{N_{CP}} \\ & \mathbf{I}_{KN} \end{bmatrix}, \tag{4.4}$$

where $\mathbf{0}_{a,b}$ and $\mathbf{I}_a$ are the all zero matrix of dimension $a \times b$ and identity matrix of dimension $a \times a$ respectively. Thus the OFDM symbol to be transmitted, including the cyclic prefix, is,

$$\mathbf{s}_b^{(CP)} = \Psi \mathbf{s}_b \tag{4.5}$$

$$= \Psi \mathbf{W}^H \mathbf{C}^E \mathbf{d}_b \tag{4.6}$$

$$= \mathbf{L}\mathbf{d}_b. \tag{4.7}$$

Here $\mathbf{L} = \Psi \mathbf{W}^H \mathbf{C}^E$ may be thought of as the modulation matrix that includes spreading, OFDM modulation and cyclic prefix addition. This representation is intuitively appealing however a more general approach to MIMO OFDM signals provides a means for analysis and receiver design.

In general a linear STBC may be represented by 2.46. In order to develop ML metrics for various linear STBCs in frequency selective channels consider the following space-time OFDM formulation [31, Ch. 8]:

Frequency selective channels imply multipath propagation effects and analogously channels with memory, therefore sequences of transmission vectors must be considered. That is, N_s sequences

$\check{\mathbf{s}}_a \equiv \check{s}_a[n],\ a = 1,2,\ldots,N_s$ and $n = 0,1,\ldots,N_{FFT}-1$ of are mapped to a sequence of matrices $\{\Phi[n]\}$ each of dimension $N_{Tx} \times N_s$ according to [31, eq. (8.2.2-8.2.3)],

$$\{\check{s}_1[n]\ \check{s}_2[n]\ \ldots \check{s}_{N_s}[n]\} \rightarrow \{\Phi[n]\}, \tag{4.8}$$

where,

$$\Phi[n] = [\phi_1[n]\ \phi_2[n]\ \ldots \phi_{N_s}[n]]\,. \tag{4.9}$$

The mapping for each n is equivalent to 2.46. Following this mapping the set $\{\Phi[n]\}$ is inverse Fourier transformed [31, eq. (8.2.4)]:

$$\mathbf{S}[k] = \frac{1}{\sqrt{N_{FFT}}} \sum_{n=0}^{N_{FFT}-1} \Phi[n] e^{j2\pi \frac{kn}{N_{FFT}}}, \tag{4.10}$$

and the cyclic prefix is appended,

$$\mathbf{S}^{(CP)}[k] = \begin{cases} \mathbf{S}[N_{FFT}+k] & k = -N_{CP},\ldots -1 \\ \mathbf{S}[k] & k = 0,\ldots,N_{FFT}-1 \end{cases} \tag{4.11}$$

The set $\{\mathbf{S}^{(CP)}[k]\} = [\mathbf{s}_1^{(CP)}[k]\ \ldots\ \mathbf{s}_{N_s}^{(CP)}[k]],\ k = -N_{CP},\ldots,N_{FFT}-1$ are then reordered into N_s matrices of dimension $N_{Tx} \times N_{FFT}$ by grouping the columns of each $\mathbf{S}^{(CP)}[k]$ by index into $\{\hat{\mathbf{S}}^{(CP)}[k]\} = \{[\mathbf{s}_n^{(CP)}[-N_{CP}]\ \ldots\ \mathbf{s}_n^{(CP)}[N_{FFT}-1]]\},\ n = 1,2,\ldots,N_s$. The row index of $\{\hat{\mathbf{S}}^{(CP)}[k]\}$ is the spatial dimension corresponding to transmit antennas and the column index is the temporal dimension corresponding to sample period. An entire OFDM symbol is made up of $N_{FFT}+N_{CP}$ samples and there are N_s OFDM symbols. This may be equivalently represented by,

$$\mathbf{S}^{(CP)}[k] \equiv \mathbf{S}_k = \frac{1}{\sqrt{N_{FFT}}} \sum_{a=1}^{N_s} \left(\mathbf{A}_a \bar{\mathbf{s}}_a^{(CP)}[k] + j\mathbf{B}_a \tilde{\mathbf{s}}_a^{(CP)}[k]\right), \tag{4.12}$$

where $\mathbf{s}_n^{(CP)} = \bar{\mathbf{s}}_n^{(CP)} + j\tilde{\mathbf{s}}_n^{(CP)}$ is defined by 4.7. The received samples after removal of the cyclic prefix may then be expressed in matrix form as [31, eq. (8.2.6)],

$$\mathbf{Y}[k] = \sum_{l=0}^{L} \mathbf{H}_l \mathbf{S}^{(CP)}[k-l] + \mathbf{N}_\sigma[k] \quad k = 0, 1, \ldots, N_{FFT} - 1, \tag{4.13}$$

where $\mathbf{H}_l$ is the lth matrix valued channel tap of a length $L+1$ channel, and $\mathbf{N}_\sigma[k]$ is a matrix containing i.i.d. AWGN samples with zero mean and variance σ_n. The ML metric for a linear STBC must be considered for detection of either OSTBC or spatial multiplexing. The ML metric for ST-OFDM with linear STBC is [31, eq. (8.2.12-8.2.14)],

$$\sum_{n=0}^{N_{FFT}-1} \left|\left|\mathbf{z}[n] - \mathbf{F}[n]\hat{\mathbf{s}}'_{ML}[n]\right|\right|^2, \tag{4.14}$$

where,

$$\hat{\mathbf{s}}'_{ML}[n] = \left[\tilde{\mathbf{s}}^T_{ML}[n]\ \tilde{\mathbf{s}}^T_{ML}[n]\right]^T, \tag{4.15}$$

$$\mathbf{z}[n] = vec\left(\mathbf{Z}[n]\right), \tag{4.16}$$

$$\mathbf{Z}[n] = \frac{1}{\sqrt{N_{FFT}}} \sum_{n=0}^{N_{FFT}-1} \mathbf{Y}[k] e^{-j2\pi \frac{kn}{N_{FFT}}}, \tag{4.17}$$

$$\mathbf{F}[n] = \left[\mathbf{F}_a[n]\ \mathbf{F}_b[n]\right], \tag{4.18}$$

$$\mathbf{F}_a[n] = \left[vec\left(\check{\mathbf{H}}\left[2\pi\frac{n}{N_{FFT}}\right]\mathbf{A}_1\right) \ \ldots\ vec\left(\check{\mathbf{H}}\left[2\pi\frac{n}{N_{FFT}}\right]\mathbf{A}_{N_s}\right)\right], \tag{4.19}$$

$$\mathbf{F}_b[n] = \left[j.vec\left(\check{\mathbf{H}}\left[2\pi\frac{n}{N_{FFT}}\right]\mathbf{B}_1\right) \ \ldots\ j.vec\left(\check{\mathbf{H}}\left[2\pi\frac{n}{N_{FFT}}\right]\mathbf{B}_{N_s}\right)\right], \tag{4.20}$$

$$\check{\mathbf{H}}[\omega] = \sum_{l=0}^{L} \mathbf{H}_l e^{-j\omega l}. \tag{4.21}$$

4.3.1 ML detection of OSTBCs and linear precoding

In section 2.5.2 an algorithmic example is presented that describes the ML detection of OSTBCs. This is however a limited approach to the detection process although it is informative. The matrix algebraic framework presented in section 4.3 provides a general means to achieve the same goal. In [31] it has been shown that,

$$\Re\left\{\mathbf{F}^H[n]\mathbf{F}[n]\right\} = \left|\left|\check{\mathbf{H}}\left[2\pi\frac{n}{N_{FFT}}\right]\right|\right|^2 \mathbf{I}. \tag{4.22}$$

The ML detection metric 4.14 in the case of OSTBCs reduces to,

$$\sum_{n=0}^{N_{FFT}-1} \left|\left|\hat{\mathbf{s}}'[n] - \hat{\mathbf{s}}'_{ML}[n]\right|\right|^2, \tag{4.23}$$

where

$$\hat{\mathbf{s}}'[n] = \frac{\Re\{\mathbf{F}^H[n]\mathbf{z}[n]\}}{\left|\left|\check{\mathbf{H}}\left[2\pi\frac{n}{N_{FFT}}\right]\right|\right|^2}. \tag{4.24}$$

The term $\hat{\mathbf{s}}'_{ML}[n]$ would normally then represent a sequence of the most likely symbols thus decoupling the detection of the data, however in this case the spreading operation prevents direct decoupling of the symbols. The spreading operation of the transmitter may be considered as linear precoding of the symbols. Typically this negates the orthogonality of the OSTBCs [31, Sec. 7.5]. In other words, when linear precoding of symbols is performed the independent ML detection of symbols at the receiver, as is the case when employing OSTBCs, is no longer possible. Conversely, in the system under study the CRCCCs do not negate orthogonality of the OSTBC and the ML detection of the decoupled symbols is still possible. This vastly simplifies the receiver structure without compromising the system performance and leverages the benefits offered by the spreading operation.

Before despreading (which may be thought of as a decoding operation) the SNR of each subcarrier or chip is,

$$\frac{\left|\left|\check{\mathbf{H}}\left[2\pi\frac{n}{N_{FFT}}\right]\right|\right|^2}{\sigma^2}. \tag{4.25}$$

This SNR indicates that a diversity order of $N_{Rx}N_{Tx}$ is achievable in multipath fading if symbols are transmitted [31]. However the processing gain associated with the despreading of spread spectrum signals predicts a further improvement in performance. 4.24 is the sufficient statistic for the despreading process which is passed from the demapping functional sub-unit of the receiver to the despreading functional sub-unit (FU: 3a in Fig. 4.1). Thus the algorithmic approach for one receive antenna (as in section 2.5.2) is generalised to multiple receive antennas.

4.3.2 Near ML detection of spatially multiplexed signals

In the case of the spatial multiplexing transmitter the sphere decoder may be used to perform near ML detection. The sphere decoder requires the received signals to be formulated as follows:

$$\mathbf{r} = \mathbf{H}\mathbf{s} + \mathbf{n}_\sigma, \tag{4.26}$$

which is detailed in section 3.5.1 and $\mathbf{H}$ takes on the form given in 3.43. The vector $\mathbf{s}$ is then given by,

$$\mathbf{s} = vec(\mathbf{S}) = [\mathbf{s}_1^T \ \mathbf{s}_2^T \ \dots \ \mathbf{s}_{N_{Tx}}^T]^T, \tag{4.27}$$

where $\mathbf{s}_i$ is defined by 4.7. Therefore the effective channel matrix, including spreading, OFDM and CP matrices is,

$$\tilde{\mathbf{H}} = \mathbf{H}\Phi^{(P)}\left(\mathbf{I}_{N_{Tx}} \otimes \mathbf{L}\right), \tag{4.28}$$

where $\Phi^{(P)}$ is a permutation matrix that performs the equivalent function to the $vec(\cdot)$ operator. With this formulation the procedure outlined in section 2.5.4 may be followed to perform joint ML detection of the symbols,

$$\mathbf{d} = vec([\mathbf{d}_1 \ \mathbf{d}_2 \ \dots \ \mathbf{d}_{N_{Tx}}]) = [\mathbf{d}_1^T \ \mathbf{d}_2^T \ \dots \ \mathbf{d}_{N_{Tx}}^T]^T, \tag{4.29}$$

in the expression,

$$\mathbf{r} = \tilde{\mathbf{H}}\mathbf{d} + \mathbf{n}_\sigma \tag{4.30}$$

which is equivalent to 4.26.

4.4 CONCLUDING REMARKS

The mathematical developments of chapters 2 and 3 have been combined in the functional design of the MIMO MC-CDMA modem in this chapter. This modem may take the form of one of two systems that respectively achieve transmit diversity or improved capacity. The matrix formulations presented thus far have been integrated into a matrix algebraic framework that facilitates the detection algorithms necessary for the receivers of two distinct systems. This chapter concludes the system design. The following chapters treat the investigation into and performance evaluation of the respective systems.

CHAPTER 5

TRANSMIT DIVERSITY MC-CDMA MODEM

5.1 RESEARCH QUESTIONS

The BER as a function of the bit energy-to-noise density ratio serves as universal measure of the performance of a communication system. It is universal in the sense that it is independent of the system bandwidth and digital modulation scheme thus allowing the performance of distinctly different systems to be compared. Typically this can be done by deriving an analytical expression based on the modulation scheme, coding algorithms, channel characteristics and receiver structure. However taking all these factors into account often makes the analytical problem prohibitively complex to solve, as is the case in this investigation. The alternative is to estimate the BER through Monte-Carlo simulation.

The preceding discussion describes many parameters that may form part of evaluation of the proposed systems. These include the numbers of transmit and receive antennas, Doppler characteristics, channel length, PDP and antenna correlation. In order to reduce the number of possible results while being able to draw meaningful conclusions the following research question have been proposed:

What is the probability of bit error (BER) given the SNR in the transmit diversity MC-CDMA MIMO wireless communication system?
What is the effect of Doppler on the BER?
What is the effect of frequency selective fading on the BER?
What is the effect of antenna correlation on the BER?
What is the BER of the proposed transmit diversity system under the LTE MIMO channel conditions?

From these questions it is obvious that the BER as a function of the normalised bit energy to noise power ratio plays a pivotal role in evaluating the proposed systems. For this reason six experiments have been performed in an effort to provide insight into each of the phenomena that affect BER. The first of the experiments serves as a benchmark of the system in AWGN (without fading). This simplistic channel, however unrealistic, provides insight into the underlying signal corruption mechanism. The subsequent experiments attempt to address each of the aspects (spatial diversity and types of fading) of wireless communication systems: multiple antennas, temporal selectivity, frequency selectivity and spatial correlation. The methodology adopted was to test the system using a channel characterised by one of the phenomena while assuming that the others are not present. The last experiment was included in order to illustrate the system performance in channel conditions with a combination of the abovementioned aspects and takes the form of a standardised channel model: the LTE MIMO channel.

5.2 AWGN EXPERIMENT

5.2.1 Hypothesis

It is hypothesised that the transmit diversity MC-CDMA system will achieve BER equivalent to that of a narrowband uncoded BPSK system in AWGN.

5.2.2 Experimental parameters

Noise is present is all communication systems. The AWGN channel therefore forms a fundamental building block of all other simulated fading channels. The transmit diversity system has been simulated with the parameters listed in Table 5.1 for various numbers of transmit and receive antennas.
The code rate in the case of this experiment (and subsequent experiment) is maximised according to equation 2.47, the maximum code rate for orthogonal designs [36]. It should be noted that the code rate is a function of the number of transmit antennas.

Table 5.1: AWGN experiment simulation parameters.

(a) System

Parameter	Symbol	Value
Sampling frequency	F_{sa}	1 MHz
Code family size	K	8
Flock size	M	8
Element code length	N	4
FFT length	N_{FFT}	MN
Code rate	R	R_{max}
Bit rate/frequency	F_{bit}	$2F_{sa}$

(b) Channel

Parameter	Symbol	Value
Maximum Doppler shift	F_D	0 Hz
Length	L	0
Antenna correlation	N/A	Low

5.2.3 Results

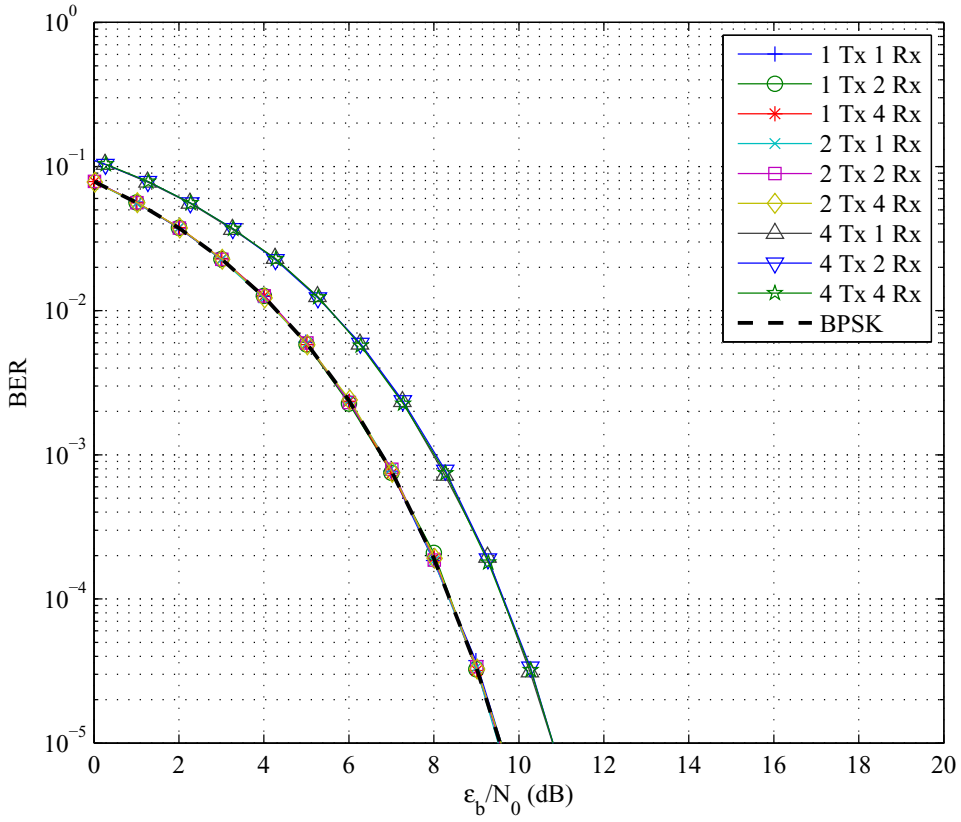

Figure 5.1: BER vs. SNR per bit for the transmit diversity system in AWGN.

The results of the AWGN experiment may be seen in Fig. 5.1. The theoretical bit error probability for narrowband BPSK in AWGN is also shown for comparison.

5.2.4 Conclusion

It can be seen that the transmit diversity MC-CDMA system achieves the same performance as uncoded narrowband BPSK (or QPSK) in AWGN. Furthermore this is independent of the number of receive antennas. The performance loss observed in cases where $N_{Tx} > 2$ is as a result of the reduced rate of the OSTBC and is equivalent to 1.25 dB.

As hypothesised the transmit diversity MC-CDMA system achieves a BER equivalent to that of an uncoded narrowband BPSK system in AWGN.

5.3 MULTIPLE ANTENNA DIVERSITY EXPERIMENT

5.3.1 Hypothesis

It is hypothesised that the transmit diversity MC-CDMA system will achieve spatial diversity order of $N_{Tx}N_{Rx}$, which is equivalent to that of an ST-OFDM system.

5.3.2 Experimental parameters

A spatial diversity order of $N_{Tx}N_{Rx}$ has been observed in narrowband BPSK systems with time-invariant Rayleigh flat fading when OSTBC are employed [31]. The transmit diversity system has been simulated under these conditions with the parameters listed in Table 5.2 for various numbers of transmit and receive antennas.

The code rate given is again the maximum code rate for orthogonal designs given by [36] as in the case of the AWGN experiment.

Table 5.2: Multiple antenna diversity experiment parameters.

(a) System

Parameter	Symbol	Value
Sampling frequency	F_{sa}	1 MHz
Code family size	K	8
Flock size	M	8
Element code length	N	4
FFT length	N_{FFT}	MN
Code rate	R	R_{max}
Bit rate/frequency	F_{bit}	$2R_{max}F_{sa}$

(b) Channel

Parameter	Symbol	Value
Maximum Doppler shift	F_D	0 Hz
Length	L	0
Antenna correlation	N/A	Low

5.3.3 Results

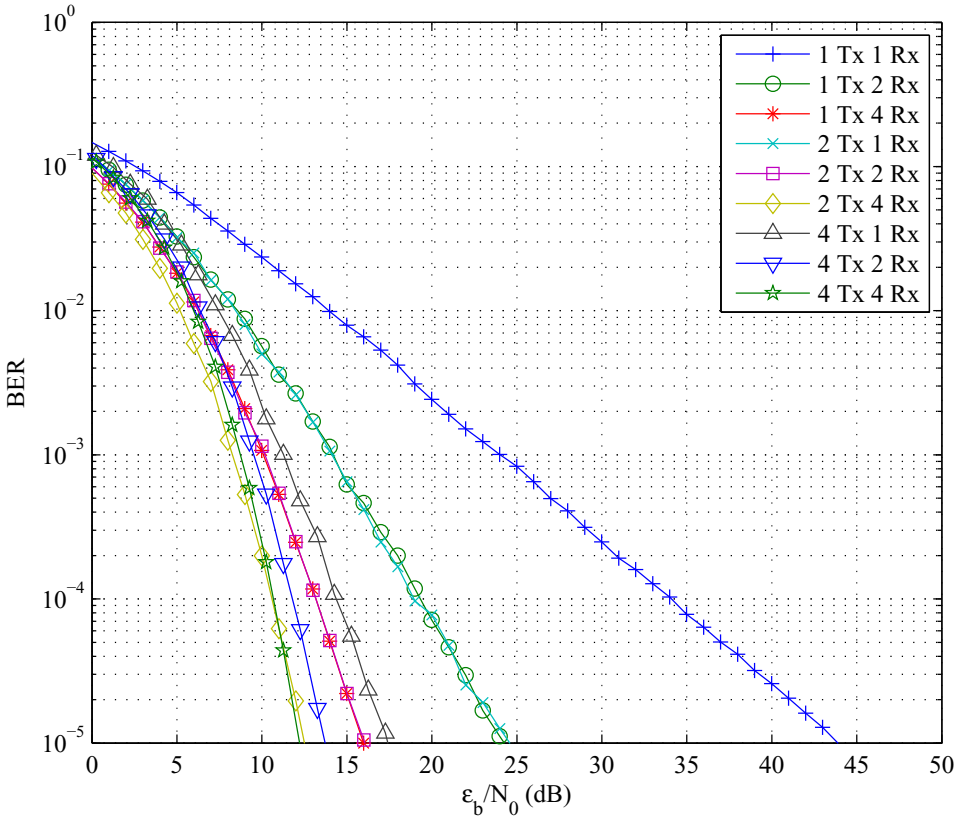

Figure 5.2: BER vs. SNR per bit for the transmit diversity system in frequency non-selective time-invariant Rayleigh fading.

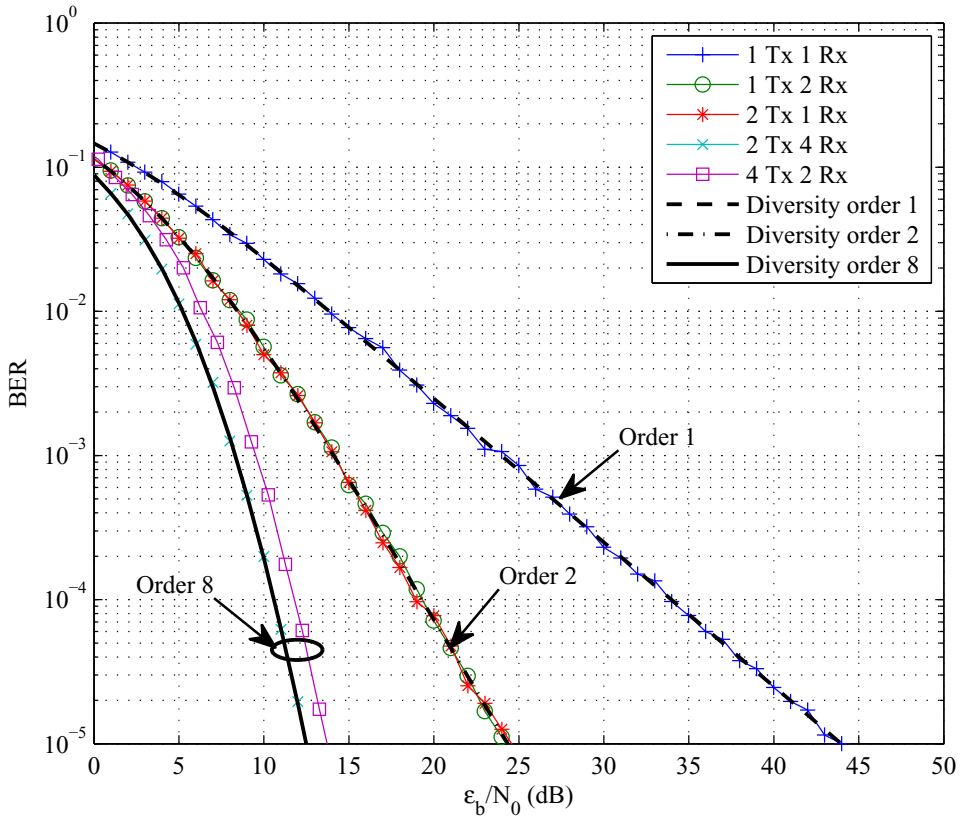

Figure 5.3: BER vs. SNR per bit for the transmit diversity system in frequency non-selective time-invariant Rayleigh fading (selected results part 1).

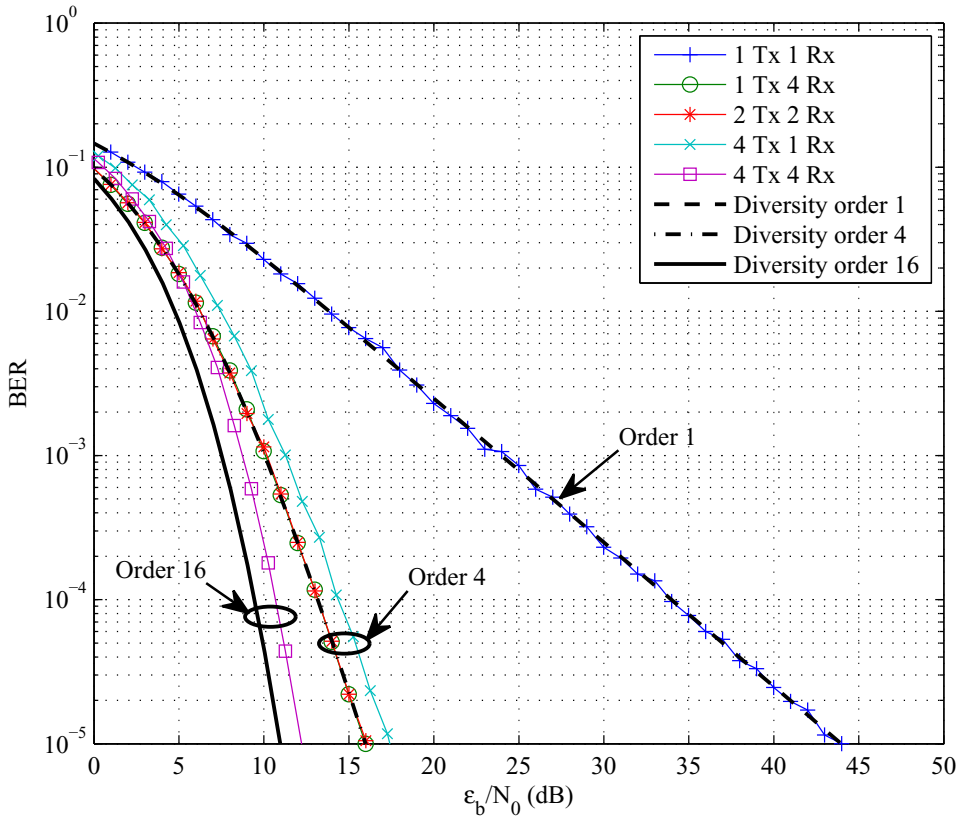

Figure 5.4: BER vs. SNR per bit for the transmit diversity system in frequency non-selective time-invariant Rayleigh fading (selected results part 2).

The results of the multiple antenna diversity experiment may be seen in Figs 5.2 - 5.4. Fig. 5.2 shows the full set of results while Figs 5.3 and 5.4 show selected results along with the theoretical bit error probabilities for systems with appropriated diversity orders, for comparison.

5.3.4 Conclusion

The most notable feature of these results is the gradients of the various curves, which are indicative of the diversity order. It can be seen from Figs 5.3 and 5.4 that the gradients of the various results equal that of systems with a diversity order of $N_{Tx}N_{Rx}$. It must also be noted that the simulations with $N_{Tx} = 4$ suffer a performance penalty compared to simulation with the same $N_{Tx}N_{Rx}$ product. This is due to the reduced rate of the OSTBCs for systems with $N_{Tx} > 2$ and is approximately equal to 1.25 dB.

As hypothesised, the transmit diversity MC-CDMA system achieves a spatial diversity order of $N_{Tx}N_{Rx}$ which is equivalent to ST-OFDM.

5.4 DOPPLER EFFECT EXPERIMENT

5.4.1 Hypothesis

It is hypothesised that while simultaneously providing multiple access, when viewed as a form of linear precoding, the CDMA encoding will allow temporal diversity to be extracted, in addition to the spatial diversity of an ST-OFDM system.

5.4.2 Experimental parameters

The Doppler effect introduces temporal variability to the channel. Rayleigh flat fading with a maximum Doppler shift ranging from 5 Hz to 300 Hz has been simulated. A 2×2 MIMO channel was adopted with simulation parameters listed in Table 5.3.

Table 5.3: Doppler experiment parameters.

(a) System

Parameter	Symbol	Value
Sampling frequency	F_{sa}	1 MHz
Code family size	K	8
Flock size	M	8
Element code length	N	4
FFT length	N_{FFT}	MN
Transmit antennas	N_{Tx}	2
Receive antennas	N_{Rx}	2
Code rate	R	1
Bit rate/frequency	F_{bit}	$2F_{sa}$

(b) Channel

Parameter	Symbol	Value
Maximum Doppler shift	F_D	{5 Hz, 30 Hz, 70 Hz, 300 Hz}
Length	L	0
Antenna correlation	N/A	Low

5.4.3 Results

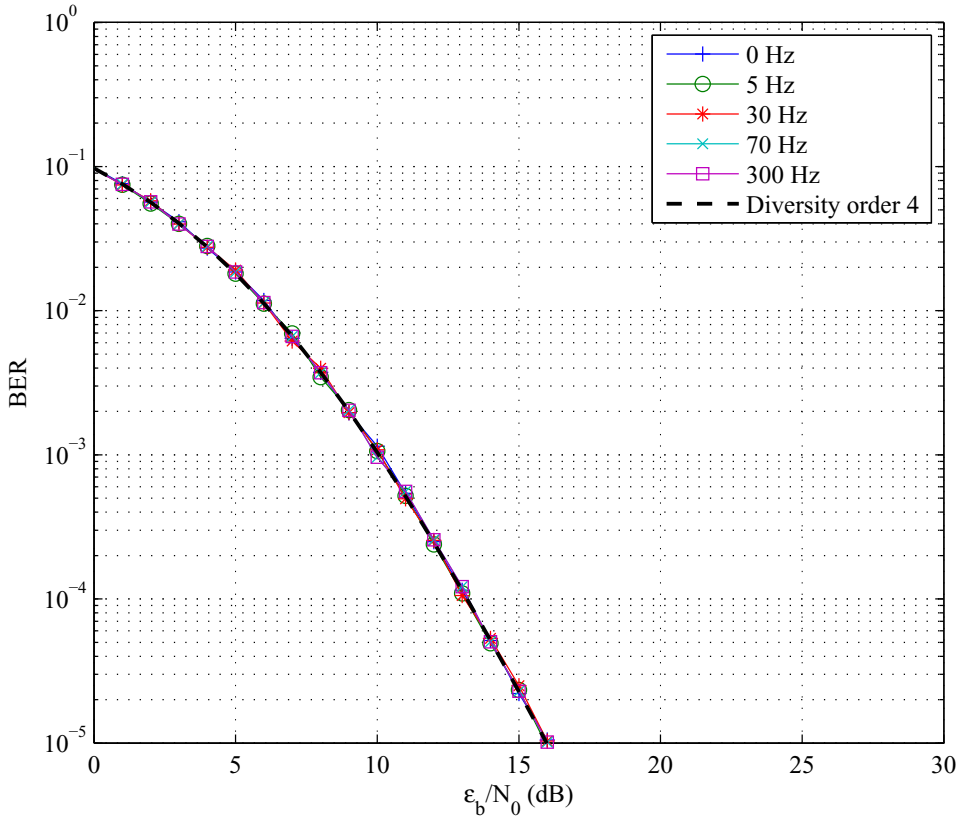

Figure 5.5: BER vs. SNR per bit for the transmit diversity system in frequency non-selective Rayleigh fading.

The results of the Doppler effect experiment may be seen in Fig. 5.5. The theoretical bit error probability for a system with fourth order diversity is also shown for comparison.

5.4.4 Conclusion

What is an initially perplexing result, the fact that the system appears to be unaffected by Doppler shift, is explained by nature of the DS spreading that is employed. The data are spread in the DS manner and the resulting signals are then transformed via the IFFT. The result of this is to distribute energy from all the symbols across all the subcarriers. This provides a means to extract multipath diversity (as will be seen is subsequent experiments) but not temporal diversity. The diversity order of the

system with Doppler is equivalent to that of the flat faded theoretical diversity system. Performance loss is however not observed since perfect channel state information (CSI) is assumed.

Opposed to the hypothesis the transmit diversity MC-CDMA system does not extract temporal diversity while providing multiple access via the CRCCCs.

5.5 MULTIPATH EXPERIMENT

5.5.1 Hypothesis

It is hypothesised that while simultaneously providing multiple access, when viewed as a form of linear precoding, the CDMA encoding will allow multipath diversity to be extracted in addition to the spatial diversity of an ST-OFDM system.

5.5.2 Experimental parameters

Multipath propagation causes frequency selectivity in the channel. The 2×2 MIMO system has been simulated with a Rayleigh faded time-invariant multipath channel. The uniform and exponential decay power delay profiles for channel lengths of 1 to 6 chip-spaced taps were utilised. The parameters of the simulation are listed in Table 5.4.

Table 5.4: Multipath experiment parameters.

(a) System

Parameter	Symbol	Value
Sampling frequency	F_{sa}	1 MHz
Code family size	K	8
Flock size	M	8
Element code length	N	4
FFT length	N_{FFT}	MN
Transmit antennas	N_{Tx}	2
Receive antennas	N_{Rx}	2
Code rate	R	1
Bit rate/frequency	F_{bit}	$2F_{sa}$

(b) Channel

Parameter	Symbol	Value
Maximum Doppler shift	F_D	0 Hz
Length	L	$\{0, 1, 2, 3, 4, 5\}$
Antenna correlation	N/A	Low

5.5.3 Results

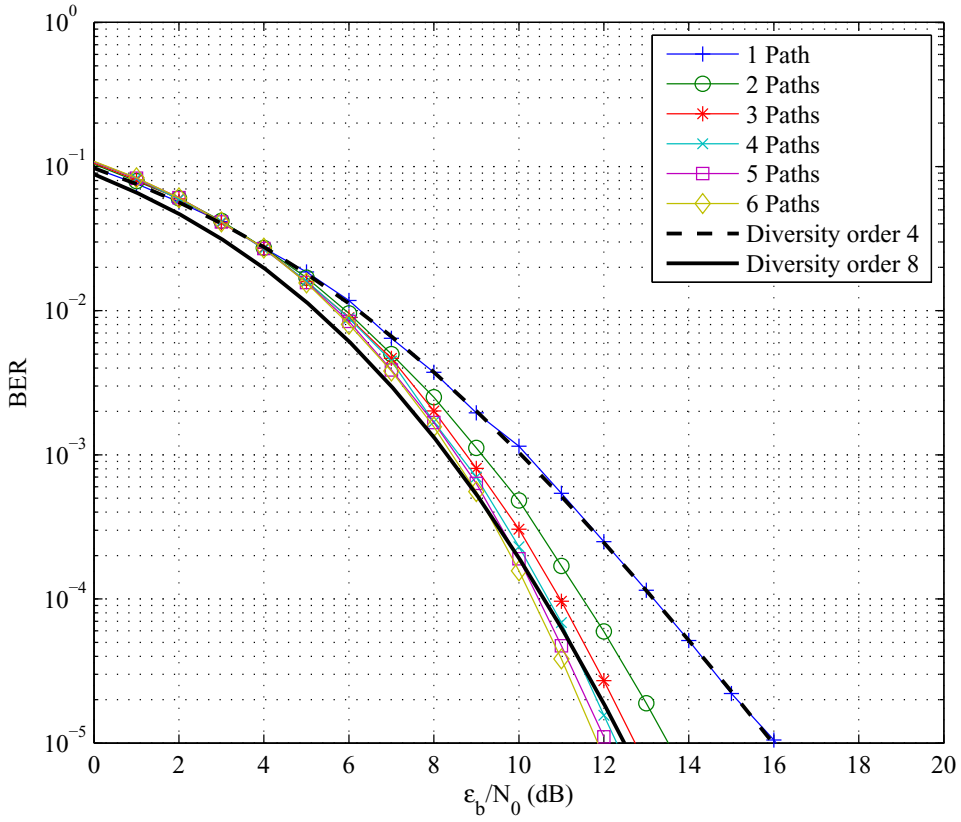

Figure 5.6: BER vs. SNR per bit for the transmit diversity system in frequency selective fading with a uniform PDP.

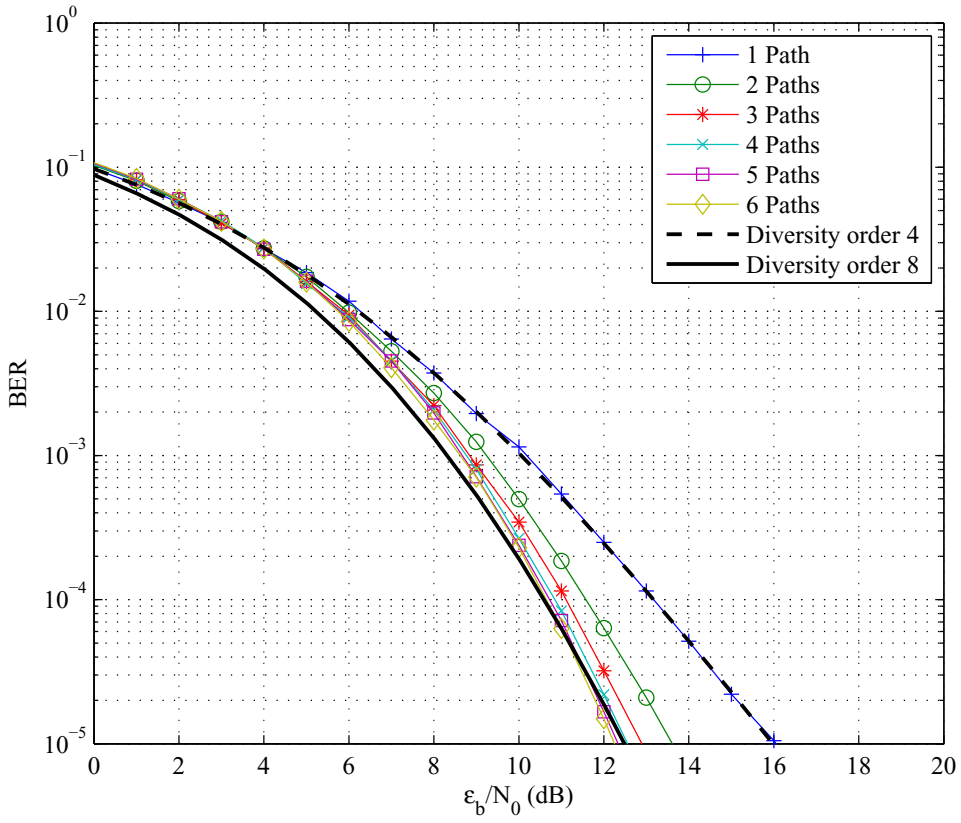

Figure 5.7: BER vs. SNR for the transmit diversity system in frequency selective fading with an exponential decay delay PDP.

The results of the multipath experiment may be seen in Figs 5.6 and 5.7. Fig. 5.6 shows the results for the system simulated with the uniform PDP channel and Fig. 5.7 with an exponentially decaying PDP channel. Both of these sets of simulations were conducted for channel with 1 to 6 paths. The theoretical bit error probabilities for systems with fourth and eighth order diversity are also shown for comparison.

5.5.4 Conclusion

Two features emerge from these results. Firstly, the sets appear to be almost identical for the different channel delay profiles. This is understandable since, as stated, perfect CSI is assumed. Secondly, and more importantly, the system gains a performance advantage for each additional path in the channel. This is due to the nature of the spreading, which allows the added multipath diversity of the channel

to be extracted. This is also a unique result, since ST-OFDM does not gain an advantage in multipath channels [31].

As hypothesised, the transmit diversity MC-CDMA system does extract additional multipath diversity while providing multiple access.

5.6 ANTENNA CORRELATION EXPERIMENT

5.6.1 Hypothesis

It is hypothesised that the performance of the transmit diversity MC-CDMA system will be degraded with correlated antennas.

5.6.2 Experimental parameters

Signals transmitted from antennas making up an array propagate through the same environment and interact with the same objects; therefore the fading exhibits certain degrees of correlation. The time-invariant Rayleigh flat fading channel was employed. Antenna correlations of low, medium and high correlation, specified in the LTE standard [62] for 2×2 MIMO channels, were adopted. The simulation parameters are listed in Table 5.5.

Table 5.5: Antenna correlation experiment parameters.

(a) System

Parameter	Symbol	Value
Sampling frequency	F_{sa}	1 MHz
Code family size	K	8
Flock size	M	8
Element code length	N	4
FFT length	N_{FFT}	MN
Transmit antennas	N_{Tx}	2
Receive antennas	N_{Rx}	2
Code rate	R	1
Bit rate/frequency	F_{bit}	$2F_{sa}$

(b) Channel

Parameter	Symbol	Value
Maximum Doppler shift	F_D	0 Hz
Length	L	0
Antenna correlation	N/A	{Low, Medium, High}

5.6.3 Results

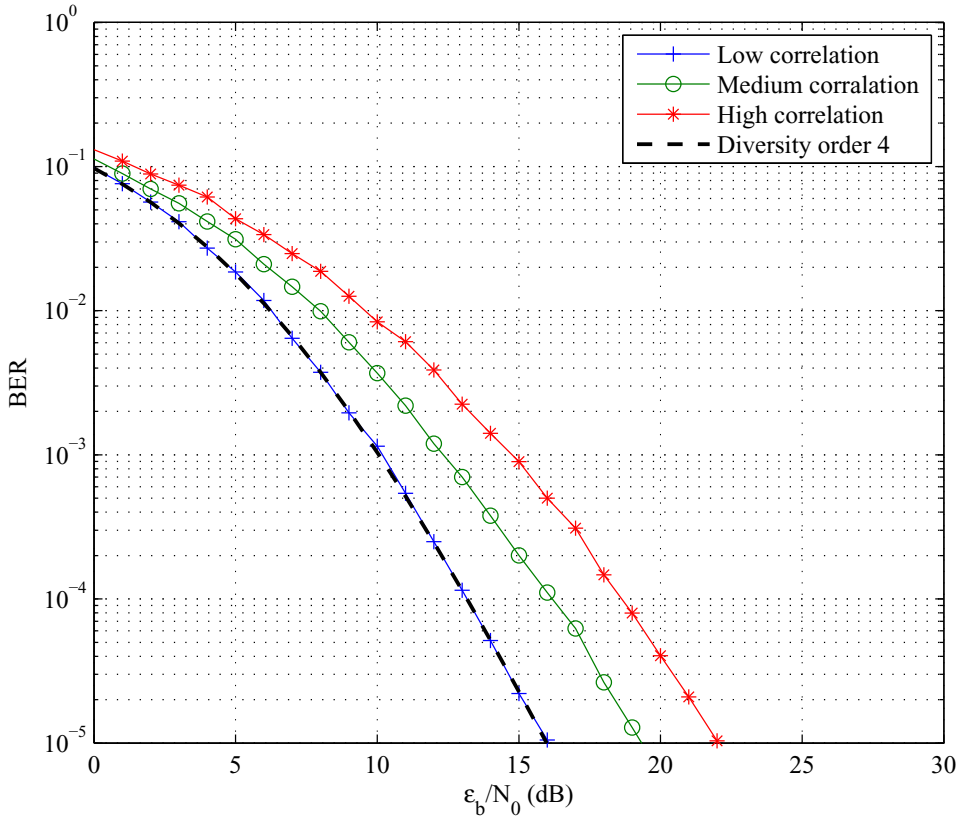

Figure 5.8: BER vs. SNR per bit for the transmit diversity system in frequency non-selective Rayleigh fading with correlated antennas.

The results of the antenna correlation experiment may be seen in Fig. 5.8. The theoretical bit error probability for a system with fourth order diversity is also shown for comparison.

5.6.4 Conclusion

From Fig. 5.8 it can be seen that the system pays a marginal penalty with respect to diversity, i.e. the reduction in gradient of the BER curves is small. Furthermore, a large penalty is paid due to antenna correlation as can be seen from the horizontal translation of the medium and high correlation bit error probabilities of 2.15 *dB* and 4.57 *dB* at a BER of 10^{-3} from the low correlation result, respectively.

As hypothesised the performance of the transmit diversity MC-CDMA system is indeed degraded with correlated antennas.

CHAPTER 6

SPATIALLY MULTIPLEXED MC-CDMA MODEM

6.1 RESEARCH QUESTIONS

As in the previous Chapter the performance of the spatially multiplexed system has been evaluated in terms of the BER as a function of the bit energy-to-noise density ratio. The same methodology has been adopted in order to estimate this quantity: namely Monte-Carlo simulation. Again in order to produce meaningful results without exhausting all parameter combinations the following research questions have been proposed:

What is the probability of bit error (BER), given the SNR in the spatially multiplexed MC-CDMA MIMO wireless communication system?
What is the effect of Doppler on the BER?
What is the effect of frequency selective fading on the BER?
What is the effect of antenna correlation on the BER?
What is the BER of the proposed spatially multiplexed system under the LTE MIMO channel conditions?

Methodology consistent with Chapter 5 has been adopted throughout simulation of the spatially multiplexed system.

6.2 AWGN EXPERIMENT

Including “experiment” in the title of this sub-section is a misnomer, since it is not possible to simulate spatial multiplexing in only the presence of noise. The reason for this is that the channel matrix, **H** in

the expression,

$$\mathbf{r} = \mathbf{H}\mathbf{s} + \mathbf{n} \tag{6.1}$$

would be populated by ones (or some single constant value). The problem is best understood when attempting to invert **H**; it turns out that this matrix is singular or that its inverse does not exist. Another way of interpreting this is that all the joint detection algorithms, whether zero forcing or sphere decoder, rely on the **H** having full rank in order to decode the transmitted data. This particular matrix has rank no greater than one. Herein lies the problem: with low rank channel matrices data detection is not possible. This problem not only exists for AWGN channels but also for real world channels with low transmit and receive antenna correlation where the presence of the "pinhole" effect can cause the channel matrix to have low rank [64].

6.3 MULTIPLE ANTENNA DIVERSITY EXPERIMENT

6.3.1 Hypothesis

It is hypothesised that the spatially multiplexed MC-CDMA system will achieve spatial diversity of N_{Rx}, which is equivalent to that of the BLAST system [6].

6.3.2 Experimental parameters

Without the temporal coding of a STBC, the spatial multiplexing system has a potential spatial diversity of only N_{Rx}. The system has been subjected to time-invariant Rayleigh flat fading with simulation parameters listed in Table 6.1 for various numbers of transmit and receive antennas.

Table 6.1: Multiple antenna diversity experiment parameters.

(a) System

Parameter	Symbol	Value
Sampling frequency	F_{sa}	1 MHz
Code family size	K	8
Flock size	M	8
Element code length	N	4
FFT length	N_{FFT}	MN
Code rate	R	N_{Tx}
Bit rate/frequency	F_{bit}	$2N_{Tx}F_{sa}$

(b) Channel

Parameter	Symbol	Value
Maximum Doppler shift	F_D	0 Hz
Length	L	0
Antenna correlation	N/A	Low

6.3.3 Results

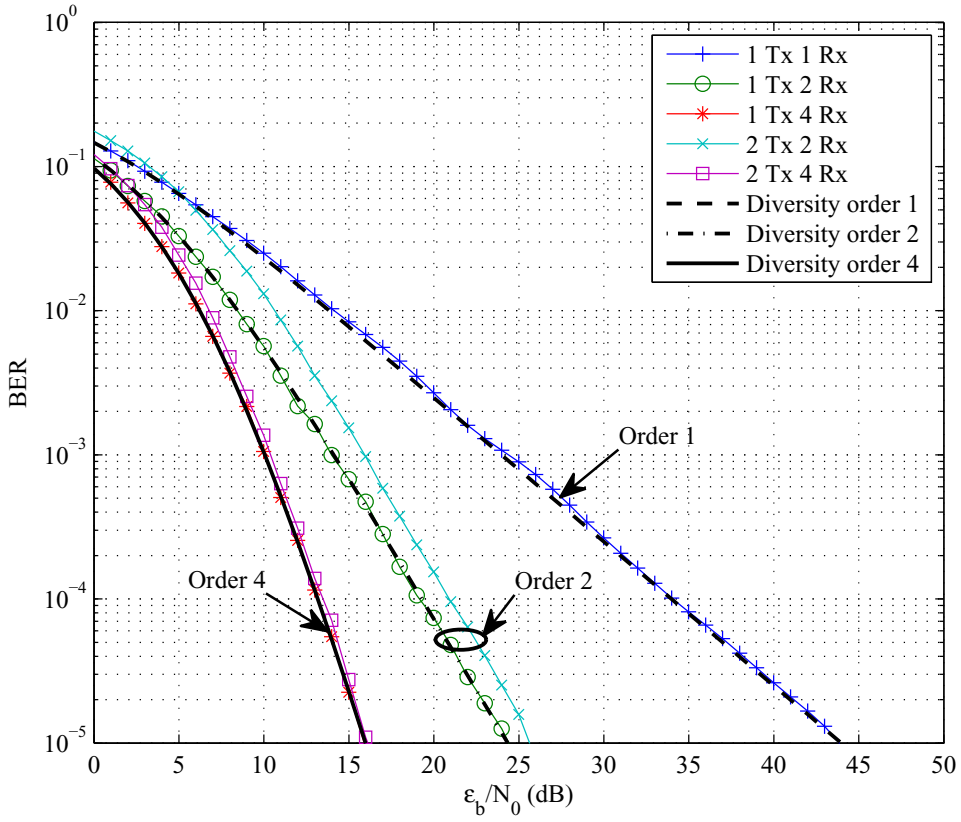

Figure 6.1: BER vs. SNR per bit for the spatially multiplexed system in frequency non-selective time-invariant Rayleigh fading.

The results of the multiple antenna diversity experiment are shown in Fig. 6.1 along with the first, second and fourth order diversity theoretical bit error probability curves.

6.3.4 Conclusion

It can be seen that the spatial multiplexing system achieves the receive diversity order predicted. It is also interesting to note that in the case of $N_{Tx} = N_{Rx} = 2$ there is a reduction of 2 dB performance at a BER of 10^{-3}. This is due to the near optimal nature of the sphere decoder coupled with the search space of 2^{128}. Also it can be seen that the performance penalty is less, 0.4 dB at a BER of 10^{-3}, when $N_{Rx} = 4$ and there is more information available to the decoder.

As hypothesised, the spatially multiplexed MC-CDMA system achieves spatial diversity of N_{Rx}.

6.4 DOPPLER EFFECT EXPERIMENT

6.4.1 Hypothesis

It is hypothesised that while simultaneously providing multiple access, when viewed as a form of linear precoding, the CDMA encoding will allow temporal diversity to be extracted in addition to the spatial diversity of a spatially multiplexed system. In contrast to this, it is further hypothesised that performance degradation will manifest due to the channel not being constant over all the transmitted OFDM symbols.

6.4.2 Experimental parameters

The receiver in the ST-OFDM based system essentially reverses the operations performed during modulation at the transmitter. This means that the FFT of the channel impulse response must be performed. The definition of ST-OFDM [31] assumes that the channel impulse response is time invariant. This directly conflicts with the Doppler channel and presents a problem. At what moment in time should the FFT of the channel impulse response be calculated? The approach that was taken herein was to assume the worst case and compute the FFT of the channel at the moment of reception of the first sample ($t = 0$ s).

The simulation parameters of the time varying flat fading channel are listed in Table 6.2. The 2×2 MIMO channel was utilised with maximum Doppler spread of 5 Hz, 30 Hz, 70 Hz, 100 Hz, 225 Hz and 300 Hz. This range of frequencies along with the sampling frequency $F_{sa} = 1$ MHz were selected to illustrate the effect of temporal variability as described by the 3GPP's LTE propagation conditions [62, Appendix B.2.2]. Furthermore the sampling frequency (equivalent to the chip rate of 1 Mcps in the system under investigation) was selected to be in the same order of magnitude as the chip rate, 3.84 Mcps, specified by the WCDMA's user equipment standard [65].

Table 6.2: Doppler experiment parameters.

(a) System

Parameter	Symbol	Value
Sampling frequency	F_{sa}	1 MHz
Code family size	K	8
Flock size	M	8
Element code length	N	4
FFT length	N_{FFT}	MN
Transmit antennas	N_{Tx}	2
Receive antennas	N_{Rx}	2
Code rate	R	2
Bit rate/frequency	F_{bit}	$2F_{sa}$

(b) Channel

Parameter	Symbol	Value
Maximum Doppler shift	F_D	{0 Hz, 5 Hz, 30 Hz, 70 Hz, 100 Hz, 225 Hz, 300 Hz}
Length	L	0
Antenna correlation	N/A	Low

6.4.3 Results

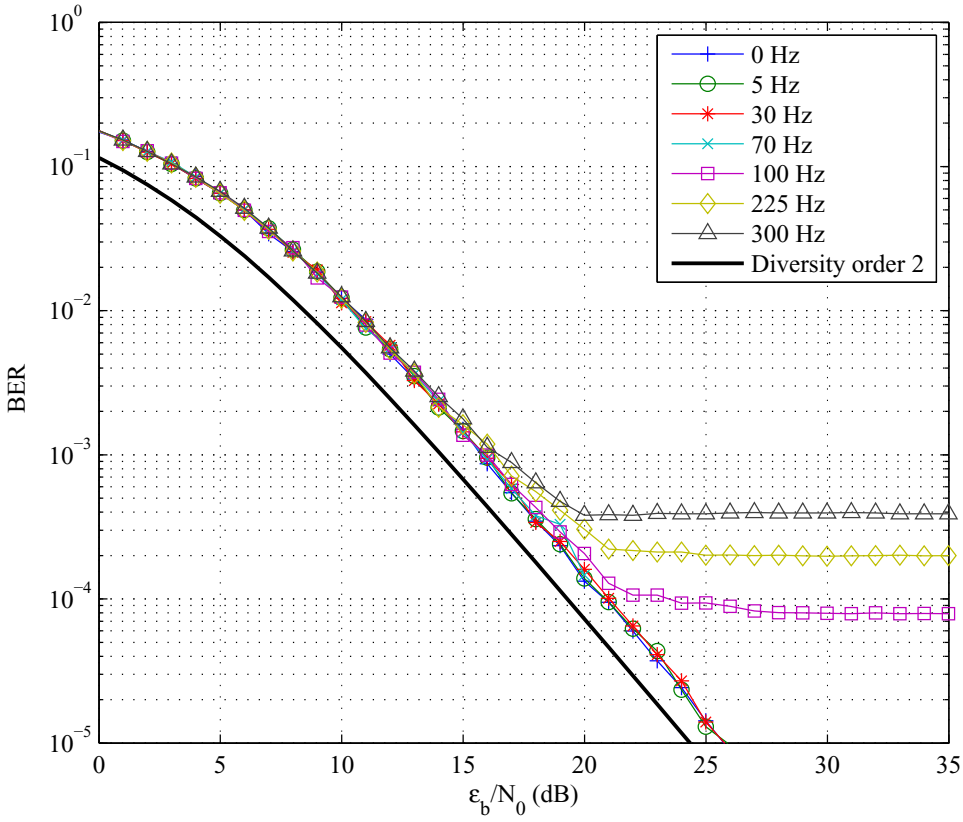

Figure 6.2: BER vs. SNR per bit for the spatially multiplexed system in frequency non-selective Rayleigh fading.

The results of the Doppler effect experiment may be seen in Fig. 6.2. The second order diversity theoretical bit error probability is also shown for comparison.

6.4.4 Conclusion

From Fig. 6.2 it can be seen that the system achieves a second order diversity. This is a result of the two receive antennas. Again the loss in performance is evident due to the near optimal decoder and the minimal received samples that it uses to detect the transmitted data. It is also notable that the sphere decoder is unaffected by Doppler at lower frequencies. The time variant nature of the Doppler effect comes into play at higher frequencies manifesting in the error floor seen from 100 Hz and

greater. In stark contrast this effect is not seen in the Doppler effect experiment of chapter 5 where the only difference is the use of OSTBCs as opposed to spatial multiplexing. The unrecoverable error floor in this experiment can only be as a result of the incomplete nature of the sphere decoding algorithm employed. To clarify, the algorithm employed lacks the post sorting stage and as a result error propagation is possible due to the aggressive reduction in hypersphere radius. This result merits further investigation since the ratio of the frame length to the sampling frequency is small. With longer spreading codes it is likely that the error floor will manifest at lower frequencies. Lastly, no temporal diversity is extracted since spreading is only performed in a single dimension. Extending this to the second dimension may yield a counter effect to that resulting in the error floor.

Contrary to the hypothesis the spatially multiplexed system does not extract temporal diversity. Furthermore, severe performance degradation is observed at higher Doppler frequencies.

6.5 MULTIPATH EXPERIMENT

6.5.1 Hypothesis

It is hypothesised that while simultaneously providing multiple access, when viewed as a form of linear precoding, the CDMA encoding will allow multipath diversity to be extracted in addition to the spatial diversity of a spatially multiplexed system.

6.5.2 Experimental parameters

Table 6.3 lists the parameters used for the multipath experiment. A uniform PDP channel model was employed, with time-invariant Rayleigh faded taps. The channel lengths were varied from 1 to 6 chip-spaced taps with 2 transmit and 2 receive antennas.

Table 6.3: Multipath experiment parameters.

(a) System

Parameter	Symbol	Value
Sampling frequency	F_{sa}	1 MHz
Code family size	K	8
Flock size	M	8
Element code length	N	4
FFT length	N_{FFT}	MN
Transmit antennas	N_{Tx}	2
Receive antennas	N_{Rx}	2
Code rate	R	2
Bit rate/frequency	F_{bit}	$2F_{sa}$

(b) Channel

Parameter	Symbol	Value
Maximum Doppler shift	F_D	0 Hz
Length	L	$\{0, 1, 2, 3, 4, 5\}$
Antenna correlation	N/A	Low

6.5.3 Results

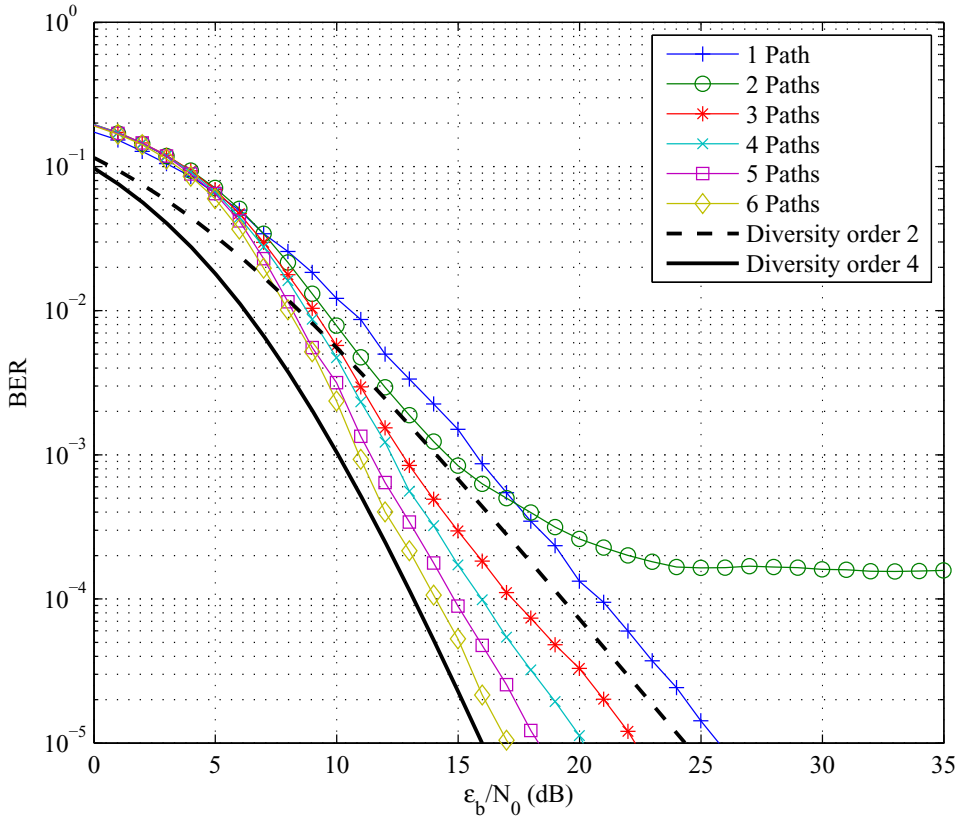

Figure 6.3: BER vs. SNR per bit for the spatially multiplexed system in frequency selective fading with a uniform PDP employing the sorted QR decomposition algoritm without post sorting at the decoder.

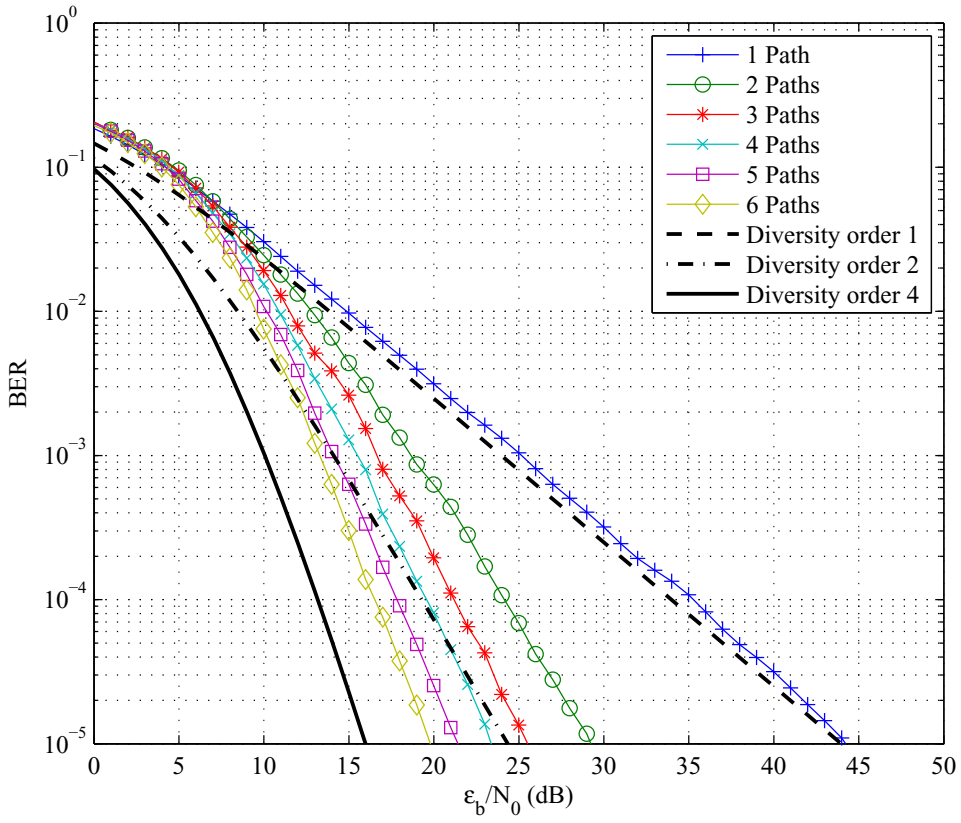

Figure 6.4: BER vs. SNR per bit for the spatially multiplexed system in frequency selective fading with a uniform PDP employing the unsorted QR decomposition algoritm at the decoder.

Fig. 6.3 shows the bit error probabilities for the spatially multiplexed system simulated in a multipath channel. The decoder employed the sorted QR decomposition algorithm without the post sorting algorithm. The next figure, Fig. 6.4 shows the results of the same experiment when the unsorted QR decomposition was employed in the decoder.

6.5.4 Conclusion

The results shown in Fig. 6.3 inspired the repeat of this experiment due to the error floor observed in the case of two paths. This may be explained by similar logic to the Doppler experiment. For the case where there is a single path all chips are faded by the same random variable with the channel offering no extra advantage. Therefore sorting the received symbols does not make any distinction with respect to the received SNR. When more paths are introduced, the received symbols begin to

have different received SNR values. Without the post sorting applied in the decoder the sorted QR decomposition sometimes results in incorrect ordering of the received symbols [59]. This in turn leads to incorrect detection of symbols early in the algorithm and subsequent propagation of errors through the block.

It seems unlikely though, that the simulation with two paths would have the worst performance. Consider that the more frequency variation in the channel, the more diversity is offered and potentially improved system performance. Thus the diversity extraction performed by the despreading of the codes counteracts the error propagation effect which manifests in the error floor.

Fig. 6.4 is a control experiment that illustrates the difference between the sorted QR and unsorted QR algorithms. When comparing the figures it can be seen that the sorted QR decomposition algorithm achieves a larger diversity order for a given channel length but is affected by the propagation errors, whereas the unsorted QR decomposition does not achieved the correct diversity but is unaffected by the propagation of errors.

These effects merit further investigation.

As hypothesised, the spatially multiplexed MC-CDMA system extracts multipath diversity however the sorted QR decomposition suffers from the error propagation effect. Furthermore the unsorted QR decomposition algorithm does not achieve spatial diversity but does extract extra multipath diversity without the propagation of errors.

6.6 ANTENNA CORRELATION EXPERIMENT

6.6.1 Hypothesis

It is hypothesised that the performance of the spatially multiplexed MC-CDMA system will be degraded with correlated antennas.

6.6.2 Experimental parameters

The spatially multiplexed system was evaluated using the LTE MIMO Low, Medium and High antenna correlation matrices for 2 transmit and 2 receive antennas. A single path Rayleigh time-invariant channel was simulated with parameters listed in Table 6.4.

Table 6.4: Antenna correlation experiment parameters.

(a) System

Parameter	Symbol	Value
Sampling frequency	F_{sa}	1 MHz
Code family size	K	8
Flock size	M	8
Element code length	N	4
FFT length	N_{FFT}	MN
Transmit antennas	N_{Tx}	2
Receive antennas	N_{Rx}	2
Code rate	R	2
Bit rate/frequency	F_{bit}	$2F_{sa}$

(b) Channel

Parameter	Symbol	Value
Maximum Doppler shift	F_D	0 Hz
Length	L	0
Antenna correlation	N/A	{Low, Medium, High}

6.6.3 Results

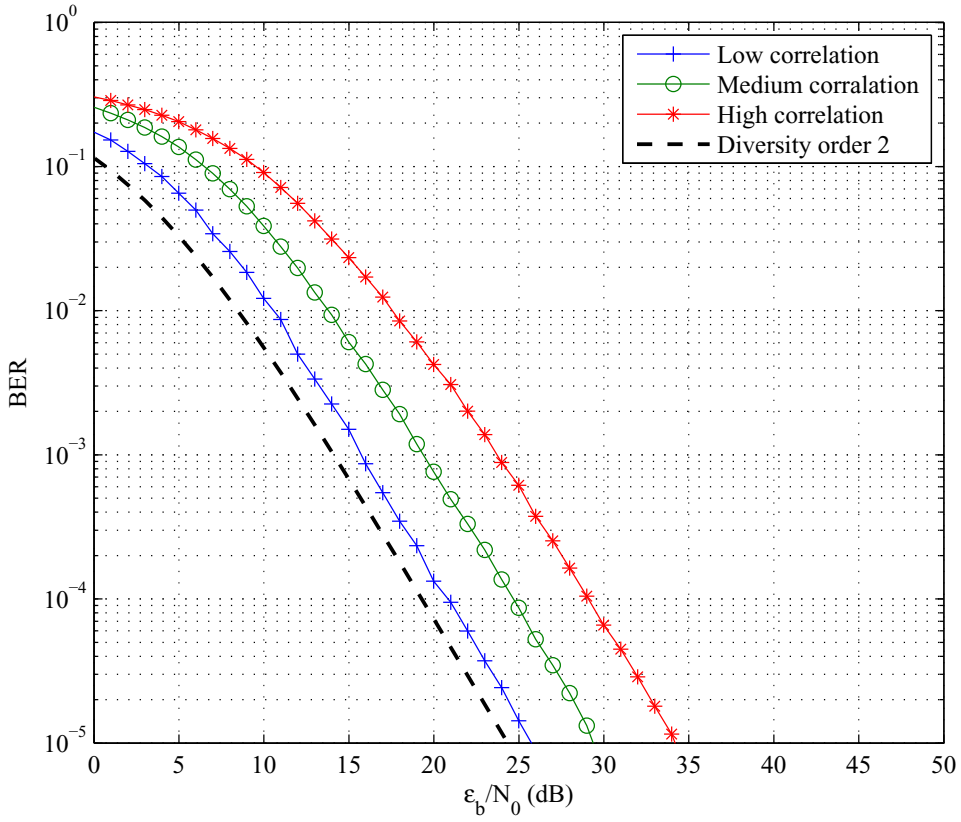

Figure 6.5: BER vs. SNR per bit for the spatially multiplexed system in frequency non-selective Rayleigh fading with correlated antennas.

The results of the antenna correlation experiment may be seen in Fig. 6.5. They are plotted along with the theoretical bit error probability for a second order diversity system.

6.6.4 Conclusion

From the results of the antenna correlation experiment is can be seen that the spatially multiplexed system responds in much the same way as the transmit diversity system. There is minimal loss of diversity but significant performance loss as seen by the horizontal translations. In the case of the medium and high antenna correlation environments there is a loss of 3.6 *dB* and 8 *dB* respectively, compared the low correlation environment. Also the initial performance loss due to the near optimal

decoder is observed.

As hypothesised, the spatially multiplexed MC-CDMA system suffers performance losses with correlated antennas.

CHAPTER 7

CONCLUSION

7.1 CONCLUDING REMARKS

A wireless communication system based on three fundamental technologies has been investigated. Work conducted on MC-CDMA employing CRCCCs has been extended to the multi antenna environment. A divergence in the field of multi antenna wireless communications was identified and provided a basis for the investigation. Two distinct and somewhat antagonistic properties exist when exploiting the spatial dimension. These are the benefit of increased capacity or higher diversity order.

Although both the spatial multiplexing concept and space time block codes can be described by unified matrix algebra, the fundamental difference lies in the necessary means for data detection at the receiver. In Chapter 2 the fundamental technologies of OFDM, CDMA and MIMO were described in vector forms. A detailed description of complementary codes, specifically the CRCCCs, was also presented. Furthermore, benefits of spatial diversity techniques as well as capacity achieving multiplexing were illustrated.

Following this in Chapter 3 was a description of the channel. This chapter began with noise and a description of the time varying SISO multipath channel. This single antenna system was modelled as a discrete FIR filter before it was shown to form the fundamental composition of the multi-antenna channel. The discrete description was further expressed in vector notation consistent with that of Chapter 2. Lastly the LTE standardised channel model was considered along with the tertiary form of fading experienced in these systems; spatial correlation.

Chapter 4 served to unify the matrix algebra of the preceding chapters in the functional context of the

system. At this point the divergence was clear in the functional description of the receiver making way for the following two chapters. The spatially multiplexed system, while transmitting at a higher rate, requires a complex non-linear detector best implemented as a variant of the sphere decoder. On the other hand the transmit diversity system, although transmitting at lower rates, requires only a linear detector.

Chapters 5 and 6 report the performance results of the two distinctly different spatial methods in the form of bit error probabilities. Of particular interest were the results of the transmit diversity system employing OSTBC in AWGN and in multipath conditions. It was observed that the system performed equivalently to uncoded narrowband BPSK (or QPSK) in AWGN independently of the number of receive antennas and only incurred a performance penalty when $N_{Tx} > 2$ and the subsequent rate was less than unity. This was also for the case where all codes in the family are used simultaneously and no performance loss due to multi-user interference was incurred. Another significant result was the extraction of added multipath diversity in multipath conditions. A further point of interest noted from the results was the apparent immunity of both systems to lower frequency Doppler spread. This was aided by the high sampling rate and the assumed perfect CSI.

7.2 FUTURE RESEARCH

As this work builds on previous research, future study may extend it in the following ways:

- As stated in Chapter 6 the sphere decoder employing the sorted QR decomposition without the post sorting algorithm is suboptimal and results in propagation of errors in certain cases. This an area for further investigation in order to determine the performance of the spatially multiplexed MC-CDMA system with an optimal decoder.

- Spreading has only been performed in one of the two possible dimensions. The obvious extension would be to employ CRCCCs to spread in both time and frequency. This may offer further benefits in terms of diversity or may uncover potential pitfalls of the technology.

- Only simulation results have been presented. The field would certainly be enriched by the inclusion of analytical analyses that confirm performance results. This would be a natural extension of the base provided in the matrix algebraic framework.

- Throughout this document perfect CSI has been assumed. A step in the direction of real world

implementation would be to analyse the effect of imperfect CSI. This includes synchronisation errors in time and frequency which may have an adverse effect on the despreading process. The other element to CSI is the knowledge of the triply selective fading of a mobile wireless MIMO channel. Channel estimation plays a large role here and is inherently imperfect, which would likely lead to reduced diversity order.

- It would be beneficial to assess the performance of both systems using the LTE standardised channels listed herein. Also high mobility should be included here since only low to medium mobility has been considered.

REFERENCES

[1] C. Xiao, J. Wu, S.-Y. Leong, Y. Zheng, and K. Letaief, "A Discrete-Time Model for Triply Selective MIMO Rayleigh Fading Channels," *IEEE Trans. Wireless Commun.*, vol. 3, no. 5, pp. 1678–1688, 2004.

[2] M. Roberts, M. A. Temple, R. Mills, and R. Raines, "Evolution of the Air Interface of Cellular Communications Systems Toward 4G Realization," *IEEE Commun. Surveys Tutorials*, vol. 8, no. 1, pp. 2–23, 2006.

[3] E. Perahia, "IEEE 802.11n Development: History, Process, and Technology," *IEEE Commun. Mag.*, vol. 46, no. 7, pp. 48–55, 2008.

[4] D. Pareit, B. Lannoo, I. Moerman, and P. Demeester, "The History of WiMAX: A Complete Survey of the Evolution in Certification and Standardization for IEEE 802.16 and WiMAX," *IEEE Commun. Surveys Tutorials*, vol. 14, no. 4, pp. 1183–1211, 2012.

[5] C. E. Shannon, "A Mathematical Theory of Communication," *Bell System Technical Journal*, vol. 27, pp. 623–656, Oct., 1948.

[6] G. J. Foschini, "Layered Space-Time Architecture for Wireless Communication in a Fading Environment when Using Multi-element Antennas," *Bell Labs Technical Journal*, vol. 1, no. 2, pp. 41–59, 1996.

[7] A. Goldsmith, S. Jafar, N. Jindal, and S. Vishwanath, "Capacity Limits of MIMO Channels," *IEEE J. Sel. Areas Commun.*, vol. 21, no. 5, pp. 684–702, 2003.

[8] J. G. Proakis and M. Salehi, *Digital Communications*, 5th ed., ser. McGraw-Hill higher education. McGraw-Hill, 2008.

[9] L. Hanzo, M. El-Hajjar, and O. Alamri, "Near-Capacity Wireless Transceivers and Cooperative Communications in the MIMO Era: Evolution of Standards, Waveform Design, and Future Perspectives," *Proc. IEEE*, vol. 99, no. 8, pp. 1343–1385, 2011.

[10] H. Yang, "A Road to Future Broadband Wireless Access: MIMO-OFDM-Based Air Interface," *IEEE Commun. Mag.*, vol. 43, no. 1, pp. 53–60, 2005.

[11] W. Zhang, X.-G. Xia, and K. Ben Letaief, "Space-Time/Frequency Coding for MIMO-OFDM in Next Generation Broadband Wireless Systems," *IEEE Trans. Wireless Commun.*, vol. 14, no. 3, pp. 32–43, 2007.

[12] M. Jiang and L. Hanzo, "Multiuser MIMO-OFDM for Next-Generation Wireless Systems," *Proc. IEEE*, vol. 95, no. 7, pp. 1430–1469, 2007.

[13] M. Juntti, M. Vehkapera, J. Leinonen, V. Zexian, D. Tujkovic, S. Tsumura, and S. Hara, "MIMO MC-CDMA Communications for Future Cellular Systems," *IEEE Commun. Mag.*, vol. 43, no. 2, pp. 118–124, 2005.

[14] S. Weinstein and P. Ebert, "Data Transmission by Frequency-Division Multiplexing Using the Discrete Fourier Transform," *IEEE Trans. Commun. Technol.*, vol. 19, no. 5, pp. 628–634, 1971.

[15] R. Scholtz, "The Origins of Spread-Spectrum Communications," *IEEE Trans. Commun.*, vol. 30, no. 5, pp. 822–854, 1982.

[16] M. J. E. Golay, "Complementary Series," *IRE Trans. Inf. Theory*, vol. 7, no. 2, pp. 82–87, 1961.

[17] C. C. Tseng and C. Liu, "Complementary Sets of Sequences," *IEEE Trans. Inf. Theory*, vol. 18, no. 5, pp. 644–652, 1972.

[18] H.-H. Chen, *The Next Generation CDMA Technologies*, 1st ed. John Wiley & Sons Ltd., 2007.

[19] H.-H. Chen, H.-W. Chiu, and M. Guizani, "Orthogonal Complementary Codes for Interference-Free CDMA Technologies," *IEEE Trans. Wireless Commun.*, vol. 13, no. 1, pp. 68–79, 2006.

[20] C. Han, N. Suehiro, and T. Hashimoto, "N-Shift Cross-Orthogonal Sequences and Complete Complementary Codes," in *IEEE International Symposium on Information Theory*, 2007, pp. 2611–2615.

[21] H. Torii, N. Suehiro, and M. Nakamura, "General Construction of Periodic Complete Complementary Codes Composed of Expanded Modulatable Orthogonal Sequences," in *Fifth IEEE Symposium on Computers and Communications*, 2000, pp. 738–743.

[22] C. Zhang, C. Han, Y. Liao, X. Lin, and M. Hatori, "Iterative Method for Constructing Complete Complementary Sequences with Lengths of 2^{mN}," *Tsinghua Science and Technology*, vol. 10, no. 5, pp. 605–609, 2005.

[23] H.-H. Chen, S.-W. Chu, and M. Guizani, "On Next Generation CDMA Technologies: The REAL Approach for Perfect Orthogonal Code Generation," *IEEE Trans. Veh. Technol.*, vol. 57, no. 5, pp. 2822–2833, 2008.

[24] C. Han, N. Suehiro, and T. Hashimoto, "A Systematic Framework for the Construction of Optimal Complete Complementary Codes," *IEEE Trans. Inf. Theory*, vol. 57, no. 9, pp. 6033–6042, 2011.

[25] A. M. Merensky, "A Multi-Dimensional Code-Division-Multiplexed OFDMA Modem Using Cyclic Rotated Orthogonal Complete Complementary Codes," *SAIEE Research Journal*, vol. 103, no. 3, pp. 94–102, Jun., 2012.

[26] G. Raleigh and J. Cioffi, "Spatio-Temporal Coding for Wireless Communication," *IEEE Trans. Commun.*, vol. 46, no. 3, pp. 357–366, 1998.

[27] E. T. Ar and I. E. Telatar, "Capacity of Multi-antenna Gaussian Channels," *European Transactions on Telecommunications*, vol. 10, pp. 585–595, 1999.

[28] H. Taoka, K. Dai, K. Higuchi, and M. Sawahashi, "Field Experiments on MIMO Multiplexing with Peak Frequency Efficiency of 50 Bit/Second/Hz Using MLD Based Signal Detection for OFDM High-Speed Packet Access," *IEEE J. Sel. Areas Commun.*, vol. 26, no. 6, pp. 845–856, 2008.

[29] A. Paulraj and C. Papadias, "Space-Time Processing for Wireless Communications," *IEEE Signal Process. Mag.*, vol. 14, no. 6, pp. 49–83, 1997.

[30] S. Sanayei and A. Nosratinia, "Antenna Selection in MIMO Systems," *IEEE Commun. Mag.*, vol. 42, no. 10, pp. 68–73, 2004.

[31] E. G. Larsson and P. Stoica, *Space-Time Block Coding for Wireless Communications*. Cambridge University Press, 2003.

[32] S. Alamouti, "A Simple Transmit Diversity Technique for Wireless Communications," *IEEE J. Sel. Areas Commun.*, vol. 16, no. 8, pp. 1451–1458, 1998.

[33] V. Tarokh, H. Jafarkhani, and A. Calderbank, "Space-Time Block Codes from Orthogonal Designs," *IEEE Trans. Inf. Theory*, vol. 45, no. 5, pp. 1456–1467, 1999.

[34] M.-O. Damen, H. El-Gamal, and G. Caire, "On Maximum-Likelihood Detection and the Search for the Closest Lattice Point," *IEEE Trans. Inf. Theory*, vol. 49, no. 10, pp. 2389–2402, 2003.

[35] Z. Safar, W. Su, and K. J. R. Liu, "A Fast Sphere Decoding Framework for Space-Frequency Block Codes," in *IEEE International Conference on Communications*, vol. 5, 2004, pp. 2591–2595 Vol.5.

[36] X.-B. Liang, "Orthogonal Designs with Maximal Rates," *IEEE Trans. Inf. Theory*, vol. 49, no. 10, pp. 2468–2503, 2003.

[37] A. Paulraj, D. Gore, R. Nabar, and H. Bolcskei, "An Overview of MIMO Communications - A Key to Gigabit Wireless," *Proc. IEEE*, vol. 92, no. 2, pp. 198–218, 2004.

[38] L.-L. Yang and L. Hanzo, "Multicarrier DS-CDMA: A Multiple Access Scheme for Ubiquitous Broadband Wireless Communications," *IEEE Commun. Mag.*, vol. 41, no. 10, pp. 116–124, 2003.

[39] H.-H. Chen, J.-F. Yeh, and N. Suehiro, "A Multicarrier CDMA Architecture Based on Orthogonal Complementary Codes for New Generations of Wideband Wireless Communications," *IEEE Commun. Mag.*, vol. 39, no. 10, pp. 126–135, 2001.

[40] B. Hochwald, T. Marzetta, and C. Papadias, "A Transmitter Diversity Scheme for Wideband CDMA Systems Based on Space-Time Spreading," *IEEE J. Sel. Areas Commun.*, vol. 19, no. 1, pp. 48–60, 2001.

[41] S. Sfar and K. Ben Letaief, "Layered Group Detection for Multiuser MIMO Wireless CDMA Systems," *IEEE Trans. Wireless Commun.*, vol. 5, no. 9, pp. 2305–2311, 2006.

[42] F. D. V. Maasdorp, "Design and Performance Evaluation of a Full Rate, Full Diversity Space-Time-Spreading Code for an Arbitrary Number of Tx Antennas," M. Eng. thesis, Department of Electrical, Electronic and Computer Engineering of the Faculty of Engineering, Built Environment and Information Technology at the University of Pretoria, 2008.

[43] L. Staphorst, "Viterbi Decoded Linear Block Codes for Narrowband and Wideband Wireless Communication over Mobile Fading Channels," M. Eng. thesis, Department of Electrical, Electronic and Computer Engineering of the Faculty of Engineering, Built Environment and Information Technology at the University of Pretoria, 2005.

[44] C. Papadias and H. Huang, "Linear Space-Time Multiuser Detection for Multipath CDMA Channels," *IEEE J. Sel. Areas Commun.*, vol. 19, no. 2, pp. 254–265, 2001.

[45] H. Huang, H. Viswanathan, and G. Foschini, "Multiple Antennas in Cellular CDMA Systems: Transmission, Detection, and Spectral Efficiency," *IEEE Trans. Wireless Commun.*, vol. 1, no. 3, pp. 383–392, 2002.

[46] G. Stuber, R. Barry, S. McLaughlin, Y. Li, D. Brunelli, and T. Pratt, "Broadband MIMO-OFDM Wireless Communications," *Proc. IEEE*, vol. 92, no. 2, pp. 271–294, 2004.

[47] H. Bolcskei, "MIMO-OFDM Wireless Systems: Basics, Perspectives, and Challenges," *IEEE Trans. Wireless Commun.*, vol. 13, no. 4, pp. 31–37, 2006.

[48] V. van Zelst and T. C. W. Schenk, "Implementation of a MIMO OFDM-Based Wireless LAN System," *IEEE Trans. Signal Process.*, vol. 52, no. 2, pp. 483–494, 2004.

[49] H. Bolcskei, M. Borgmann, and A. Paulraj, "Impact of the Propagation Environment on the Performance of Space-Frequency Coded MIMO-OFDM," *IEEE J. Sel. Areas Commun.*, vol. 21, no. 3, pp. 427–439, 2003.

[50] C. Ibars and Y. Bar-Ness, "Analysis of Time-Frequency Duality of MC and DS CDMA for Multiantenna Systems on Highly Time-Varying and Wide-Band Channels," *IEEE Trans. Wireless Commun.*, vol. 4, no. 6, pp. 2661–2667, 2005.

[51] M. El-Hajjar, O. Alamri, R. Maunder, and L. Hanzo, "Layered Steered Space-Time-Spreading-Aided Generalized MC DS-CDMA," *IEEE Trans. Veh. Technol.*, vol. 59, no. 2, pp. 999–1005,

2010.

[52] M.-L. Ku and C.-C. Huang, "A Complementary Codes Pilot-Based Transmitter Diversity Technique for OFDM Systems," *IEEE Trans. Wireless Commun.*, vol. 5, no. 3, pp. 504–508, 2006.

[53] A. F. Molisch, *Wireless Communications*, 2nd ed. John Wiley and Sons Ltd., 2011.

[54] E. O. Brigham, *The Fast Fourier Transform and its Applications*, 1st ed., ser. Prentice Hall Signal Processing Series, A. V. Oppenheim, Ed. Prentice-Hall International, 1988.

[55] L. L. Hanzo, L. L. Yang, E. L. Kuan, and K. Yen, *Single and Multi-Carrier DS-CDMA: Multi-User Detection, Space-Time Spreading, Synchronisation, Networking and Standards*, 1st ed. John Wiley & Sons Ltd., 2003.

[56] E. W. Weisstein, *The CRC Encyclopedia of Mathematics*, 3rd ed. Chapman and Hall/CRC, 2009, vol. 1.

[57] A. Ben-Israel and T. N. E. Greville, *Generalized Inverses: Theory and Applications*, 1st ed., ser. Wiley Interscience Series of Texts, Monographs and Tracts, P. H. Lipman Bers and H. Hochstadt, Eds. John Wiley & Sons Ltd., 1974.

[58] G. H. Golub and C. F. V. Loan, *Matrix Computations*, 2nd ed., ser. John Hopkins Series in the Mathematical Sciences. The John Hopkins University Press, 1990.

[59] D. Wubben, R. Bohnke, V. Kühn, and K. D. Kammeyer, "MMSE Extension of V-BLAST Based on Sorted QR Decomposition," in *IEEE 58th Vehicular Technology Conference*, vol. 1, 2003, pp. 508–512 Vol.1.

[60] T. S. Rappaport, *Wireless Communications: Principles and Practice*, 2nd ed. Prentice Hall PTR, 2002.

[61] A. Papoulis, *Probability, Random Variables, and Stochastic Processes*, 3rd ed., ser. McGraw-Hill series in electrical engineering. Communications and signal processing. McGraw-Hill, Inc., 1991.

[62] *Evolved Universal Terrestrial Radio Access (E-UTRA); User Equipment (UE) Radio Transmission and Reception*, Third Generation Partnership Project Long Term Evolution Advanced Std.

Release 11, Rev. 11.4.0, Apr., 2013.

[63] M. Patzold, *Mobile Fading Channels*, 1st ed. John Wiley & Sons Ltd., 2002.

[64] D. Gesbert, M. Shafi, D. shan Shiu, P. Smith, and A. Naguib, "From Theory to Practice: An Overview of MIMO Space-Time Coded Wireless Systems," *IEEE J. Sel. Areas Commun.*, vol. 21, no. 3, pp. 281–302, 2003.

[65] *Universal Mobile Telecommunications System (UMTS); User Equipment (UE) radio transmission and reception (FDD)*, Third Generation Partnership Project Std. Relesase 11, Rev. 11.9.2, Apr., 2014.

APPENDIX A

GENERATION OF ORTHOGONAL COMPLETE COMPLEMENTARY CODES

Beginning with an $N \times N$ orthogonal matrix **A**,

$$\mathbf{A} = \begin{bmatrix} a_{1,1} & a_{1,2} & \cdots & a_{1,N} \\ a_{2,1} & a_{2,2} & \cdots & a_{2,N} \\ \vdots & \vdots & & \vdots \\ a_{N,1} & a_{N,2} & \cdots & a_{N,N} \end{bmatrix}, \tag{A.1}$$

with elements $a_{i,j}, i, j = 1, 2, \ldots N$ of magnitude $|a_{i,j}| = 1$. **A** is orthogonal in the sense that its columns are mutually orthogonal, that is,

$$\sum_{i=1}^{N} a_{i,k} a_{i,m}^{*} = 0 \quad k \neq m. \tag{A.2}$$

The autocorrelation function of the sequence defined by **A** is zero for all N-multiple shifts except the zero shift.

Next, by defining matrix **B** in the same way as **A**, N sequences of length N^2 can be constructed in the following manner:

$$\mathbf{C} = \begin{bmatrix} b_{1,1}\mathbf{A}_1 & b_{1,2}\mathbf{A}_2 & \cdots & b_{1,N}\mathbf{A}_N \\ b_{2,1}\mathbf{A}_1 & b_{2,2}\mathbf{A}_2 & \cdots & b_{2,N}\mathbf{A}_N \\ \vdots & \vdots & & \vdots \\ b_{N,1}\mathbf{A}_1 & b_{N,2}\mathbf{A}_2 & \cdots & b_{N,N}\mathbf{A}_N \end{bmatrix}, \tag{A.3}$$

where $\mathbf{A}_i$ is the ith row of matrix $\mathbf{A}$. This may be rewritten as,

$$\mathbf{C} = \begin{bmatrix} c_{1,1} & c_{1,2} & \cdots & c_{1,N^2} \\ c_{2,1} & c_{2,2} & \cdots & c_{2,N^2} \\ \vdots & \vdots & & \vdots \\ c_{N,1} & c_{N,2} & \cdots & c_{N,N^2} \end{bmatrix}. \tag{A.4}$$

The rows of $\mathbf{C}$ exhibit the ideal correlation properties described in section 2.4.2.

Now taking a third orthogonal matrix $\mathbf{D}$,

$$\mathbf{D} = \begin{bmatrix} d_{1,1} & d_{1,2} & \cdots & d_{1,N} \\ d_{2,1} & d_{2,2} & \cdots & d_{2,N} \\ \vdots & \vdots & & \vdots \\ d_{N,1} & d_{N,2} & \cdots & d_{N,N} \end{bmatrix}, \tag{A.5}$$

again defined in the same way as $\mathbf{A}$, a complementary code family may be constructed as,

$$\mathbf{E} = \begin{bmatrix} \mathbf{E}_{1,1} & \mathbf{E}_{1,2} & \cdots & \mathbf{E}_{1,N} \\ \mathbf{E}_{2,1} & \mathbf{E}_{2,2} & \cdots & \mathbf{E}_{2,N} \\ \vdots & \vdots & & \vdots \\ \mathbf{E}_{N,1} & \mathbf{E}_{N,2} & \cdots & \mathbf{E}_{N,N} \end{bmatrix}, \tag{A.6}$$

with,

$$\mathbf{E}_{i,j} = [c_{i,1}\ d_{j,1}\ \ldots\ c_{i,N}d_{j,N}\ c_{i,N+1}d_{j,1}\ \ldots\ c_{i,2N}d_{j,N}\ \ldots \tag{A.7}$$

$$c_{i,N^2-N+1}d_{j,1}\ \ldots\ c_{i,N^2}d_{j,N}] \tag{A.8}$$

$$= [e_{i,1}\ e_{i,2}\ \ldots\ e_{i,N^4}], \tag{A.9}$$

where the row $\mathbf{E}_i = [\mathbf{E}_{i,1},\ \mathbf{E}_{i,2},\ \ldots\ ,\mathbf{E}_{i,N}]$, represents the ith flock of the family with jth element code $\mathbf{E}_{i,j}$.